



Dipl.-Ing. Johannes Hiesmayr, MEng, BSc

Experimental Investigation and Simulation of Gaseous Emissions and Fuel Consumption in Real World Driving Scenarios for Two-Wheeler-Applications

DISSERTATION

Submitted at the

Graz University of Technology

in fulfilment of the requirements for the
degree of Doctor of Technical Science (Dr.techn.)

First supervisor:

Ao.Univ.-Prof. Dr. Stefan Hausberger
Institute of Internal Combustion Engines and Thermodynamics
Graz University of Technology

Second supervisor

Assoc.-Prof. Dr. Leonidas Ntziachristos
Laboratory of Heat Transfer and Environmental Engineering
Aristotle University of Thessaloniki

Graz, May 2019



Institute of Internal Combustion Engines and Thermodynamics
Head: Univ.-Prof. Dr. Helmut Eichlseder

Foreword

I was always fascinated by the unknown and new. It gets boring as the initial rush is over, when things get settled and turn normal or become daily business. However, it is not usual to get the chance of starting a PhD thesis in a specialized technical area after some years working in a completely different field with hardly any specific background on the upcoming challenges. Hence and foremost, I want to thank Dr. Stephan Schmidt for this chance and for his trust in my engagement and skills to handle the tasks in my research project. Special thanks go to the Head of the Research Area Design, Assoc. Prof. DI Dr. Roland Kirchberger, and all my friends and colleagues for the extraordinary pleasant working atmosphere, the inspiring technical discussions and all their support; especially, thank you Ritschi, Pacl and Jandlman. In fact, no publication would have been released in its linguistic perfection without Mag. Claudia Melde – Thank you!

Moreover, for the preparation of the first and second assessment document and for taking the role as my supervisors for this thesis, I want to gratefully thank Univ.-Prof. Stefan Hausberger from Graz University of Technology and Assoc.-Prof. Leonidas Ntziachristos from Aristotle University of Thessaloniki.

The most important things in my life are family and friends (and cycling). Without education, guiding light and unreserved support of my parents I would have never become the free minded person I am – thank you! My girlfriend, my relatives and all my friends endured the times when I had not been with them due to my studies and nevertheless, even after many weeks or even months, it is always as if I have never been away; that is the greatest gift – Thank you.

Last but not least, my daughter Sara means everything to me. She shaped me as a completely new person and she is the greatest gift ever to me. Sara, I am endlessly thankful for every single day with you. I want you to be healthy and happy for the rest of your life and I will support you with anything in every possible way I can. My graduation is dedicated to you.

Content

FORMULA SYMBOLS AND ABBREVIATIONS.....	2
STATUTORY DECLARATION.....	5
ABSTRACT	7
ZUSAMMENFASSUNG.....	9
1 INTRODUCTION	11
1.1 PROBLEM STATEMENT AND OBJECTIVE	14
1.2 STRUCTURE AND METHODOLOGY	14
1.2.1 <i>Identification of publications and the authors' inputs respectively</i>	15
1.2.2 <i>Acknowledgements</i>	15
1.3 RELEVANCE OF REAL DRIVE EMISSION MEASUREMENT	15
2 MEASUREMENT METHODOLOGY FOR RDE	19
2.1 TEST OBJECTS	19
2.2 TEST RIG EMISSION MEASUREMENT.....	23
2.2.1 <i>Technical limits of on-road tests and chassis dynamometer measurements</i>	24
2.3 REAL DRIVE EMISSION MEASUREMENT	27
2.3.1 <i>Installation of the measurement equipment</i>	27
2.3.2 <i>Measured Values</i>	28
2.3.3 <i>Adaptions to measurement equipment</i>	29
2.3.4 <i>Calibration and measurement season</i>	30
2.4 EVALUATION OF MEASUREMENT EQUIPMENT	31
2.4.1 <i>Cross influences and side effects of the measurement equipment</i>	36
2.5 EVALUATION OF MOTORCYCLE DRIVING DYNAMIC	44
2.5.1 <i>Real world traffic situations</i>	45
2.5.2 <i>Representative single on-road micro-trips</i>	47
2.5.3 <i>Motorcycle driving dynamic and legislative boundaries</i>	49
2.5.4 <i>Selecting and processing single micro-trips</i>	53
2.5.5 <i>Influences of driver and traffic flow on trip indicators</i>	54
2.5.6 <i>Evaluation of the single micro-trips</i>	55
2.5.7 <i>Deliberation on additional or changed trip indicators for motorcycles</i>	60
2.6 REAL DRIVE TEST CYCLES FOR CHASSIS DYNAMOMETER.....	62
2.6.1 <i>Assessment of Real Drive Cycles</i>	69
3 RESULTS OF THE RDE MEASUREMENT METHODOLOGY.....	73
3.1 ON-ROAD MEASUREMENT RESULTS.....	73
3.2 CHASSIS DYNAMOMETER MEASUREMENTS	80
3.3 NON-REGULATED GASEOUS EMISSIONS.....	85
3.4 CONSOLIDATING DISCUSSION OF THE EMISSION RESULTS	89
4 METHODOLOGY FOR REAL DRIVE EMISSION SIMULATION.....	94
4.1 SIMULATION MODEL DESCRIPTION	94
4.1.1 <i>Longitudinal vehicle simulation model</i>	94
4.1.2 <i>Introduction to machine learning and related work</i>	95
4.1.3 <i>Artificial neural network modelling</i>	97
4.1.4 <i>Emission and fuel economy simulation</i>	109
4.1.5 <i>Model adaption to other motorcycles</i>	118
5 CONCLUSIVE DISCUSSION	119
5.1 RDE MEASUREMENT METHODOLOGY FOR MOTORCYCLES	120
5.2 RDE SIMULATION METHODOLOGY.....	122
6 LITERATURVERZEICHNIS.....	123

Formula symbols and abbreviations

Formula symbols

s	-	Standard deviation
t	s	Time
v	m/s	Velocity
h	m	Geodetic altitude
\dot{V}	m ³ /s	Volume flow
\dot{m}	kg/s	Mass flow
T	K	Temperature
n	rpm	Engine speed
a	m/s ²	Acceleration
d	M	Distance
N	-	Number of ... (e.g. measurement points)
Y	-	Target Vector
F	-	Transfer function
X	-	Vector for learning input
W	-	Weight vector
c	-	Bias
tq	Nm	Torque
a	%	Throttle angle
P	W	Power

Abbreviations

ANN	Artificial Neural Network
ATC/ACC	European Topic Center on Air and Climate Change
CAT	Catalytic converter
CVS	Constant Volume Sampling System
EC	European Commission
EFM	Exhaust Flow Meter
EGR	Exhaust gas recirculation
EU	European Union
FID	Flame Ionization Detector
FTIR	Fourier Transform Infrared Spectroscopy
GPS	Global Positioning System
GVWR	Gross vehicle weight rating
ICE	Internal combustion engine
IDC	Indian Drive Cycle
LVD	Longitudinal Vehicle Dynamic
NDIR	Nondispersive infrared sensor
NDUV	Nondispersive Ultra Violet Spectroscopy
NEDC	New European Drive Cycle
NEFZ	New European drive cycle (Neuer Europäischer Fahrzyklus)
OBD	On board diagnosis
PEMS	Portable Emission Measurement System
PM	Particulate Matter
PTW	Powered-Two-Wheeler
RDC	Real Drive Cycle
RDE	Real Drive Emissions
RDM	Real Drive cycle Moped
RPA	Relative positive acceleration
SCR	Selective catalytic reduction system
VA _{pos}	Vehicle times positive acceleration
WMTC	World Motorcycle Test Cycle

Statutory Declaration

I declare that I have authored this thesis independently, that I have not used other than the declared sources/resources, and that I have explicitly indicated all material which has been quoted either literally or by content from the sources used. The text document uploaded to TUGRAZonline is identical to the present dissertation.

Johannes Hiesmayr

Graz, _____
Date

Signature

Abstract

In recent times it turned out that real world operating scenarios have a major influence on regulation and homologation of emissions and fuel consumption. Having in mind the worldwide ambitions to reduce emissions of climate-relevant and environmentally harmful gases and the exploitation of fossil resources, deep understanding concerning the real drive behavior of mobile sources has to be acquired. For passenger cars, it is a well-known fact that emissions and fuel consumption in real world conditions, considerably differ from the officially published values [1].

Emissions of passenger cars and of commercial vehicles are officially regulated by the European Commission by means of real driving with Euro 6d-temp since September 2019 for passenger cars and with EURO VI since 2013 for commercial vehicles. A methodology to measure RDE real drive emissions is therefore well approved for heavy duty vehicles and automotive applications but was not adapted for two-wheeler-applications yet. Hence, measurements have been performed for motorcycles with the state-of-the-art measurement equipment at the Graz University of Technology to be prepared for possible future legislation. Moreover, as the number of different engine and vehicle concepts for powered-two wheelers is very high and will even rise with hybridization, the simulation of emissions and fuel consumption is indispensable for further development towards more environmentally friendly mobility. Hence, the content of the present work is separated in three thematic areas.

The first area describes an RDE measurement methodology for motorcycles. Test objects, measurement gauge and the measurement effort are described. The collected data led to insights into driving dynamic of motorcycles to be introduced in coherence with state of the art on-road driving assessment for passenger cars. One exemplary output was the synthetic assembly of real drive cycles for motorcycles that will be evaluated in terms of their dynamic on chassis dynamometer in comparison to on-road driving. Moreover, so called trip indicators as stated in the regulation “Commission Regulation (EU) 2016/646” for light passenger and light commercial vehicles will be discussed for two-wheeler-applications to better reflect driving dynamic for motorcycles. All these insights will be introduced to gain a better understanding of influencing factors for RDE and to compare and assess the data with automotive applications. In this context, the evaluation and assessment of herein used portable emission measurement system (PEMS) equipment is presented.

In the second area, results and a comparison of on-road and test bench emission measurements are demonstrated to build the bridge between the relevance of different measurement methodologies including their assessment and a possible RDE assessment process for motorcycles. The goal is to give an idea of how to represent real word driving of two-wheeler-applications with state-of-the-art measurement and assessment technologies and additionally to reflect on possible adaptations in terms of state-of-the-art measurement technology and methodology for homologation combined to existing RDE legislation.

The third area introduces an adaptive artificial neural network based predictive model for emission and fuel consumption simulation of motorcycles. The model is developed in Matlab and Simulink and is integrated into a longitudinal vehicle dynamic simulation whereby it is possible to simulate various and not yet measured test cycles. Subsequently, it is possible to predict real drive emissions and on-road fuel consumption by a minimum of previous measurement effort. The modelling approach is adaptive in terms of usability for different engine and exhaust gas treatment systems as the model does not require specific knowledge about technical vehicle parameters, which can be unknown due to manufacturers’ concealment. Backpropagation is used as supervised learning technique for training the neural networks and various learning inputs are investigated and evaluated.

The simulation expands on the previously presented research of possible measurement methodologies for real drive emissions for motorcycles. The purpose of the simulation is to minimize the effort in estimating real world effects and to serve as a tool for further improvement towards upcoming more stringent legislative emission limits. Therefore, the adaptation of an investigated Euro 3 motorcycle is presented as an example. Moreover, tools are presented to assign emission relevant scenarios to specific driving patterns and to assess them according to the vehicles driving dynamic.

Finally, there is a conclusive discussion on the presented research topic. Some further issues are addressed for the measurement and simulation methodology and current applications of the presented findings are introduced.

Zusammenfassung

Reale Fahrscenarien haben bei allen Fahrzeugen mit Verbrennungsmotor signifikanten Einfluss auf deren Emissionen. Bei Nutzfahrzeugen und Personenkraftwagen gibt es bereits entsprechende gesetzliche Grundlagen zum Nachweis der Emissionen im praktischen Fahrbetrieb. Diese gesetzlichen Grundlagen sind bisher nicht auf Zweiräder mit Verbrennungsmotor übertragen worden.

Die vorliegende Doktorarbeit beschäftigt sich in diesem Zusammenhang mit der Evaluierung und Bewertung von möglichen Methodiken zur Messung und Simulation von Emissionen und Kraftstoffverbrauch im realen Fahrbetrieb. Für ein besseres Verständnis der gegebenen Randbedingungen für Motorräder und Mopeds werden dazu vorerst Untersuchungen zur Fahrdynamik vorgestellt. Auf Basis der daraus gewonnenen Erkenntnisse werden verschiedene sogenannte Real Drive Cycles (RDC) vorgestellt. Diese entstanden aus den Untersuchungen zur Fahrdynamik und sollen Messungen am Zweirad-Rollenprüfstand mit realitätsnahem Fahrverhalten ermöglichen. Des Weiteren wurde ein portables Emissions-Mess-System (PEMS), welches bereits bei Automobilen und Nutzfahrzeugen Anwendung findet, adaptiert und an insgesamt drei Versuchsobjekten getestet. Es werden die gemessenen Emissionsergebnisse von Typprüfzyklus, RDC und aus dem realen Fahrbetrieb verglichen und diskutiert. Aufbauend auf den Messergebnissen wurde auf Basis neuronaler Netze mit Matlab und Simulink ein Simulationsmodell für Emissionen von Realfahrscenarien entwickelt und in eine bestehende Längsdynamik Simulation integriert. Die Simulationsergebnisse werden den Messergebnissen gegenübergestellt.

Abschließend werden die unterschiedlichen Mess- und Simulationsergebnisse gegenübergestellt. Auf Basis der gewonnenen Erkenntnisse wird als Ergebnis dieser Arbeit eine mögliche Methodik für RDE-Tests für motorisierte Zweiräder diskutiert.

1 Introduction

We are in the great ages of mankind; the human being is shaping the world in a way that has never happened before by the cause of any living species. Our desire for a chance of good living causes our planet to suffer for our success in terms of the proceeding depletion of resources and alarming devastation of biological ecosystems. Figure 1 shows a highway interchange embedded in the megacity of Shanghai as an example for our reshaped environment. Infrastructure and industry, mobility and transportation, food and water production and supply, and the residential sector have direct, significant effects on the world environment as these are the main causes for global energy consumption.



Figure 1: Nanpu Bridge Interchange in Shanghai, China [2].

The energy demand is directly driven by population and economic growth [3]. Figure 2 shows the total primary energy supply by source from 1990 until now in 5-year increments on the left-hand side. Even though renewables are on the rise and predicted for an increased share on total energy supply [4], the fossil-based energy demand will not bottom out as a full life cycle assessment is considered for any technology that arrogates to substitute carbon-based sources.

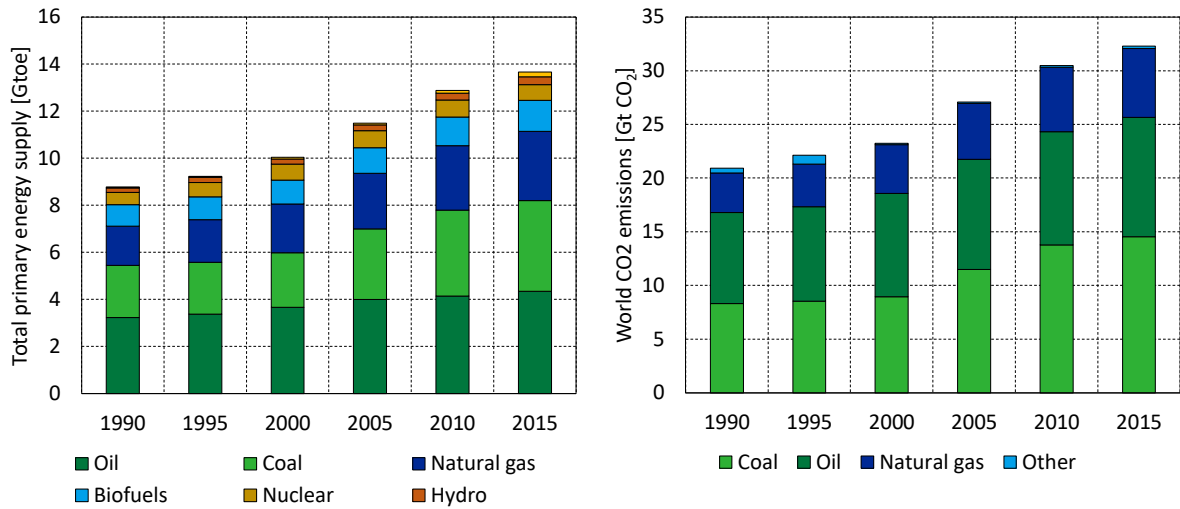


Figure 2: Total primary energy supply by source and world CO₂ emissions from fuel combustion [5].

Energy consumption of hydro-carbon-based sources results in emissions due to thermodynamic energy conversion by oxidation processes wherein the combustion process is the most common one. Hence, the main resulting emissions are CO₂, CO, NO_x, SO_x, HC and PM. CO₂ is a non-health-damaging gaseous pollutant which is directly linked to total fossil energy consumption. Figure 2 shows the world CO₂ emissions from fuel combustion from 1990 until now in 5-year increments on the right-hand side. CO₂ is the main reason for the greenhouse effect and global warming which will not decline until an effective sink for that molecule is found as counterweight to fossil energy sources. Further on, CO, NO_x, SO_x, HC and PM emissions are environmentally and health relevant emissions partly caused by incomplete combustion processes (CO, HC). Figure 3 shows the consumption of global energy and feedstock fuels, with the transport sector accounting around 20% in 2018. Nowadays, this sector mainly relies on the use of carbon-based energy. Thus, mobility is a main source for these emissions.

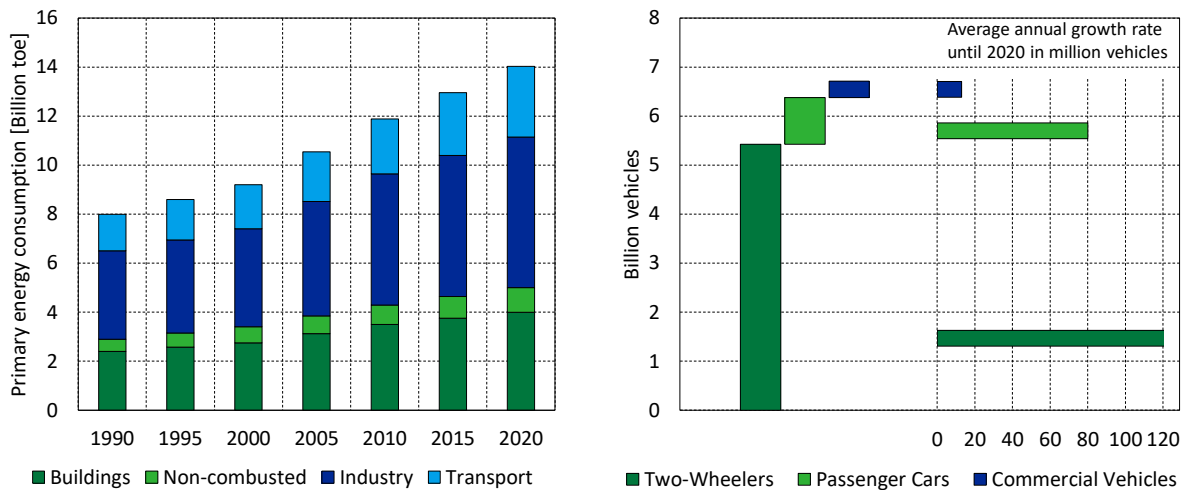


Figure 3: Primary fossil energy consumption by end use sector¹ [6] and estimated segmentation of the transport sector worldwide in 2015 [7] [8] [9] [10] [11].

Furthermore, Figure 3 shows the estimated segmentation of the transport sector worldwide in 2015, based on production statistics on the right-hand side. It can be seen, that powered two-wheelers are by far the most commonly used vehicles with the highest production so far with an estimated total number of 5.5 billion units. Their share on total vehicles will even rise as in developing countries a motorcycle is more likely to be used as primary mobile. Therefore, emission level regulation is indispensable for this kind of mobile source to protect human and environmental health within a long-term perspective. A lot of countries, also in Eastern Asia, use the legislative regulations of the European Commission for the certification and homologation process for motorcycles or at least follow their directives.

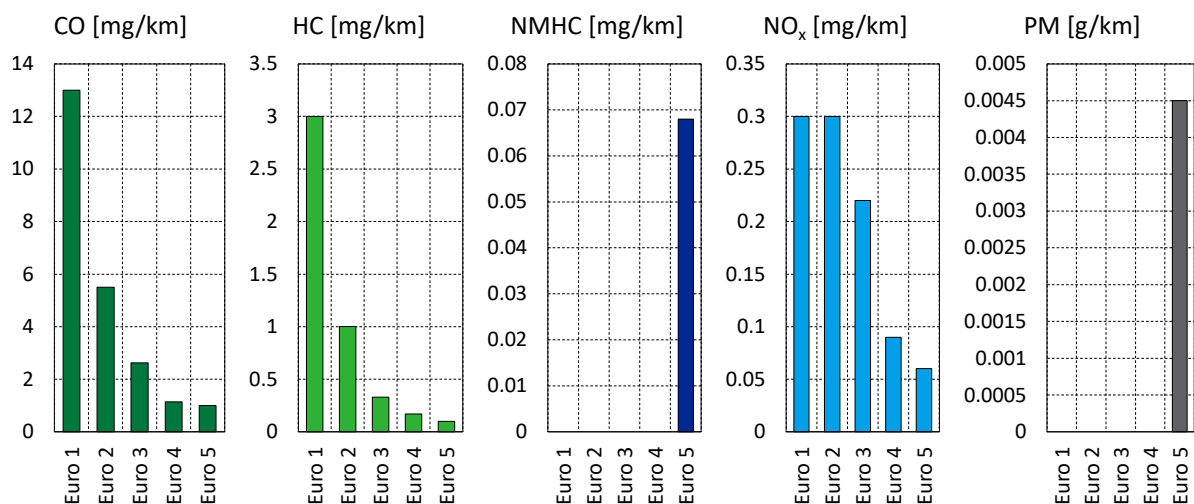


Figure 4: Legislative emission regulation and limits for powered two-wheelers [12] [13] [14].

¹ Primary energy use in power plants is allocated according to final sector electricity consumption; Industry excludes non-combusted use of fuels;

Figure 4 illustrates the emission limits for the European Union from Euro 1 to Euro 5 certification for motorcycles. Euro 4 certification is obligatory since 2018. Euro 5 certification is already defined and will be introduced in 2020 [15]. The legislative limits are becoming more stringent and even mass of particulate matter must be controlled in the future. But all these limits rely on type approval test measurements on the test rig. It is a well-known issue for passenger cars and commercial vehicles that test results considerably differ from real world operation results [1] [16]. Thereto, measurement procedures for real drive emissions RDE are established for passenger cars and these are relevant for certification since Euro 6c [14]. Motorcycles might show the same discrepancies in their emission and fuel consumption performance. This issue leads to the objective of the current doctoral thesis.

1.1 Problem statement and objective

Real world operating scenarios have a major influence on emissions and fuel consumption. To reduce climate-relevant and environmentally harmful gaseous emissions and the exploitation of fossil resources more efficiently, deep understanding concerning the real drive behavior of mobile sources is needed. Due to legislative regulations by the European Commission a methodology to measure real drive emissions is well approved for heavy duty vehicles and automotive applications but may not be applicable directly to two-wheelers.

The objective of this doctoral thesis is the investigation and assessment of real world behavior of motorcycles in terms of driving dynamic, emission levels, and fuel consumption. The goal is to find a methodology to determine and evaluate these parameters. The relevance of real drive emission measurement for motorcycles in particular will be discussed in section 1.3 in more detail to give deeper insights into the prerequisites of this work.

1.2 Structure and methodology

Followed by the relevance of RDE measurement in section 1.3, this thesis is separated in four main parts.

The first part treats the elaboration of a suitable measurement methodology for RDE for motorcycles. Treated test objects are introduced and measurement equipment is assessed. The applicability of measurement gauge for specific motorcycle classes as well as driving dynamic of two-wheelers are important issues which will be discussed in detail. Main findings of this part are so-called Real Drive Cycles RDC to reflect typical on-road behavior.

The second part introduces measurement results for real drive emissions for two-wheelers. Euro 3 and Euro 4 motorcycles will be compared and the further use of RDE measurement results with regard to the development towards more stringent legislative limits will be stated.

The third part expands on a fast and adaptive simulation methodology for RDE. The emission simulation model is based on machine learning and integrated in a longitudinal vehicle dynamic model LVD in Matlab. With this tool, quick assessments of on-road behavior concerning gaseous emissions and fuel economy are possible, whereby the needed data base for the simulation can be gained by very few chassis dynamometer measurements.

The fourth and last main part is a conclusive discussion of the herein presented RDE measurement and simulation methodologies with a quick look on their possible further use. Some parts of the herein presented methodologies are already in use, and is also mentioned

more detailed in this chapter.

1.2.1 Identification of publications and the authors' inputs respectively

Publications have been released by the author within the scope of this doctoral thesis. In particular, the four papers “Current findings in measurement technology and measurement methodology for RDE and fuel consumption for two-wheeler-applications” [17], “Results, assessment and legislative relevance of RDE and fuel consumption measurement of two-wheeler-applications” [18], “Artificial neural network based predictive real drive emission and fuel economy simulation of motorcycles” [19] and “Evaluation of measurement technologies for RDE and fuel consumption for two-wheeler-applications” [20]. Furthermore, masters' and bachelors' theses have been elaborated during this research project. The author acted as project leader and junior scientist within that project and all the herein presented work and results emerged from his own contribution if not cited or marked otherwise. Figures or text passages from the aforementioned papers are not additionally marked as they are made or written by the author himself.

1.2.2 Acknowledgements

The present thesis emerged within the framework of the K-project “ECO-Powerdrive²”, funded by the Austrian government, the Styrian and the Upper Austrian government within the excellence initiative COMET. A full portable emission measurement system PEMS was provided by AVL List GmbH. Motorcycles were provided by BMW Motorrad GmbH, Munich or rented and bought from local retailers. The simulations and some calculations described in this publication were carried out with Matlab and Matlab Simulink.

1.3 Relevance of real drive emission measurement

Combustion engine powered mobile sources are one of the major pollution sources in urban areas. According to ETC/ACC (2009) data, road transport contributes about 42% of total NO_x emissions, 47% of total CO emissions and 18% of total PM emissions at EU25 level [21]. In order to assess both the environmental impacts and the impact on human's health, it is necessary to gain reliable data from emission measurements to monitor the evolution of mobile sources. Furthermore, these data provide the base for regulatory measures and their control of effectiveness. Due to the progress in reducing regulated emissions of gasoline and Diesel passenger cars and other mobile sources, the contribution of powered two-wheeler-applications PTW to the overall fleet emissions of mobile sources becomes more important in the future. Figure 5 illustrates that for HC and CO emissions. It can be seen that the sum of emissions of all road transport sources is decreasing as more stringent legislative limits are applied. Even though, the share on total emissions of powered two-wheelers is on the rise as their emission regulation lags behind. The need for a better regulation in this area is even more obvious, as their share is bigger and their number is rising in urban areas in developing countries [22]. Additionally, although current regulatory measures seem efficient to stabilize the CO share, further measures will be required for HC emissions which are estimated to reach an even bigger share of total emissions in the next years [22].

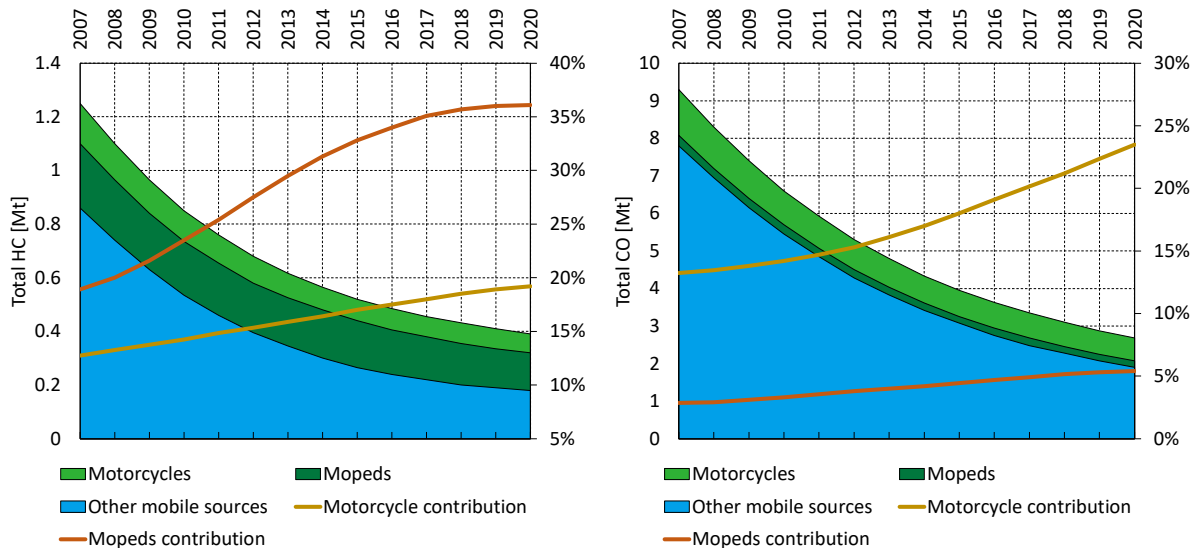


Figure 5. Evolution of PTWs HC and CO emission in Europe in comparison with emissions of all other road transport sources [22].

Yet, this is enforced by the fact that the amount of PTW in urban regions of emerging countries in Asia is around 50% of the total vehicle population and its absolute number is increasing at an annual rate of over 10% [23] [24]. Thereto, Figure 6 illustrates registered vehicles in million units and population in billion units for main regions or countries in the world. Additionally the annual new registrations of vehicles in million units is shown. This figure implies and thereto demonstrates the potential of upcoming mobilization as one compares developed and developing countries. Personal mobility is a desirable good and annual growth rates are on the rise. To more clearly illustrate the scale of this issue, in absolute numbers for Jakarta, capital city of Indonesia, this means a daily increase of at least 1000 motorbikes (around 1200 vehicles in total) in average in July 2011 [25]. Furthermore, Figure 7 illustrates the contribution of PTWs gaseous emissions compared to the total number of mobile sources in a representative Asian country, Vietnam, on the left-hand side. Europe's mix is additionally shown on the right-hand side. The figure underlines the relevance of treating powered two-wheelers with high priority to develop and implement pollution control strategies if Asian and Indian cities are to achieve clean and healthy air in the near future [24].

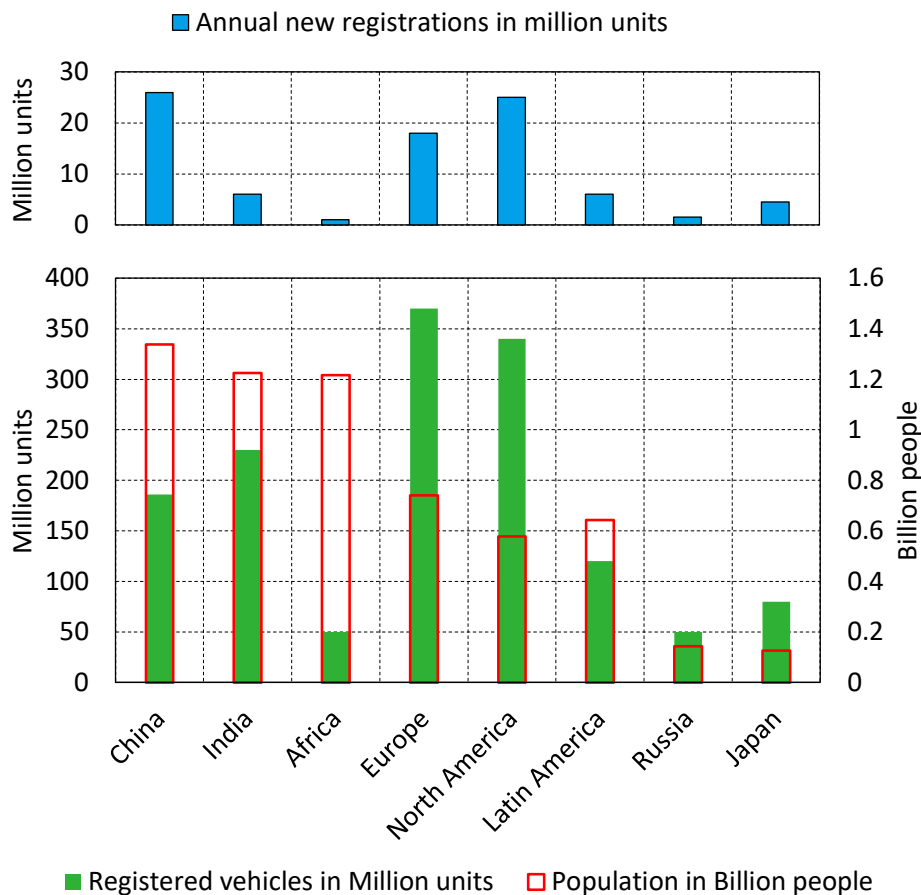


Figure 6: Vehicles and population [26] [27] [28] [29] [30] [31] [32] [33].

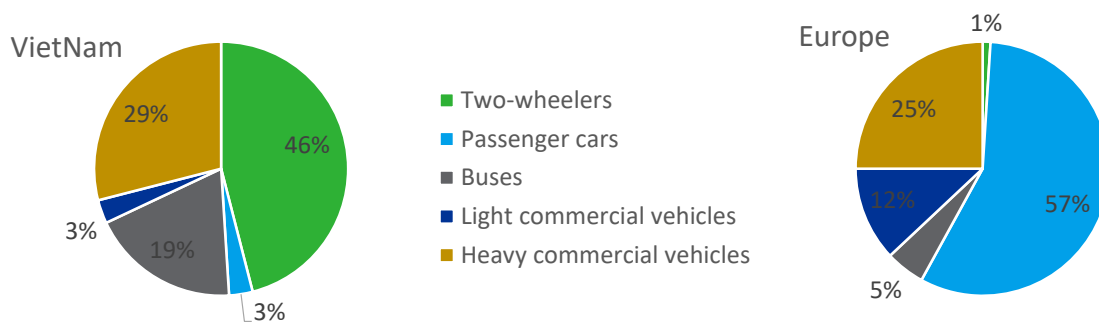


Figure 7. Vietnam's road transport CO₂ emissions by vehicle type in 2010 [23] (left-hand side) and Europe's road transport CO₂ emissions in 2016 (right-hand side) [34].

Nowadays, numerous test cycles for emission certification on chassis dynamometer are available in different countries like the NEDC, WMTC, and IDC amongst others [35]. Also test cycles have been developed by real world data that shall not be based on fixed legislative driving standards anymore, but reflect local driving conditions [36]. According to these test cycles for laboratory purpose, attempts have been made in automotive industries to use random cycle generators for homologation process to prevent not only cycle beating but also to stop the optimization of engine behavior towards specific engine loads and drive cycles respectively. Concurrently, plenty of studies show that factors such as driving conditions, driver behavior, traffic flow, road characteristics and vehicle drivability significantly affect emissions and fuel

consumption in real drive scenarios. Along with these arguments and recapitulating the need to improve emission behavior and to reduce fuel consumption of PTWs, the possibility of extending the planned Euro 5 regulation for PTWs by RDE investigations seems to be very likely. Figure 8 exemplarily shows the differences in engine operation for different automotive test cycles and a real world test cycle. The greater variety of load points is obvious.

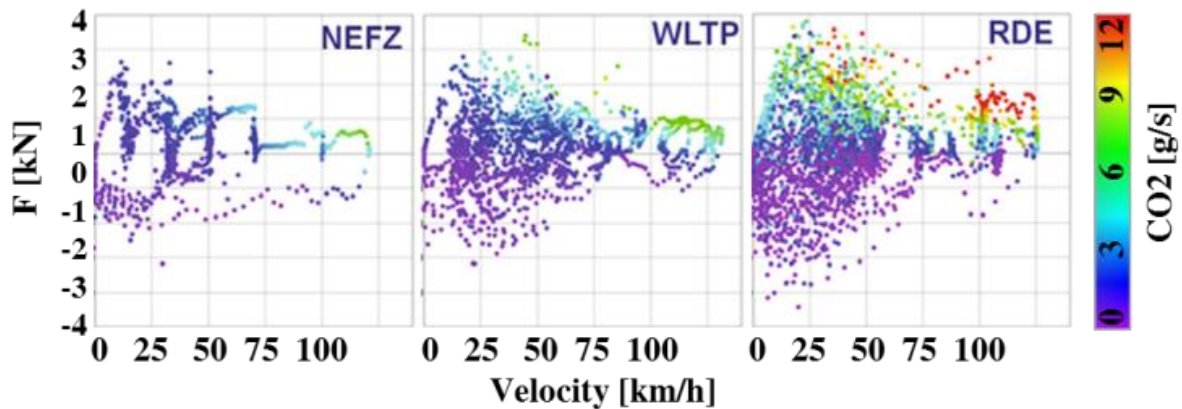


Figure 8. Load points (F/v) and their CO_2 emissions for different automotive drive cycles and a real world test cycle (RDE) for passenger cars [37].

However, the already applied RDE measurement equipment and methodologies are not committed to be taken similar for two-wheeler-applications. Nevertheless, the acquisition of expertise in RDE measurement technology, methodology, evaluation and assessment is essential to be prepared for future development in this segment of mobile sources.

For this purpose, state of the art RDE and fuel consumption measurement technology, originally used for automotive applications, was investigated to apply all the needed gauges on a motorcycle.

2 Measurement methodology for RDE

The use of PEMS in the homologation process also became legislatively embedded for mobile sources as already the “Commission Regulation (EU) 715/2007” contains provisions to ensure that the emission limits are respected under normal vehicle operation and use [38]. Especially in Europe and America the public interest increased due to the Volkswagen emission scandal in 2015 and therefore the on-road measurement to show real world behavior has gained more importance. Exemplarily, the amending regulation “Commission Regulation (EU) 2016/646” for light passenger cars and commercial vehicles includes test procedures for RDE within September 2017 for Euro 6c homologation process. The legislative development shows that real word measurement of emissions and fuel consumption can be introduced for two-wheeler-applications even though it is not planned yet in an upcoming stage of Euro 5 regulation scheduled in 2020.

In order to develop a comprehensive measurement methodology for RDE for motorcycles, the established type approval tests for all categories of powered two-wheelers have to come into consideration. Furthermore, commercially available measurement equipment has to be evaluated with regard to the proliferation of different vehicle and engine concepts. Last but not least, the driving pattern itself has to be investigated as this is mainly determined by vehicle categories and engine capacity respectively so that this might differ from other mobiles. These facets lead to the theoretical background from which a comprehensive measurement methodology will be developed in this study.

Therefore, the first section of this chapter describes the test objects which had been used to elaborate the measurement methodology for RDE. To give a more general overview of the topic, the following section 2.2 introduces to test rig emission measurements for motorcycles on the chassis dynamometer. This is relevant as the presented RDE measurement methodology for motorcycles includes tests on the dyno. Section 2.3 steps into detail for RDE measurement. Test equipment is introduced and evaluated. Further on, motorcycles’ driving dynamic is investigated in section 2.5 and leads to the upcoming section 2.6 wherein afore mentioned Real Drive Cycles RDC are introduced. With these cycles a comprehensive measurement methodology for powered two-wheelers can be consolidated which is conclusively described in the final section 5.1.

2.1 Test objects

Several different motorcycles were investigated starting from less than 50ccm and reaching up to 1200ccm. Figure 9 shows these powered two-wheelers: BMW 1200GS Euro 4, BMW F800R Euro 4, BMW F800GT Euro 3, BMW G650GS Euro 3, KTM Duke 125 Euro 3, Peugeot Speedfight 2 Euro 2, Honda Zooma Euro 2.



Figure 9: Test objects for real word behavior investigations of motorcycles.

These motorcycles were considered to be representative for their corresponding engine category. All of them have water-cooled four stroke engines, except the Peugeot moped has a water-cooled two stroke engine. All of the illustrated motorcycles have been investigated according to their driving dynamic behavior. Furthermore, emission test have been carried out for all of the on chassis dynamometer but on-road emission measurements were made for the BMW 1200GS and both BMW F800 motorcycles only. The following Figure 10 shows vehicle and engine specific parameters for all investigated test objects.

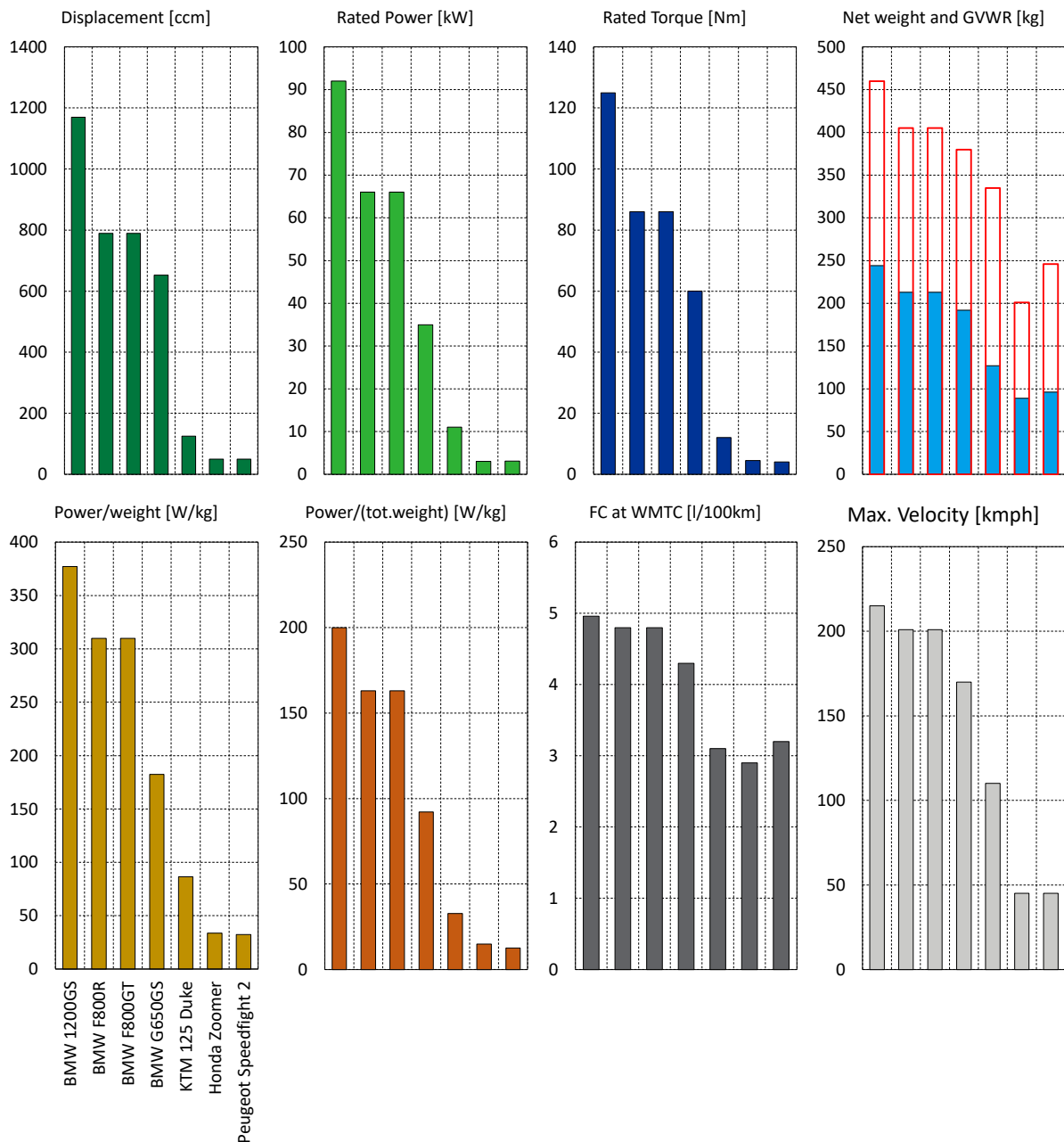


Figure 10: Vehicle and engine specific parameters for all investigated test objects.

Aside displacement, rated power and rated torque, the power to weight ratios and net weight to gross vehicle weight rating (GVWR) ratios are relevant for on-road investigations with on-board measurement equipment. This results from the need of additional measurement gear and especially from the need of additional power supply, as batteries are still relatively heavy nowadays. Batteries are used because the vehicle integrity should not be broken by any measurement cause as this will very likely influence the vehicle functionality and test results respectively. Further influencing factors will be discussed in section 2.3.

Chapter 2.3.1 will introduce the herein utilized portable emission measurement system PEMS which is originally used in automotive applications and therefore heavy and big for motorcycles or mopeds. Hence, concerns about drivability and safety for such an application must be considered. Main deliberations are as follows:

additional weight in Figure 11. Out of driving experience, all motorcycles smaller than 550ccm were considered to be too weak for on-road measurements with the herein used equipment for the following reasons. A state of the art PEMS for CO₂, CO and NO_x gaseous emission sensors and additional equipment for measuring stoichiometric ratio, engine speed, exhaust mass flow and some temperatures has around 80kg including batteries for at least four hours of continuous measurement. Hence, for the two smaller classes, the additional load will shift engine operation load points towards maximum load in a way that emissions and fuel consumption are influenced significantly. This influence is also present for the other classes but in alleviated terms as these classes include motorcycles which are also intended and constructed for road trips with additional luggage bags and/or pillion passengers. Chapter 2.3 introduces the BMW F800GT as main test object for the herein used PEMS. The influences of the measurement equipment will be presented in section 2.4 and in section 2.4.1. With an engine displacement of 800ccm, rated power of 66kW at 8000rpm and maximum torque of 86Nm at 5800rpm, the influence of a full measurement equipment in normal driving operation is not noticeable for the BMW F800GT. Sport-orientated driving behavior with an ambitious driving pattern was also investigated with this test object and, of course, this pushes the vehicle to its limits, but mostly because of the altered weight distribution and its influence on drivability. However, this motorcycle can be driven sport-orientated with a pillion passenger. These influences will be discussed more detailed in chapter 2.5.

Further on-road tests with a full PEMS were made with the BMW 1200GS motorcycle and this one does not show noticeable influence on drivability (for non-professional motorcycle drivers) as well as on emission level due to its high engine capacity.

2.2 Test rig emission measurement

To meet the targets of a comprehensive real drive emission measurement methodology, test rig emission measurements must be considered according to above mentioned limitations of on-road measurements with state of the art PEMS. Thereto, a chassis dynamometer was used with an electromagnetical brake with maximum absorbing power of 42kW at 90kph vehicle velocity and a maximum possible vehicle speed of 160kph. The dyno can be used in stationary and transient operating mode. Typical applications of transient mode are type approval test cycles where a driver rides the motorcycle on the dynamometer according to a predefined velocity profile. Road slope can be additionally adjusted in real time but has not been designated for any type approval test yet.

The test rig is equipped with a constant volume sampling system CVS which provides AVL AMA i60 gas analyzers with diluted exhaust gas emissions and also feeds measurement bags to analyze cumulated gaseous emissions for test cycle sections (e.g. urban, rural, motorway in WMTC test cycle). Additionally, a Fourier Transformed Infrared Spectroscopy measurement system FTIR was used for special measurements of non-regulated gaseous emissions and to evaluate the used PEMS for some test cycles (see chapter 2.4).

Findings of motorcycle driving dynamic investigations in chapter 2.5 will illustrate that the real driving behavior of two-wheelers is more dynamic than it is represented by type approval tests according to the investigated category of motorcycles. Thereto, it is indispensable to illuminate the technical limits of chassis dynamometer measurements for its utilization for the presented RDCs.

2.2.1 Technical limits of on-road tests and chassis dynamometer measurements

RDE and fuel consumption measurements are technically limited by several parameters. As the current commercially available portable emission measurement systems for on-road RDE and fuel consumption measurement are generally designed for heavy duty and passenger car applications, these systems are limited in their use for PTWs. Influencing factors are, e.g., the mounting position and the mounting pipes of the EFM, as packaging is an issue. The exhaust gas pipes of motorcycles are shorter than in automotive applications so that the velocity profile of the gas flow might not be homogenous at all installation positions. Straight parts of the pipes for sufficient homogenization of the velocity profile cannot be applied in many cases due to packaging issues and road safety. Another influencing factor is the additional mass added by the measurement equipment, which can be quantified for above mentioned full RDE equipment by about 80kg. This has an influence on the utilization of the engine map and also affects driving dynamic and emission formation respectively [17]. Very compact and light systems are already commercially available but not with sufficient power supply and with sufficient exhaust gas analyzing methods and accuracy for legislative purpose so far [39]. Exemplarily, the batteries of the herein used PEMS last for two and a half hour of measurement but also demand a third of the packaging of the whole equipment and are heavy in weight (see Figure 15). Another point is the exhaust gas analyzing method which is discussed in section 2.4.1.2.

Concerning chassis dynamometer measurements on the test rig, the limiting factors are total brake power and wheel slip between powered wheel and roller. The available brake power of the dynamometer is 42kW implicating a limitation of maximum measurable engine capacity depending on the test cycle. Especially when it comes to acceleration tests, which can be relevant for total emission output of a PTW, this is a limiting factor. Usually, a motorcycle on the chassis dynamometer is not strapped down because this would influence back wheel slip. To quantify the slip and to compare it with real world on-road driving, tests with constant velocity were made on-road and on the chassis dynamometer. On chassis dynamometer the relative difference between roller brake and powered wheel speed were compared. The speed of the powered wheel was measured by an optical speed indicator. At on-road measurements the front and the rear wheel speed were compared and the mean slip for a constant speed test was calculated like illustrated in the following diagram.

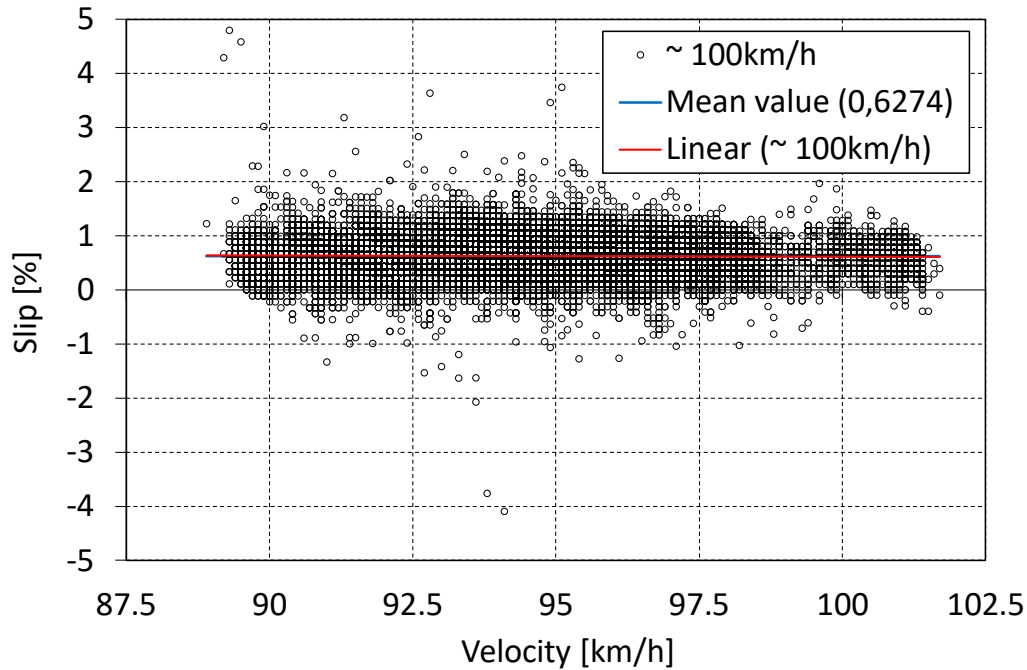


Figure 12: Estimation of mean slip for a constant speed test.

Table 1 sums up the test results. It is conspicuous that the values for driving on the chassis dynamometer slightly differ from the values for on-road driving. This effect is enforced for acceleration and deceleration phases in highly transient test cycles.

Table 1. Calculated back wheel slip at on-road and chassis dynamometer tests with constant velocity with a BMW F800GT motorcycle.

	Velocity target [km/h]	Mean resulting velocity [km/h]	Throttle angle [%]	Calculated mean slip [%]
On-road driving	100	94.7	11.2	0.63
	130	112.7	18.9	0.76
	150	140.7	32.5	1.24
Chassis dynamometer driving	100	92.1	11.2	1.45
	130	122.3	18.9	1.65
	150	138.4	32.5	1.97

To pursue these investigations, there were further slip tests on the test rig. Acceleration phases based on on-road real world driving were examined on the chassis dynamometer. These real world driving profiles represent motorway acceleration phases beginning at a motorway lay-by. Figure 13 illustrates the target velocity profile in black on the left-hand side. The green curve indicates the measured slip at on-road driving whereas the brown one indicates back wheel slip on chassis dynamometer. Once again, the same differences, as shown in Table 1, are obvious, especially at phases with very high velocity gradient. The right-hand sided diagram completes that with the corresponding acceleration in black.

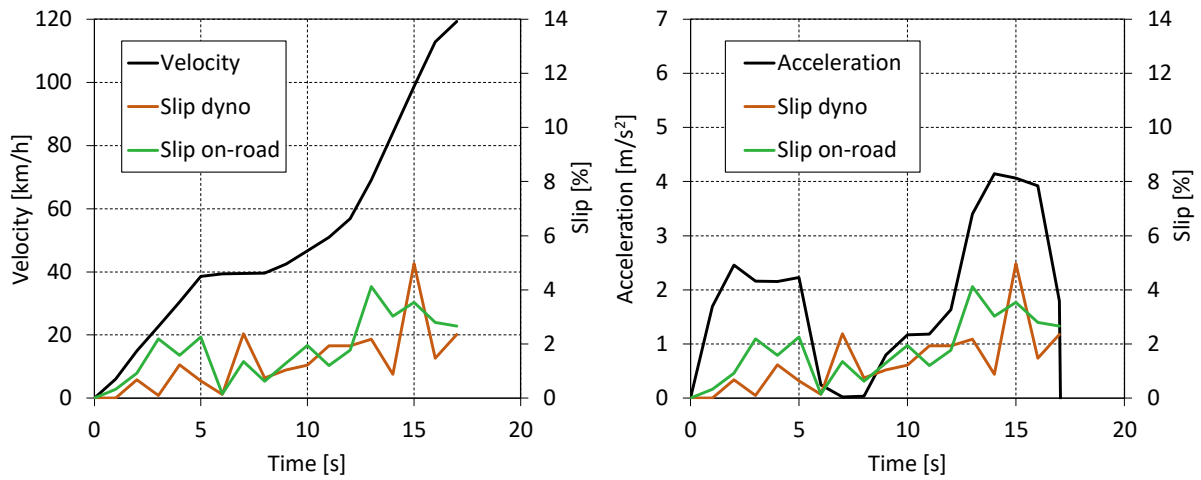


Figure 13. Back wheel slip comparison for a real world acceleration phase between on-road driving and chassis dynamometer driving.

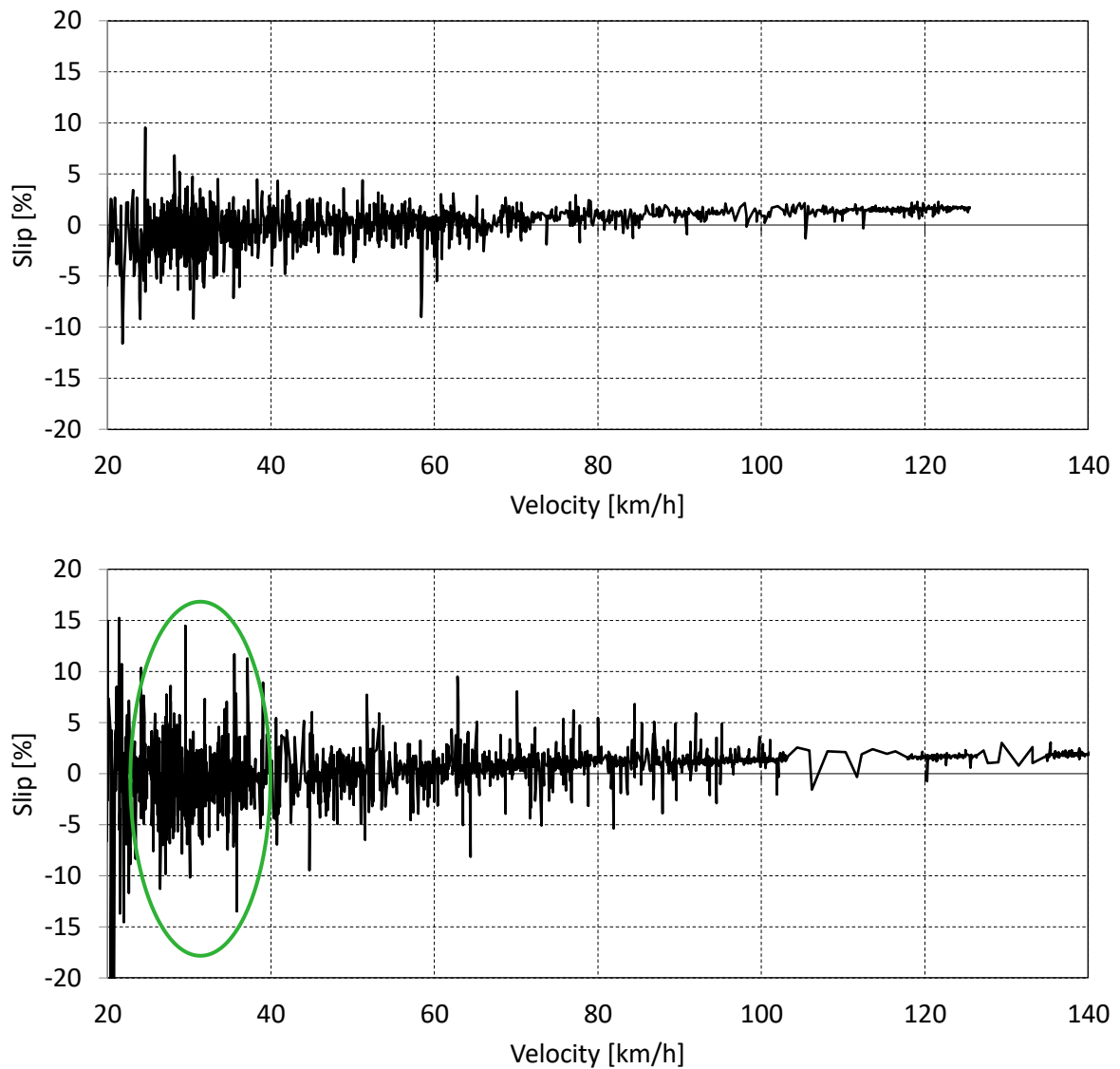


Figure 14. Back wheel slip sorted over driving speed on chassis dynamometer measurements for a driven WMTC (top) and RDC1 (bottom) with a BMW F800GT.

Moreover, the slip was monitored for a RDC in comparison to the type approval test WMTC. By its nature, the RDC test cycle implicates a more dynamic driving pattern and, therefore, steeper velocity gradients; and the slip is higher than it exemplarily occurs at WMTC, respectively. Figure 14 illustrates a comparison between the back wheel slip sorted over driving speed on chassis dynamometer measurements for these test cycles with a BMW F800GT motorcycle. The area from zero to 20 [km/h] contains values up to 15 [%] slip which can be ascribed to many acceleration phases in rural areas and bad correlation of GPS speed and measured speed at the motorcycles' wheel. The values of the marked area in the RDC that are significantly higher than expected, can be assigned to the sport-orientated uphill driving section where a constant slope was adjusted on the chassis dynamometer; this zone is marked with a green circle. The mean values of slip for WMTC and RDC for the velocity range of 20 [km/h] to 145 [km/h] are 0.4 [%] and 0.6 [%]. This comparison depicts that the synthetic real driving cycles can be driven on chassis dynamometer without restrictions, as overall mean slip is negligibly higher than for an established WMTC test cycle.

2.3 Real drive emission measurement

Real drive emission measurement equipment was installed on a BMW F800GT motorcycle to evaluate its functionality for PTWs. With this first test object the measurement set up was validated and influences on emission formation and fuel consumption measurement were investigated to establish RDE tests for further motorcycles (see chapter 2.4). This section sums up the installation process and introduces some occurred challenges.

2.3.1 Installation of the measurement equipment

AVL LIST GmbH provided state of the art equipment for full RDE and GPS measurement as it is commonly used for automotive applications nowadays. Measurements of hydrocarbon and particle emissions was not possible with the equipment used for motorcycles. The frame of the BMW F800GT was extended in a way to arrange all the measurement equipment on it, as shown in Figure 15. Also, the side carrier bags were used for auxiliary devices and additional batteries.



Figure 15. Full RDE measurement set up on a BMW F800GT motorcycle.

Figure 16 shows the installed equipment from another perspective including devices for tapping CAN parameters and multiple temperatures. The used measurement units are as listed below.



Figure 16. Measurement configuration for RDE and GPS data collection on a BMW F800GT.

1. AVL M.O.V.E GAS PEMS iS: It is a portable emission measurement system for analyzing NO, NO₂, CO and CO₂ gaseous emissions. A storage battery is also included that guarantees the electricity supply for most of the other measurement units for about four hours.
2. AVL M.O.V.E EFM: This unit is an exhaust mass flow meter. It is based on difference pressure measurement and therefore sensitive to its mounting position due to condensate in the exhaust. The control unit for the EFM is integrated in the left case (see 5 in Figure 16). Figure 28 illustrates the EFM more in detail.
3. AVL PLU116H Flow Meter: The fuel consumption is measured by a PLU displacement flow meter that is situated inside the right case.
4. AVL M.O.V.E System Control: This system is a personal computer based on Windows 7 that functions as communicator and measurement data logger between the single modules. An extension box is also used for additional signal inputs.
5. The case mounted on the left side of the motorcycle is additionally used for integrating the equipment for exhaust oxygen measurement (lambda meter), cables and accessory electricity supply. A SIM-Lambda meter logs the values of two lambda meters (before and after catalyst) to forward the signal to the CAN where it is read by the system control aside other variables.
6. A GPS logger and sensors for ambient temperature as well as humidity are mounted on the top side of the system control unit.

2.3.2 Measured Values

A lot of parameters can be monitored with the above described measurement equipment. The following Table 2 sums up the minimum required raw data to measure during an on-road test with full RDE and GPS measurement equipment.

Table 2. Measured raw data for full RDE and GPS measurement configuration.

Variable	Designation	Unit	Gauge
t	Measurement time	s	PEMS
v	GPS ground speed	km/h	GPS
h	GPS altitude	m	GPS
\dot{V}	EFM exhaust gas flow	m ³ /s	EFM
\dot{m}	EFM exhaust mass flow	kg/h	EFM
T _{EFM}	EFM gas temperature		EFM
n	Engine speed	1/min	CAN
ANG_THR	Throttle angle	%	CAN
GPiS_CO ₂	CO ₂ concentration (5°C dry)	%	PEMS
GPiS_CO	CO concentration (5°C dry)	ppm	PEMS
GPiS_NO	NO concentration (25°C semidry)	ppm	PEMS
GPiS_NO ₂	NO ₂ concentr. (25°C semidry)	ppm	PEMS
GPiS_O ₂	O ₂ concentration (5°C dry)	%	PEMS
Lambda1	Air ratio before catalyst	-	CAN
Lambda2	Air ratio after catalyst	-	CAN
\dot{m}_{fuel}	PLU fuel consumption	g/s	PLU
T _{GAS}	Gas temperature @ tapping pos.	°C	PEMS

Aside from this base configuration, additional values for several special measurements are recorded if needed, e.g. extra temperatures nearby the catalyst for light-off behavior and other investigations. They are not listed, but mentioned later if relevant.

2.3.3 Adaptions to measurement equipment

Some adaptions have been made in accordance to a correctly use of this PEMS, i.e. that the tapping position for the exhaust gas sampling was installed in front of the muffler. Figure 17 illustrates a side view of the PEMS and its marked tapping position for the exhaust gas on the left-hand side. The PEMS analyzer continuously extracts exhaust gas with a sample flow rate of up to 3.5 [l/min] which is fed to the sensors by a heated line.

Usually, the tapping position should be after the EFM where the exhaust gas flow mass is measured, the fluid velocity oscillation is damped and the flow profile is fully developed. Moreover, it is demanded not to exceed ± 70 [mbar] of pressure amplitude not to damage the sensors. Due to occurring pressure pulsations in the exhaust pipe, caused by the highly transient engine behavior, the recommended tapping position cannot be used. Investigations showed that ambient air is sucked into the exhaust end pipe at several load scenarios. Subsequently, this would have distorted emission measurements so that the tapping position was chosen before the muffler, like illustrated. As this falsifies the measured mass flow, the deviation was quantified by experiment. For a maximum flow rate of 3.5 [l/min] the discrepancy results in a maximum of 0.8 [%] for gaseous emissions and is, therefore, in-between the measurement

inaccuracy. Nevertheless, this difference was corrected in the evaluation.



Figure 17. Detailed view of PEMS and exhaust gas tapping position, left-hand side. Former vertical mounting position of the EFM, right-hand side.

Another adaptation worth mentioning is the change of the mounting position of the EFM from a vertical to a horizontal position (compare Figure 17 left- and right-hand side). The vertical mounting position should have theoretically shown better results for mass flow measurement as the flow calming sections with straight tubes are longer than it is possible with a horizontal mounting position. Nevertheless, condensate became an issue due to the longer pipes and the faster cooling of the exhaust gas with a vertical positioning of the EFM respectively. This falsifies the emission analysis as well as the mass flow measurement as the small differential pressure measurement tubes inside the EFM are affected by the condensate.

2.3.4 Calibration and measurement season

Before each measurement, a calibration procedure for PEMS and EFM has to be performed. PEMS is gauged by a special mixture of gas and an additional calibration unit that also checks background concentrations of ambient air. The prescribed procedure by the manufacturer AVL List GmbH was applied. The exhaust flow meter, additionally, has to be cleared and flushed with clean air so that the thin pipes for difference pressure measurement are free of condensate water and other debris from exhaust gas. The condensate is of special interest in the warming up phase of a test cycle when it comes to the optimal mounting position, as it is described below.

The question of where and how to measure RDE and fuel consumption on-road can be answered by the evaluation of driving factors that characterize driving dynamic for separated road segments [18]. It does not directly affect the measurement equipment but, in fact, it is directly linked to a measurement season according to a country's local weather conditions. Due to the situation in Central and Northern Europe, there are limited times of the year when it is not possible to measure two-wheelers due to wintry road conditions. As ambient temperature is

influencing both the exhaust flow measurement (e.g. condensate when pipes are cold) and the emissions (e.g. catalyst light-off time) at the beginning of each on-road test drive, these primary sections of an RDE test drive have to be kept under observation too. That effect is enforced by the relatively exposed exhaust pipes in comparison to automotive applications the measurement gauges are made for.

2.4 Evaluation of measurement equipment

As the measurement equipment was not originally developed for motorcycles, the measurement data were validated with tests on the chassis dynamometer. Therefore, a comprehensive measurement setup was installed; using not only the full RDE equipment but also as afore mentioned constant volume sampling dilution system CVS and a Fourier Transform Infrared Spectroscopy gas analyzer FTIR. Hence, some results are also presented in this section to clarify coherences, whereas the main measurement results for the investigated PTWs are consolidated in chapter 3. Figure 18 schematically illustrates the one possible test rig setup for cross checks of the measurement equipment. As PEMS and FTIR are portable, the equipment was used on different positions during several cross checks (raw emission and diluted emission measurements). Additionally, Figure 19 illustrates one installation on the chassis dynamometer and Figure 20 shows the installation of the EFM for a test rig measurement of raw emissions like it is intended to be, with sufficiently long tubes before and after the flow meter to ensure flow calming for a correct measurement. In this case, the tapping position of the exhaust gas can be located after the EFM and additional measuring points for stoichiometric ratio and temperatures are installed.

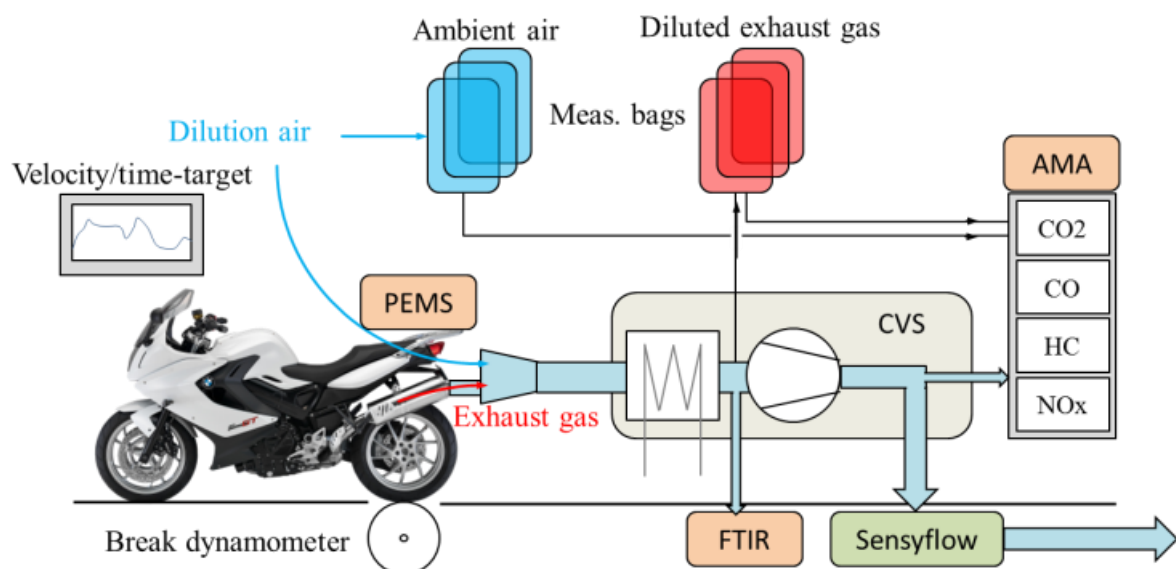


Figure 18. Chassis dynamometer measurement for validating multiple measurement gauges.



Figure 19: Chassis dynamometer with additional measurement equipment for cross checks.

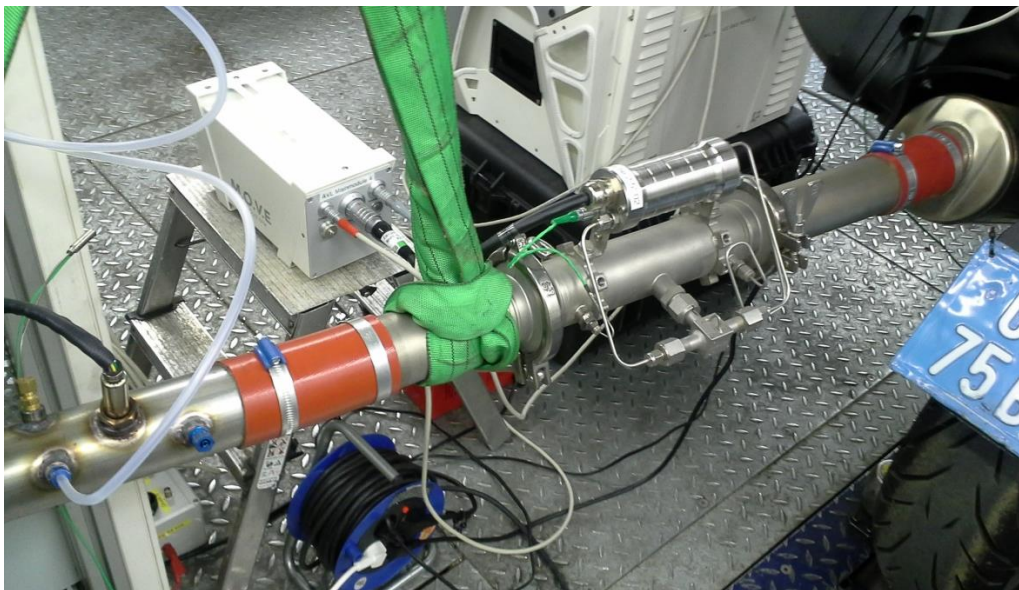


Figure 20: Installation of the EFM for test rig measurements with required standard length of the flow calming tubes before and after the measurement section.

The orange boxes in Figure 18 indicate possible installation positions of the three different gas analyzers that have been used for cross checks. The CVS system analyzes diluted gaseous emissions by multiple analyzer principles: Chemo Luminescence system for NO, NO₂ and NO_x; Flame Ionization Detector FID for HC detection; Nondispersive infrared sensor NDIR for CO and CO₂ detection. The FTIR analyzer detects gaseous compounds by their absorbance of infrared radiation. It simultaneously measures multiple components in a complex gas matrix, detecting virtually all gas-phase species. The FTIR analyzer was applied as link between the gauges as it was used to analyze the diluted gaseous emissions from the CVS tunnel (as illustrated in Figure 18) and also to analyze the undiluted gaseous emissions at the same tapping positions as the PEMS for additional measurements. Figure 21 exemplary illustrates the cumulated exhaust out CO emissions for a test cycle measured on the chassis dynamometer

with two different analyzers. Note that the mass base for the different measurement equipment is different as described and discussed further on (compare with Figure 23).

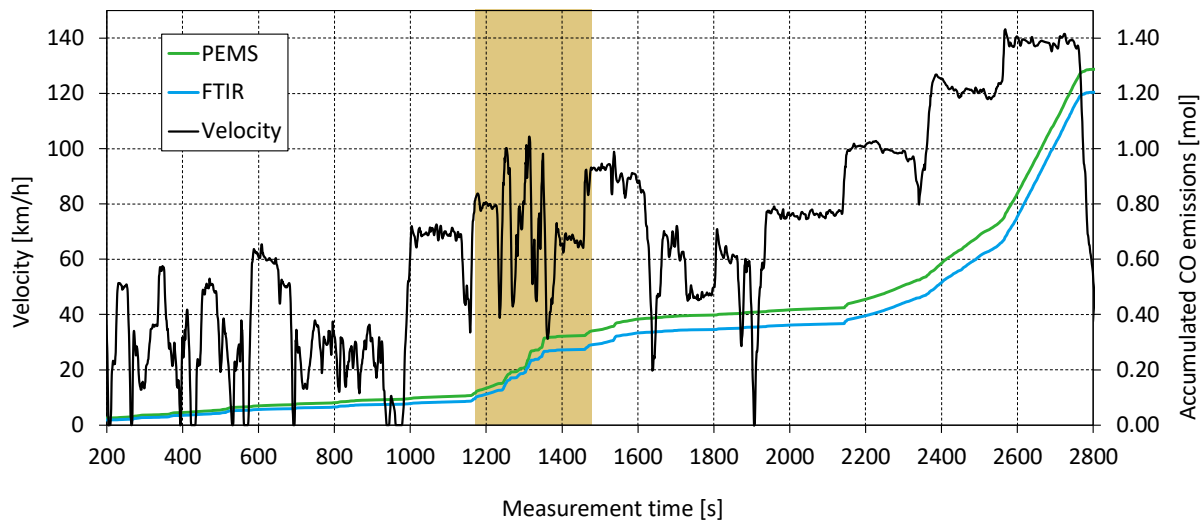


Figure 21. Accumulated exhaust out CO emissions and velocity profile of RDE test cycle.

Good correlations between FTIR and PEMS were found and also very good correlations between FTIR and CVS after catalyst light-off [18]. Discrepancies mainly emerge in the marked section where the motorcycle is driven in a highly transient way as a hilly and sport-orientated part of the test cycle (including slope on the test rig) is simulated on chassis dynamometer with high accelerations and decelerations. As all analyzers are very fast in response time, the discrepancies might emerge from the EFMs setup as it is not optimized in terms of fluid mechanics standards yet, due to packaging reasons [18]. Section 2.4.1.3 expands on that topic in terms of a possible substitution of the EFM.

Note that by measurement principle the concentrations are not measured at the same base conditions; this also causes slight differences in the calculated values: FTIR measures all components at wet condition; whereas PEMS measures CO/CO₂ by NDIR principle at 5°C and NO/NO₂ by NDUV principle at 25°C (“semi wet”). There are also factors for conversion and further calculations of PEMS values on a wet basis combined with the rules of the amending regulation “Commission Regulation (EU) 2016/427 of 10 March 2016”.

In addition to the above-mentioned measurement equipment, an AVL PLUtron™ was installed for fuel consumption measurement on the chassis dynamometer. The PLUtron™ was applied to validate the on-road used AVL PLU116H fuel volume flow measurement. In combination with two installed Lambda-meters. This data additionally enable more accurate carbon balance calculations and the validation of measured exhaust gas mass flow.



Figure 22. AVL PLUtron™ for highly accurate dynamic fuel measurement, additionally used on chassis dynamometer.

Section 2.4.1.2 introduces measurement results concerning a comparison of the measured exhaust gas flow and the calculated mass flow from fuel consumption and stoichiometric ratio measurement. Section 2.4.1.3 expands on that topic in terms of a possible substitution of the EFM.

The tests on chassis dynamometer also deliver data for comparing and characterizing the dynamic behavior of the measurement gauges. This generates additional added value as for engine operation evaluation, combustion evaluation and exhaust gas after treatment assessment an accurate mapping is indispensable and it is necessary to get the most accurate time allocation of emission data for further use, e.g. as learning input for an emission simulation model (see chapter 0). At chassis dynamometer a CVS system is usually used which analyzes with sampling technique. The transport delays of the sampling and dilution system, as well as axial dispersion phenomena, etc. cause high distortion of the initial tailpipe emission concentrations, removing much of the dynamic content of the signal and flattening the recorded emissions [40]. With mathematical approaches it is possible to get partly rid of this fluttering, but as most approaches are volume based, this very much depends on the geometry, not only of the analyzing system (CVS), but also of the vehicles' gas pipes. Thus, the direct way of using high responsive measurement gear like PEMS or FTIR, with the shortest measurement pipes possible, seems to be a more robust approach for further use of the measurement results. Additionally, the possible impact of the CVS on tailpipe backflow has to be mentioned at this point. As described above, pulsations of the exhaust gas volumes can occur during transient load operations which could cause the backflow of fresh air into parts of the exhaust pipes. This pulsations can be masked down by the depression induced by the CVS.

Summing up, Figure 23 shows the cross comparison of mass emissions (left) and concentration measurement (right) for the introduced measurement gauges (PEMS as base measurement, FTIR and AMA relative to PEMS results).

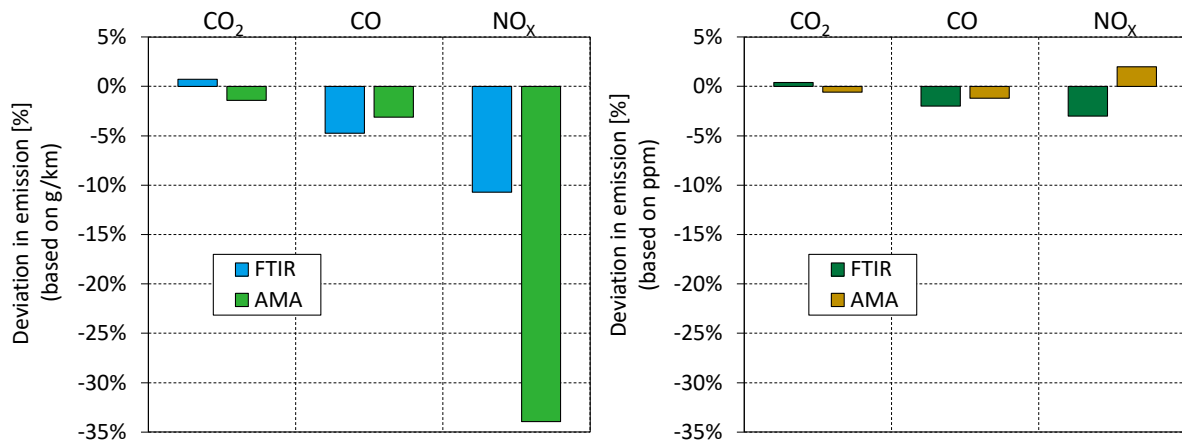


Figure 23: Cross check of mass emissions (left-hand side) and concentration measurement (right-hand side) with three different measurement gauges; PEMS measurement represents the base value 0%.

Results of the PEMS had the EFM as its exhaust gas mass flow base and indicate the baseline in the above diagrams; results of the AMA had the CVS system as its mass flow base; results of the FTIR had a Sensyflow as its mass base, which operates according to the principle of the hot-film anemometry. The installed position of the measurement equipment was chosen as indicated in Figure 18 for the results depicted in Figure 23 on the left side. For comparison, the measurement results of diluted emissions were converted to exhaust out emissions and corrected by the aspirated amount of the previous equipment. Calculated mass emissions were summed up to g/km for each test cycle. Multiple approval test were performed for this comparison and the diagrams show mean values in deviation. The deviation in mass emissions may mainly result due to differences in mass flow measurement in combination with the dilution of the exhaust gas and the time delay of the sensors. The slowest sensor in terms of time delay from a specific emission scenario to the detection of the same in the sensor is the AMA analyzer. As NO_x emissions mainly occur intermittently and with high peaks, the diminishing effects are worst for the AMA results. Moreover, this is enforced in combination with rather slow reaction time of the Rootsblower of the CVS to a changing exhaust gas temperature. Hence, the allocation of a correct mass flow value to the correct corresponding concentration value in its correct level is weak spot.

The right diagram in Figure 23 shows an additional comparison of concentration measurements for the three different measurement installations. For these tests, the PEMS and the FTIR analyzers were installed in the tube for diluted exhaust gas. Multiple type approval tests were driven and the deviations based on the PEMS measurements were recorded. The illustrated values indicate mean deviations in percentage from PEMS measurements. In fact, these deviations are in-between standard deviation of multiple test cycle measurements (compare to Table 5).

Thus, the main deviations arise from the mass flow measurement and its altered and incorrect allocation to emission concentrations as previously discussed. Therefore, the herein presented measurement principles must be used with caution for RDE measurements for motorcycles and alternatives will be discussed and presented in the following sections 2.4.1.2 and 2.4.1.3.

2.4.1 Cross influences and side effects of the measurement equipment

As by the nature of multiple measurement gauges, it is obvious that they influence each other and have side effects on the measured values. The following section introduces investigations to determine them by reference measurements. Moreover, the herein used EFM is discussed as it is the main cause for insufficient accuracy of measurement results and possible solutions for its substitution are discussed.

2.4.1.1 Influence of the additional mass

The overall measurement equipment has about 80 [kg] weight. Figure 24 illustrates the tested BMW F800GT with full measurement equipment and driver by a snapshot at an on-road RDE testing trip. As all measuring units are adapted from automotive usage, they are also big in terms of their frontal surface. As part of this work, the influence on air resistance and additional mass was not differentiated.

One has to keep in mind that the measurement equipment has clearly a different influence on different motorcycles. As for the investigated BMW F800 GT (66 kW at 8.000 rpm, 86 Nm at 5.800 rpm, 213 kg net weight but fully fueled) [41] this is comparable with a pillion passenger and some extra weight, e.g., for baggage. These gauges shall not be used on motorcycles smaller than the test object, as adequate driving behavior and road safety should be maintained (compare to the discussion in section 2.1).



Figure 24. Fully equipped BMW F800 for RDE and GPS measurement.

For the tested BMW F800GT motorcycle a clear impact on the engine map can be derived as the relative additional mass is about 40 [%] of the tare weight. The influence of an additional mass on emission formation and fuel consumption was investigated on the chassis dynamometer. Two different values for the overall mass were adjusted, namely 350 [kg] and

270 [kg]. A WMTC was driven for comparison.

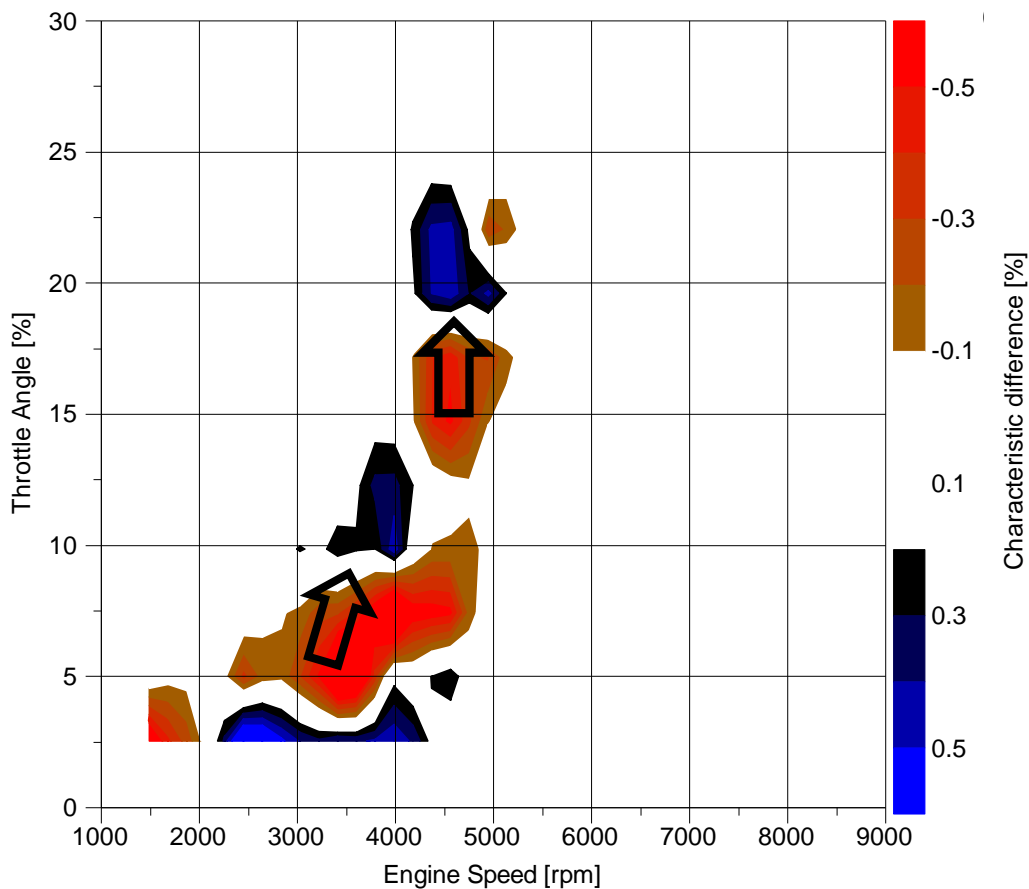


Figure 25: Characteristic difference of engine map utilization (% in time) for tests with and without RDE measurement equipment on a BMW F800GT motorcycle.

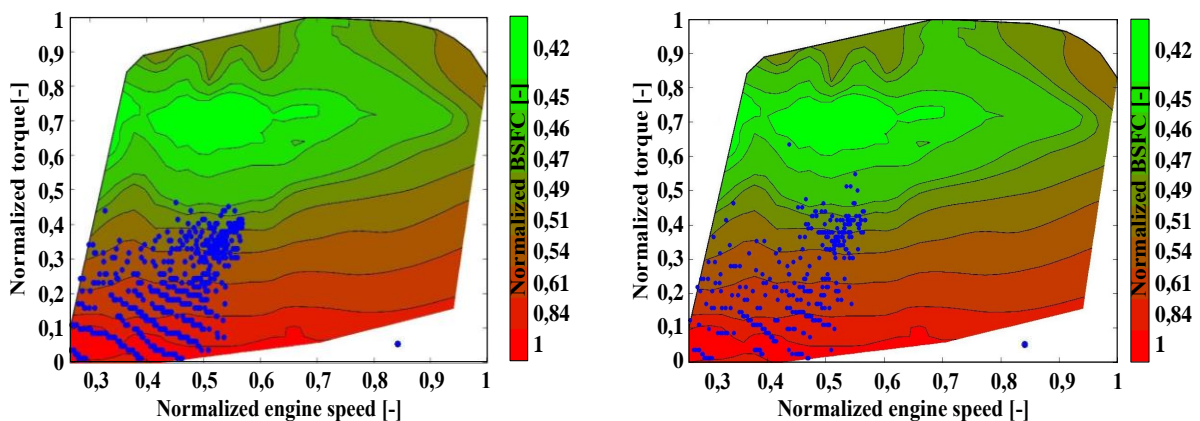


Figure 26. Engine map for driven WMTC with 270kg (left-hand side) and with 350kg (right-hand side) total weight of the BMW F800GT motorcycle; each dot represents one second in the test cycle.

Figure 25 illustrates the influence on the frequency distribution of throttle angle over engine speed without and with the whole measuring equipment mounted. A clear shift towards higher engine speeds and loads can be seen in the characteristic difference of engine map utilization, as indicated by the arrows. Additionally, Figure 26 illustrates the single engine maps for the driven test cycles with different weight and with the brake specific fuel consumption BSFC

map in background. The blue dotted measurement data shows that the utilization of the engine map is shifted towards higher engine efficiency. This results in a lower fuel consumption and CO₂ emissions for the test with higher weight, what might not be expected at first glance. The following Table 3, Table 4 and Figure 27 sum up the measurement results.

Table 3. WMTC (Stage 2 3-2; EU4) Evaluation with 270kg overall weight.

	Overall [mg/km]	DF [-]	Limit [mg/km]	Percentage of limit [%]
HC	132	1.2	170	93
CO	763	1.3	1140	87
NO _x	116	1.2	90	155
F.C.	4.8 [l/100km]			

Table 4. WMTC (Stage 2 3-2; EU4) Evaluation with 350kg overall weight.

	Overall [mg/km]	DF [-]	Limit [mg/km]	Percentage of limit [%]
HC	102	1.2	170	72
CO	796	1.3	1140	91
NO _x	184	1.2	90	245
F.C.	4.57 [l/100km]			

NO_x emissions are significantly deteriorated by the additional mass (compare also standard deviations in Table 5). This could be affiliated to the higher loads in the engine map. One has to keep in mind that the engine load is higher for the more transient real world test cycles RDC and, therefore, the raising of emission component, especially for NO_x, might be even enforced. Nevertheless, this emission measurement result is a valid result as the additional weight is in-between above-mentioned boundaries (see section 2.1) and the same results would be met with a pillion passenger. These measurement results are expanded and discussed more detailed in section 3.1 (see Figure 66 and Figure 67).

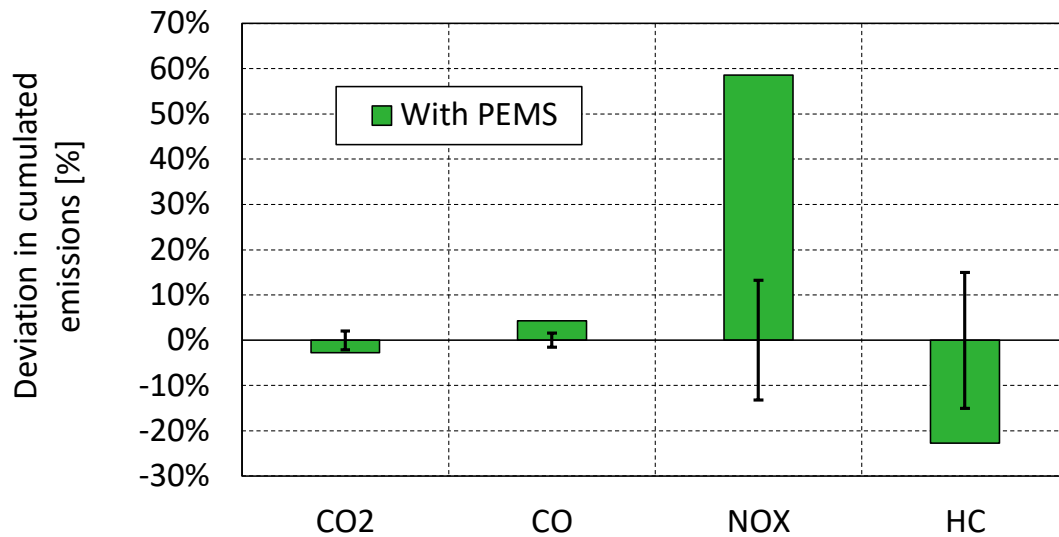


Figure 27: Deviation in cumulated emissions for WMTC type approval test with 80 kg additional weight compared to normal tare weight of 270 kg.

The presented results may lead to the conclusion that, for assessing RDE for motorcycles with state of the art PEMS technology, a factor for additional loaded mass might be introduced or at least a conformity factor is used until lighter on-road measurement equipment is available. Thus, to respect the influence on emission formation and fuel consumption according to the tare weight of a motorcycle due to the relative differences e.g. when driving with a pillion passenger. Moreover, these effects are depending on the type of motorcycle (displacement, tare weight, etc.) and its engine calibration as well, which complicates these considerations. In order to reduce the above mentioned influences, better adoption of PEMS for motorcycles is needed in terms of weight and packaging.

2.4.1.2 Influence of the EFM and its mounting pipes

As mentioned before, the exhaust mass flow meter is based on difference pressure measurement and, therefore, sensitive to its mounting position due to condensate in the thin pressure tubules. A test procedure was implemented to be fulfilled before each test trip to verify its functionality. Moreover, it must be ensured by the mounting position that the tapping positions for pressure measurement are protected from direct impingement by any condensate or particle as illustrated in Figure 28.



Figure 28. Exhaust flow meter mounted to respect road safety and measurement functionality.

Furthermore, the exhaust flow meter has to be connected with some additional pipe elbows to ensure road driving safety. Hence, this might have an influence on engine operation, and on fuel consumption and emission formation respectively due to changing gas dynamics in the exhaust pipes. Comparative measurements with the WMTC as test cycle were made on chassis dynamometer to determine the impact. The results were matched with previous evaluations of data deviation from its mean value from several WMTC measurements without tail pipe modifications, according to following formula.

Equation 1

$$s^2 = \frac{1}{n-1} \sum_{i=1}^n (x_i - \bar{x})^2$$

- \bar{x} Mean value
- x_i Measurement value
- n Number of measurements
- s Standard deviation

For one and the same driver and with special awareness of particular driving behavior, the scattering of the measurement values was known even before the comparative tests as shown in Table 5. It lists the results for emission and fuel consumption measurement and the resulting mean value with its standard deviation for each component on the very right side.

Table 5. Emission and fuel consumption measurement results of WMTC measurement.

No.	Emissions [mg/km]						
	1	2	3	4	5	\bar{x}	s
HC	102	108	107	132	128	115.4	13.59
CO	651	645	684	763	727	694	50.50
NO _x	106	124	118	116	119	116.6	6.62
CO ₂	106464	105478	109074	109156	111734	108381	2471
F.C. [km/l]	21.60	21.84	21.02	20.84	20.24	21.11	0.63

Compared against the illustrated results in Table 6, the measured values for a mounted EFM with additional pipes are not significantly exceeding the standard deviation of overall measurement data for accumulated emissions or fuel consumption. Figure 29 graphically illustrates these results.

Table 6. Difference in emission formation and fuel consumption for mounted and dismounted EFM.

No.	Emissions [mg/km]	
	<i>with EFM</i>	<i>without EFM</i>
6		7
HC	113	100
CO	745	731
NO _x	108	109
CO ₂	109703	110510
F.C. [km/l]	20.84	20.78

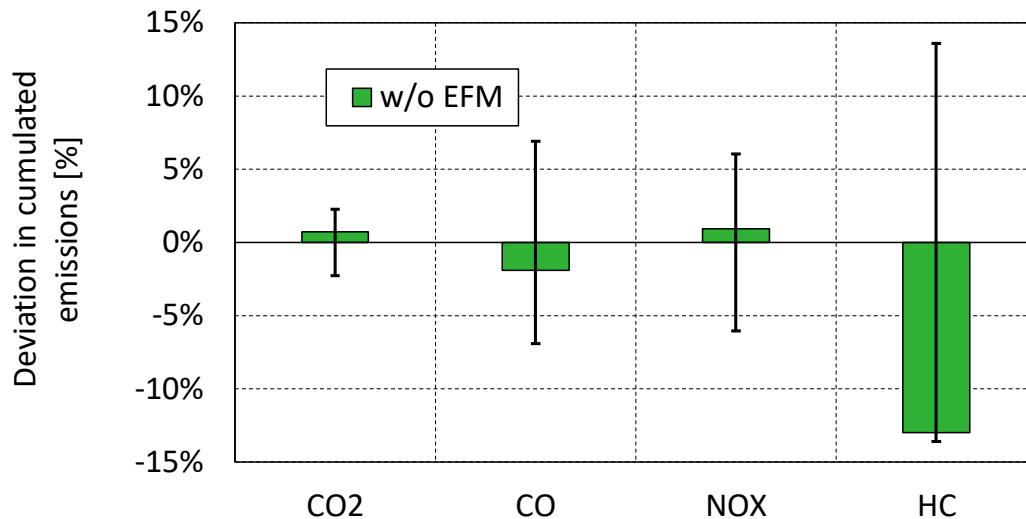


Figure 29: Deviation in cumulated emissions from mean values over multiple WMTC type approval tests without mounted EFM.

Irrespective of the outcome of above presented results, the dynamic behavior of the exhaust flow meter EFM is very bad compared to calculated exhaust mass flow from fuel consumption and stoichiometric ratio. Thereto, Figure 30 shows mass flow results for different measurement and calculation methods and corresponding throttle angle position for a low load section (urban area) of the BMW F800GT motorcyle. The blue measurement trace shows the calculated exhaust mass flow based on fuel consumption measurement (PLUtron™) and stoichiometric ratio measurement. The orange trace shows the measurement result from the exhaust flow meter EFM. Deviations up to ± 18 [%] between calculated and measured values can be seen as indicated with the green and blue cycle. These deviations occur randomly and are not triggered by any obvious cause or dependent on specific engine load conditions.

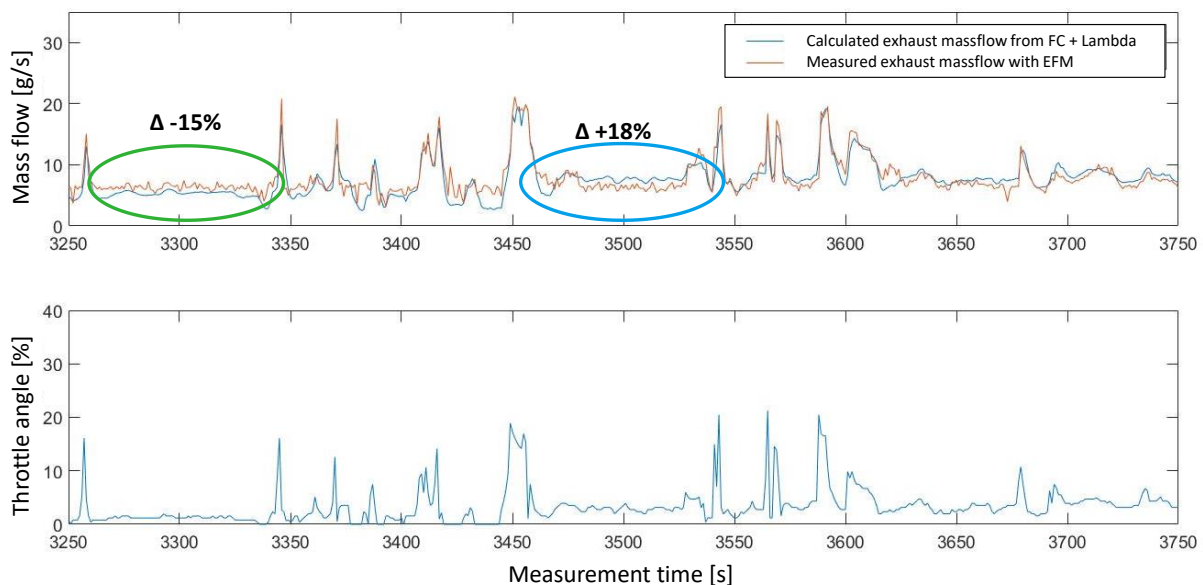


Figure 30: Mass flow results for different measurement and calculation methods and corresponding throttle angle position for a low load section (urban area) of a BMW F800GT motorcyle.

In this context, another comparison of fuel flow measurement signal monitored with CAN and calculated by PLUtron™ is shown in Figure 31. This measurement includes constant speed ramps in a first part and highly transient driving behavior in a second part. This comparison leads to the conclusion that the comparative fuel consumption measurement is accurate.

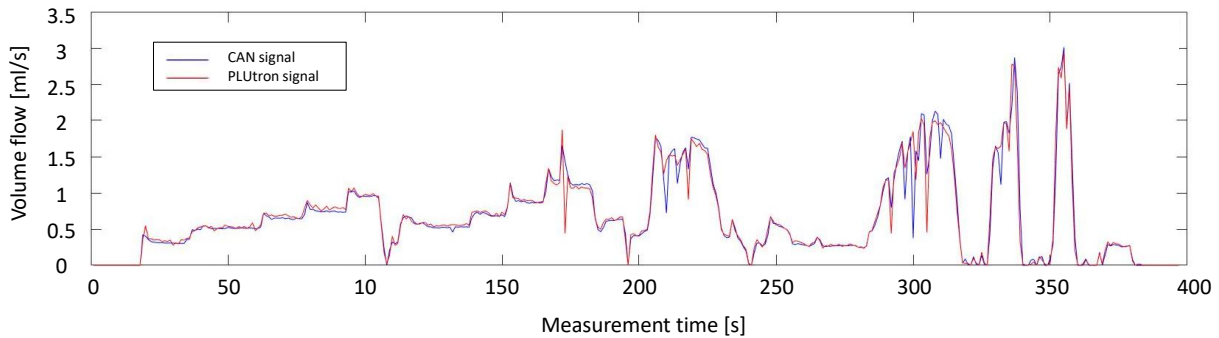


Figure 31: Comparison of volume flow measurement signal monitored with CAN and calculated by PLUtron™.

In combination with above presented cross measurement results for emission concentrations (see section 2.4), the presented inaccuracy of the here used exhaust gas mass flow measurement should be eliminated for further measurements. A substitution of the exhaust gas mass flow measurement was considered. This is discussed in the following section alongside other possible adaptations.

2.4.1.3 Better adaption of PEMS to motorcycles

As on-board emission validation and on-road emission measurement are already mandatory for heavy duty vehicles and passenger cars, the use of emission assessment systems is already mainstream. Hence, there are compact systems commercially available nowadays that measure around 11x11x3-in, but only for analyzing regulated emissions and GPS [39]. The question remains: which sensor technology has to be used and under which condition should the single gaseous components be measured (“dry”, “semi dry”, “wet”) to fulfill accuracy requirements for emission measurement in combination with an adequate mass flow measurement methodology for motorcycle on-road tests.

Currently, there are available sensors for emission measurement based on different measurement principles like FID, NDIR, etc. (compare to chapter 2.4). But these sensors have high energy demand and have packaging issues for mobile applications on motorcycles. Small NO_x sensor devices on zirconia technology basis are already in serial use for novel gasoline direct injection engines as well as for heavy duty ammonia based selective catalytic reduction (SCR) systems for on board diagnosis OBD. But it is in discussion whether the sensors are accurate enough to meet requirements for RDE analysis. Moreover mobile HC and PN/PM sensors are available but these gauges have energy and packaging issues as well. Hence, for motorcycle applications, the available sensors cannot be used in combination with the HC and PN/PM sensors yet available, what makes them useless for possible RDE legislation for motorcycles [42] [43] [44]. Furthermore, an adequate measuring system for emission mass flow also remains unsolved for motorcycles in terms of packaging and accuracy. Recapitulating can be said, that technology for RDE measurement for motorcycles is available but not

commercially useable for on-road measurement for all sorts of PTWs yet.

In terms of packaging and weight the main issues to solve will be low energy consumption for continuous measurement (storage battery's weight and space) and an adequate exhaust mass flow measurement methodology that concurrently meets standardized mass flow measurement norms and road safety whilst solving the packaging issue on motorcycles. A possible solution is the above introduced combination of fuel consumption and stoichiometric ratio measurement to calculate exhaust gas mass flow. It was shown that this measurement method is even more accurate than the tested EFM. A further reduction in weight can be achieved by replacing the fuel consumption measurement – which breaks vehicle integrity anyway – by the CAN parameter for fuel consumption. This measure relies usually on injection duration and the injector's characteristic curve. The investigated test object shows a highly accurate measurement trace of this CAN parameter as shown in Figure 31. However, its accuracy must be checked within comparative measurements at the test rig before testing on-road. Around 13 [kg] of weight and a lot of space can be saved by replacing the EFM with necessary tubes and its evaluation unit as well as the fuel consumption measurement equipment with its auxiliary batteries.

2.5 Evaluation of motorcycle driving dynamic

RDE and fuel consumption measurements on PTWs are not commonly performed in any homologation process yet. As there is also no legislative regulation so far, there are no established methods to assess the representability of on-road trips yet. Purpose of the presented evaluation of motorcycle driving dynamic is to give an overview of the on-road behavior of this vehicle category and to show these results in the context of already established type approval test cycles.

In order to get a broad database for motorcycles operated under real world conditions, four different types of measurements in a broad field campaign were investigated. Firstly, automotive RDE test routes, fulfilling the regulations for passenger car RDE tests, were used to run different PTWs. These data enable the categorization of two-wheelers driving dynamics relative to passenger cars in order to derive appraisal criteria whether a test drive is valid or not [18]. Three well approved routes are available in the vicinity of Graz. Secondly, on-road measurements for different traffic situations were performed in accordance to [45]. The resulting single micro-trips were elected by the categories region (urban, rural, motorway), road type (e.g. access road or inner city road), speed limit, and traffic situation (fluent, depending, jam). These categories result in a matrix of a specific driving pattern that represents customer usage in the investigated field of 125ccm to 800ccm [46]. The collected data of these measurements are consequently available for analyzing any of the combinations of above-mentioned categories to assess special driving scenarios and its contribution to RDE. Further purpose of these tests was to collect parameters of driving dynamics for developing a synthetic RDE test cycle from joining micro-cycles (shortened micro-trips) to a complete test cycle for chassis dynamometer tests for further investigations. So, thirdly, these RDE driving cycles (named RDC – real drive cycle) were elaborated for the test rig to build the bridge between on-road and chassis dynamometer tests. Fourthly, very common test cycles like the WMTC and additional special measurements, like acceleration tests, were performed on the chassis dynamometer. With these results, on-road measurements were compared.

All tests have been performed by multiple driver and motorcycle combinations to cover the differences in vehicle operating behavior between drivers, so called driver variability. These differences may include variations in the duration, frequency or intensity of different driving

modes such as cruise, acceleration and deceleration [47] [18]. Full RDE and GPS measurement gear was only used for tests with the BMW F800GT motorcycle. All other PTWs were driven with a GPS logger which also recorded engine speed and throttle angle. Hence, a broad dataset was collected as basis for further investigations concerning the development of any possible measurement method for PTWs RDE and fuel consumption in future.

The driven on-road test trips were evaluated in terms of their driving dynamics. Referring to the amending regulation “Commission Regulation (EU) 2016/646”, two main trip indicators to characterize the trips are chosen, e.g. the relative positive acceleration RPA and the 95th percentile of the product of vehicle speed and positive acceleration $(v \cdot a_{\text{pos}})_{95}$. These values can be plotted for specified parts of a trip (called micro-trips) whereas a commitment of limits determines whether a trip is valid or not, as described further on and illustrated in Figure 35. For sure, this is a first assessment of the applicability of these parameters for PTWs as there are no officially published values for motorcycles yet. Comparisons with passenger cars show that investigated PTWs are driven more dynamic in general [18].

The following sections introduce the investigated real world traffic situations, representative single on-road traffic situations and the evaluation of driving dynamic parameters as well as the influences on these trip indicators. So, the following chapter 2.6 expands on the derived real drive test cycles RDC for chassis dynamometer based on the herein gained insights.

2.5.1 Real world traffic situations

To assess driving dynamic of motorcycles, two different test routes have been driven that are already in use for passenger car tests from TU Graz. The on-road test cycles meet the demand of Commission Regulation (EU) 2016/646 [14].



Figure 32. On-road RDE test cycles “Arzbert” and “Ries”.

Figure 32 illustrates the driven routes in the vicinity of Graz, Austria. They consist of three parts each: an urban, a rural, and a motorway part. The respective velocity and height profiles are added in the appendix. The RDE test cycles were driven with all mentioned test objects by four drivers, different in age and physics, to cover the influence of particular driver behavior. Moreover, a subjective estimation of traffic flow was monitored for the single stages of each test cycle. Each driver also tried a variation in his driving style by subjective perception, as each route was driven in eco-style, normal and ambitious mode. This was performed in order to get the most variety in driving pattern and, therefore, a broad coverage of motorcycle driving behavior for this area. In addition to the shown test routes, a third route was driven in the vicinity of Munich to gather more representative data for flat surrounding area of a big European city. The following Figure 33 shows one measured velocity profile for the three test routes each including the geodetic altitude.

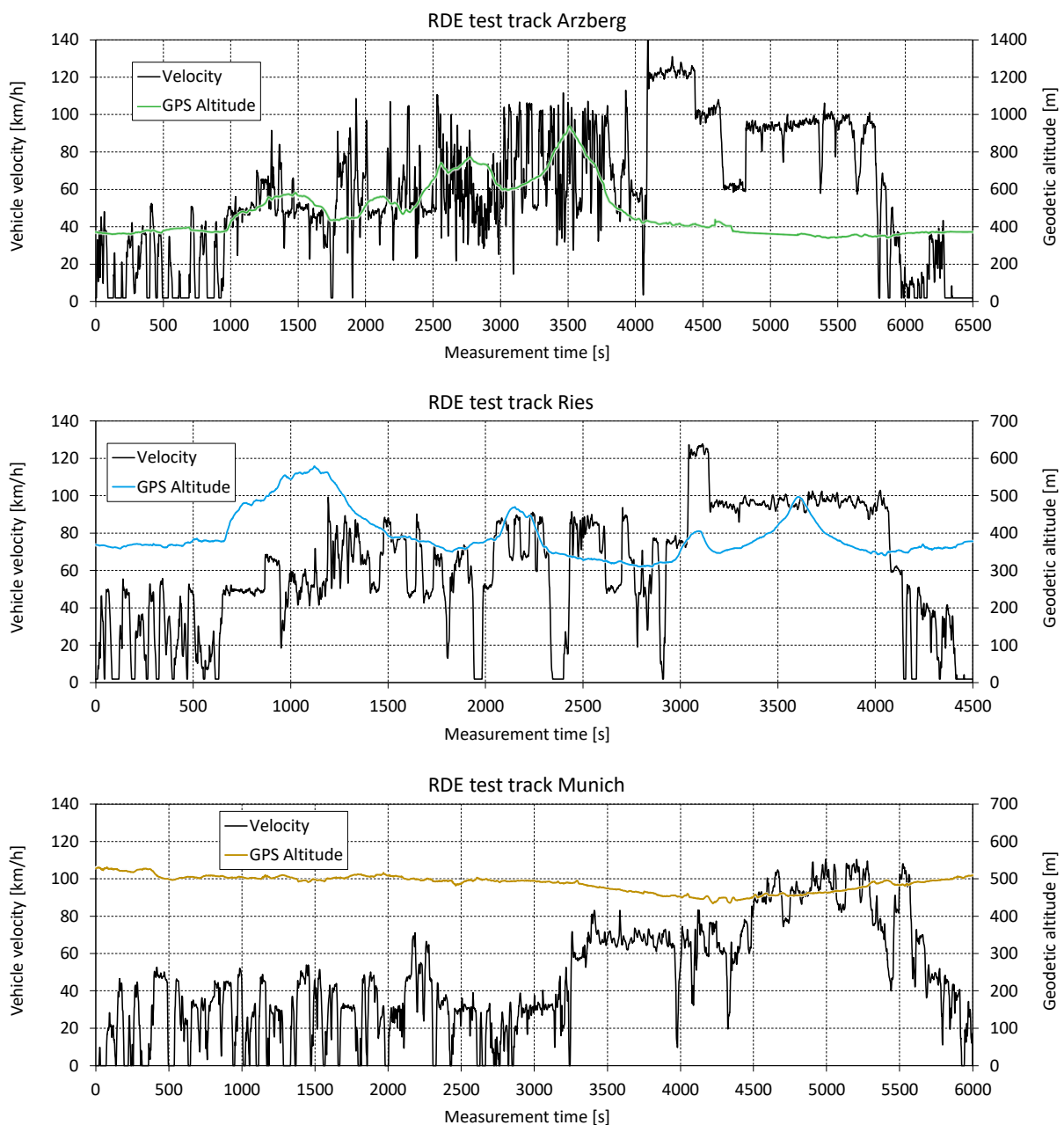


Figure 33: Measured velocity profile and geodetic altitude for three different RDE test routes.

The tests on these routes served data for a first estimation of dynamic trip indicators in comparison with passenger cars to get an idea of driving behavior and illustration for urban, rural, and motorway stages. Also real drive emission and fuel consumption data were collected for the BMW F800GT motorcycle that serve as a base for further comparison on the test bench and also for better understanding of emission relevant real world driving scenarios. These test cycles were also used to get another reference for comparing later described RDCs for chassis dynamometer. Table 7 sums up main parameters of the “Arzberg” and “Ries” test routes.

Table 7. Main parameters of automotive real world test routes driven with motorcycles.

Measurement route	Arzberg	Ries
Length [km]	104.37	75.16
Duration [s]	5956	4424
Mean velocity [km/h]	63.16	61.46
Maximum velocity [km/h]	132.06	132.86
Stop time duration [s]	287	311

The tests on the automotive real driving routes were used as reference to classify trip indicators of the single micro-trips to be introduced later on. In this case, two different speed limits were investigated in terms of the resulting trip indicators which will also be described later on.

2.5.2 Representative single on-road micro-trips

In order to better understand the influence of driving pattern and type of road on dynamic trip indicators, and to create a synthetic real driving cycle, single on-road micro-trips were selected and investigated. The following Table 8 sums up all representative micro-trips with arrangement based on [45].

Table 8. Summary of selected single on-road micro-trips with corresponding classifications.

	Measurement index	Type of road	Characterization	Speed limit [km/h]	Traffic flow	
Urban roads	S1	Main street	City entrance/exit	50-70	free	
	S2	Main street	City entrance/exit	50-60	free	
	S3	Main street	City entrance/exit	50	free	bounded
	S4	Main street	Center of town	50	free	bounded
	S5	Side street	general	50	free	
	S6	Side street	general	30	free	
Rural roads	AO 50-75	Federal highway	-	50-70	free	bounded
	AO 75-100			80-100	free	bounded
	AO-K	Roundabout		-	-	
Motorway	A-80	Motorway A2 und A9	-	80	-	
	A-100			100	-	
	A-130			130	-	
	A-free			-	-	
	Rest area			-	-	

Six different micro-trips for urban roads, characterized by their purpose and speed limit, were investigated. The same was made for rural roads and motorway by differentiating the measurement routes by speed limits. The trips themselves were selected in the immediate surroundings of Graz. The tests were made in order to be able to distill not only a synthetic driving cycle but also to build the base for compiling a real world driving cycle for specific on-road measurements for PTWs. Figure 34 illustrates the selected micro-trips. The very upper part of Figure 34 illustrates urban trips on the left side and rural trips on the right side wherein the circles for S5 and S6 do not mark a specific route, but an area of similar roads to be chosen by the driver itself when measuring. The map at the very bottom and left side shows motorway trips which were investigated. Thus, the testing procedure included continuous on-road measurements and the separation of the overall collected data according to the above described matrix in Table 8. Additionally, the map at the very bottom and right side shows a sport-orientated traffic situation that was investigated to take into account the use of motorcycle for riding for pleasure at leisure, which – for sure – has an unneglectable share on total driving time with powered two-wheelers. These investigations are discussed more detailed in section 2.5.7.

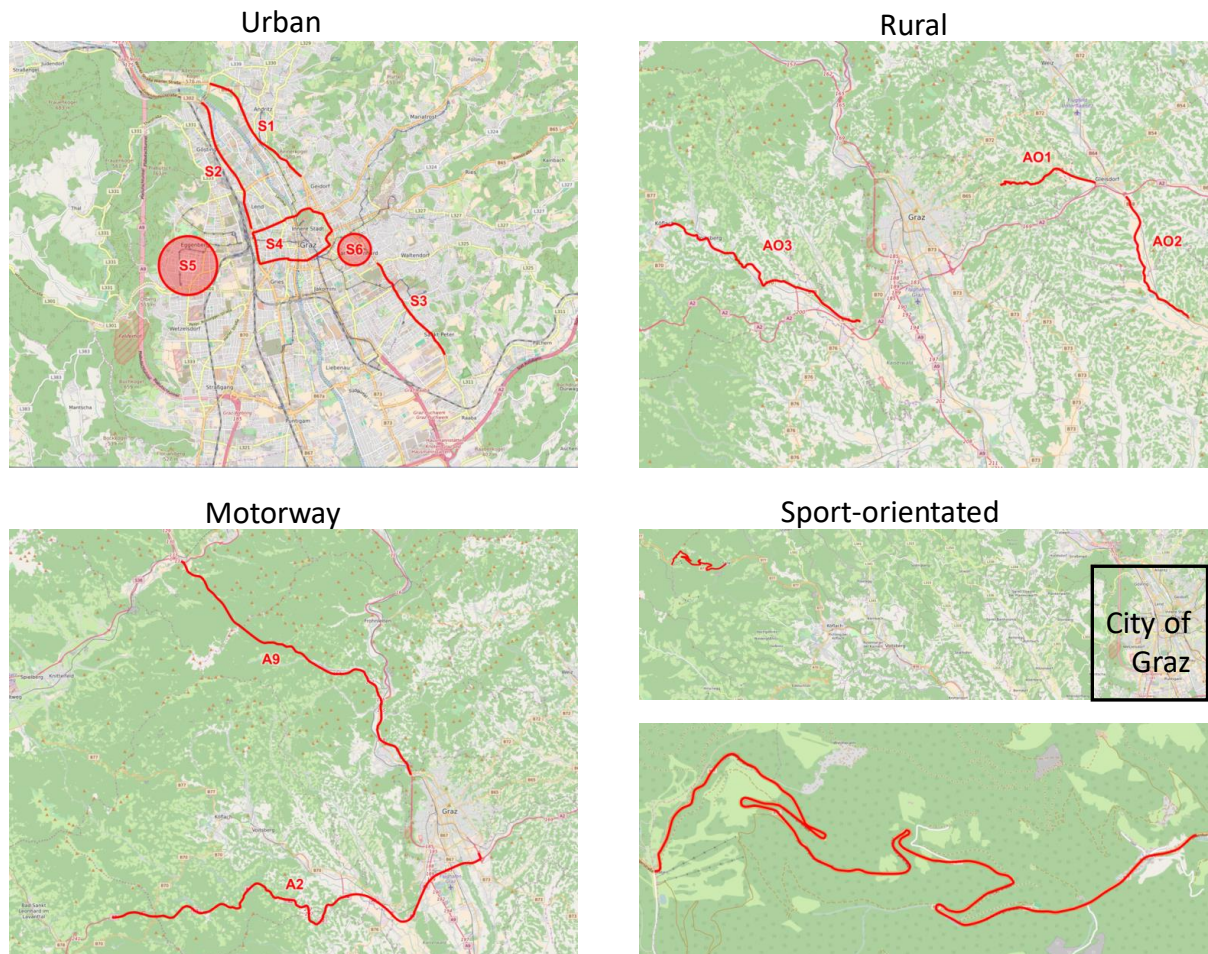


Figure 34. On-road trips for urban, rural, motorway and sport-oriented driving situations.

All test trips were done with different vehicle and driver combinations as it was done for the RDE on-road driving tests as described above. Moreover, Table 8 contains the characterization of traffic flow differentiated in free flow, bounded, and jam; wherein the bounded traffic situation describes the state in which the driving velocity cannot be chosen by the driver itself but is determined by a vehicle in front. The additional row with speed limit marks the given limit on the road segments. The rural tests additionally contain micro-trips for roundabouts. The motorway tests also contain differentiated micro-trips for driveway and exit to rest areas.

2.5.3 Motorcycle driving dynamic and legislative boundaries

In order to classify the driving dynamic of motorcycles compared to other vehicles, the above-mentioned measurements were evaluated and assessed. The following section introduces trip indicators to illustrate driving dynamics and presents some influencing factors that determine, among others, the selection of representative traffic situations for a subsequent compilation of RDCs.

2.5.3.1 Trip indicators to assess driving dynamics

The evaluation of single micro-trips is made in accordance to the Commission Regulation (EU) 2016/646 [14] that was published as for amending Regulation (EC) No 692/2008 on type-approval tests for motor vehicles with respect to emissions from light passenger and commercial vehicles (Euro 5 and Euro 6). Therein, a real driving emission test procedure is established that alludes to a possible methodology for motorcycles. While it is important that all possible driving situations are potentially covered by RDE testing, it should be avoided that the tested vehicles are driven in a biased manner, i.e. with the intention to generate a passed or failed test not by virtue of the technical performance of the vehicle but due to extreme driving patterns. Therefore, complementary boundary conditions for RDE testing are introduced in order to address such situations. These boundary conditions are set by so-called trip indicators by which the overall excess or insufficiency of driving dynamics during the trip shall be checked. For assessing the real driving cycles, speed ranges are established for allocating the test data to urban, rural, and motorway conditions, as illustrated in Table 9. As it turned out that motorcyclists in Austria often exceed these speed ranges in terms of average driving pattern, this was part of further investigations. In a first step the speed ranges were raised to the shown levels.

Table 9. Speed ranges for allocation of test data to different driving conditions.

	Urban driving [km/h]	Rural driving [km/h]	Motorway [km/h]
Regulation (EU) 2016/646	$v_i \leq 60$	$60 < v_i \leq 90$	$v_i > 90$
Analyzed additionally for	$v_i \leq 60$	$60 < v_i \leq 110$	$v_i > 110$

The appealed trip indicators include, among others, two main parameters for evaluating the overall trip dynamics; the relative positive acceleration RPA and the 95th percentile of the product of vehicle speed per positive acceleration $(v \cdot a_{\text{pos}})_{95}$, “VA_{pos}“, which physically describes a specific power. The values can be plotted for specified parts of a trip, whereas a commitment of limits determines whether a trip is valid or not, as schematically illustrated in Figure 35. As said above, these trip indicators are determined for passenger cars and the calculation schemes and boundary conditions are exemplarily used for comparisons to motorcycles and to develop insights to motorcycle driving dynamic. Section 2.5.6 expands on the test results for motorcycles.

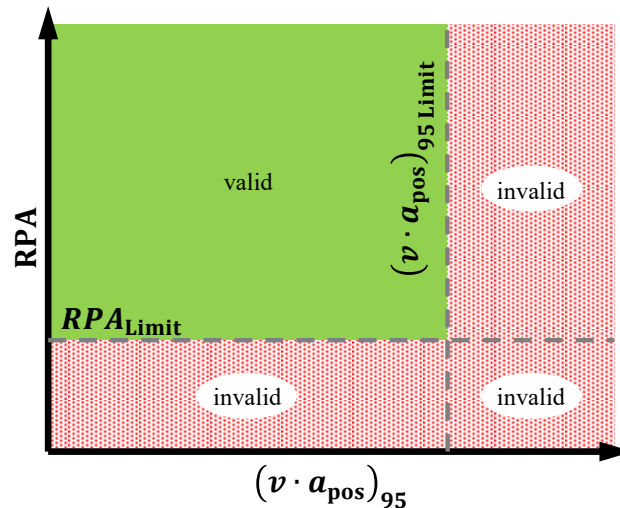


Figure 35. Limits of driving dynamic by two main parameters.

The evaluations of trip indicators are made by the software CLEAR version 2.0, which includes all calculations regarding the assessment method for RDE tests for cars and LCVs described in [13]. The CLEAR tool covers the actual state of afore mentioned RDE legislation in all details. It uses the power binning method for calculation of weighted emissions for RDE trips [48]. In this case, as there is no legislative indication for motorcycles, the evaluation of emissions is excluded; but the tool is used for assessment of driving dynamics. Thus, the input data for CLEAR included the measurement time as well as the GPS velocity and the GPS altitude for calculating the trip indicators. The analysis was made for single micro-trips whereby the computed values for above mentioned parameters RPA and VA_{pos} were evaluated for the total micro-trip and not differentiated into speed ranges. This arises from the variability of speed during single segments, which would cause defocusing of the values when split into the appropriate parts. As to satisfy the requirement for a correctly assessed trip indicator, single micro-trips were processed to fit for the mentioned chosen speed ranges for motorcycles, as described above. The following sections expand on the trip indicators.

2.5.3.1.1 95th percentile of the product of vehicle speed times positive acceleration – VA_{pos}

$(v \cdot a_{\text{pos}})_{95}$ is the 95th percentile of the product of vehicle speed and positive acceleration greater than 0.1 [m/s²] for the calculated measurement interval in [W/kg]. For calculating VA_{pos} all values of the considered interval are sorted ascending for the values of $(v \cdot a_{\text{pos}})_i$ for each corresponding column j where the acceleration is $a \geq 0,1$ [m/s²]. The sum of the number of all columns j is memorized as M_k . The searched value for VA_{pos} is found in the column where $j/M_k = 95$ [%] is valid.

2.5.3.1.2 Relative positive acceleration – RPA

RPA_k is the relative positive acceleration for the given interval k in [m/s²], calculated by the following Equation 2.

Equation 2

$$RPA_k = \frac{\sum_j \Delta t \cdot (v \cdot a_{\text{pos}})_{j,k}}{\sum_i d_{i,k}}, \quad j = 1 \text{ to } M_k, \quad i = 1 \text{ to } N_k$$

- $d_{i,k}$ – Is the distance travel [m] for the time step i in the interval k
 N_k – Is the number of measurement columns with $a \geq 0,1 \text{ m/s}^2$ [-]
 Δt – Is the time duration of one measurement column i (= 1 s) [s]

2.5.3.1.3 Mean vehicle velocity of interval k – \bar{v}_k

\bar{v}_k is the mean vehicle velocity in the given interval k in [km/h], calculated by the following Equation 3.

Equation 3

$$\bar{v}_k = \frac{\sum_i v_{i,k}}{N_k}, \quad i = 1 \text{ bis } N_k$$

- $v_{i,k}$ – Is the vehicle speed [km/h] of measurement column i in the interval k

2.5.3.2 Checking the validity of a measured micro-trip

In accordance to [13] the validity of a measured micro-trip, e.g. one measured section S1 out of Table 8 is checked for the current automotive RDE legislation by the criterion shown in Table 10 and Table 11. The boundary for VA_{pos} , therefore, describes the maximum values for an evaluated micro-trip k at the corresponding mean velocity \bar{v}_k to be valid if undershot. Equally, the values for RPA out of Table 11 describe the minimum boundary for each micro-trip k at the corresponding mean velocity \bar{v}_k to be exceeded for a valid trip segment.

Table 10: Checking the validity of measured micro-trip k for VA_{pos}

Validity		
$\bar{v}_k \leq 74.6 \text{ km/h}$	& $(v \cdot a_{\text{pos}})_{95,k} > (0.136 \cdot \bar{v}_k + 14.44)$	invalid
$\bar{v}_k > 74.6 \text{ km/h}$	& $(v \cdot a_{\text{pos}})_{95,k} > (0.0742 \cdot \bar{v}_k + 18.966)$	invalid

Table 11: Checking the validity of measured micro-trip k for RPA.

Validity		
$\bar{v}_k \leq 94.05 \text{ km/h}$	& $RPA_k < (-0.0016 \cdot \bar{v}_k + 0.1755)$	invalid
$\bar{v}_k > 94.05 \text{ km/h}$	& $RPA_k < 0.025$	invalid

Figure 42 clarifies these boundaries as the automotive values of [13] are illustrated with black dashed lines as a reference.

2.5.4 Selecting and processing single micro-trips

Selected single micro-trips were chosen from the measurements of on-road routes, always in accordance with Table 8. As one measurement includes a mixture of multiple micro-trips - as one compares Figure 34 with the following Figure 36, which indicates speed limits on a rural route - the route was separated pursuant to the specified type of roads, illustrated in Table 8.

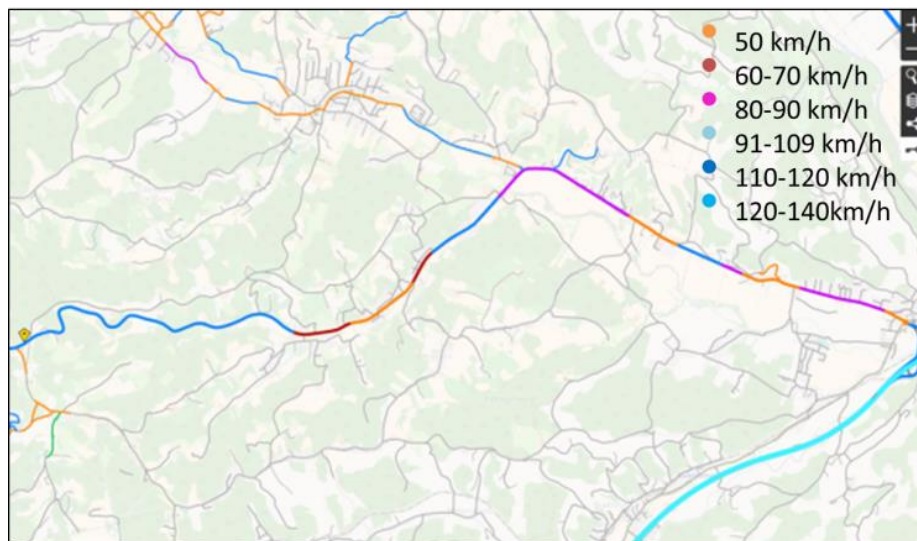


Figure 36: Speed limits on a rural test route.

Nevertheless, to differentiate the single parts into urban, rural, and motorway, the trips were edited as illustrated in Figure 37, depicting the velocity over time for a section of a rural trip. The differentiation between an urban access road embedded in a rural micro-trip is represented with the red marked area. This area was cut from the raw data, whereby rural data was only provided for further calculations of trip indicators.

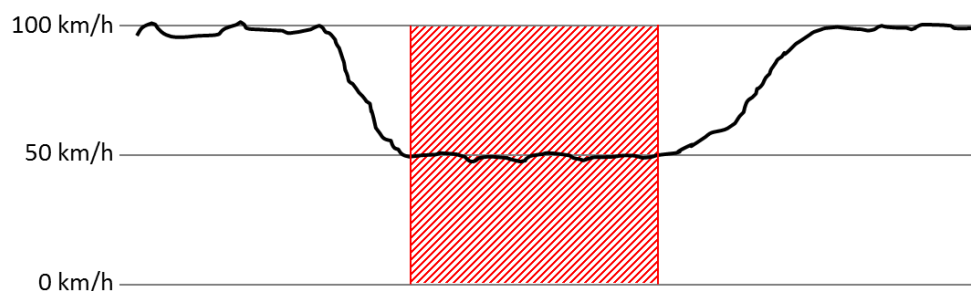


Figure 37: Schematic separation of a rural on-road route with embedded urban access road into representative micro-trips for urban and rural driving.

After processing the data, the calculation of trip indicators was made for all files by CLEAR, as described above. The software's output includes all values to assess the trips dynamics by means of the Regulation (EC) No 692/2008 [14]. Table 12 illustrates an exemplary shortened list of results for three on-road urban micro-trips S3 for free traffic flow conditions.

Table 12. Exemplary evaluation of urban trip segments.

Trip segment name	S3_BMWG650_#1	S3_BMWG650_#2	S3_BMWF800_#1	...
95 percentile $v_{0.1}$	41.48	29.80	19.48	...
Mean $v_{0.1}$	11.02	8.017	5.121	...
Weighted $v_{0.1}$	3.520	2.886	1.472	...
Mean RPA [m/s^2]	0.3672	0.2975	0.2167	...
Trip length [m]	1143	973	3273	...
Trip duration [s]	121	102	482	...
Mean v [km/h]	33.99	34.33	24.44	...
⋮	⋮	⋮	⋮	

2.5.5 Influences of driver and traffic flow on trip indicators

Since the operation of a vehicle directly affects its exhaust gas concentrations, driver variability was to be investigated. It describes the differences in vehicle operation behavior between drivers. These differences may include variations in the duration, frequency or intensity of different driving modes such as cruise, acceleration and deceleration [47]. In order to assess the influence of different drivers on the trip indicators, several additional on-road measurements on a representative motorcycle uphill route (see bottom right of Figure 34) were performed. Thus, the impact of specific driving patterns can be emerged in a better way as if urban or rural micro-trips are used for comparison.

The following Figure 38 sums up the frequency distribution of throttle angle position over engine speed for different drivers. On the left side, the uphill road was driven in cruise mode whilst on the right side the diagrams show the same trip driven ambitiously. Each column is assigned to a driver 1 to 3. A significant difference between the driving patterns and also between the drivers is obvious.

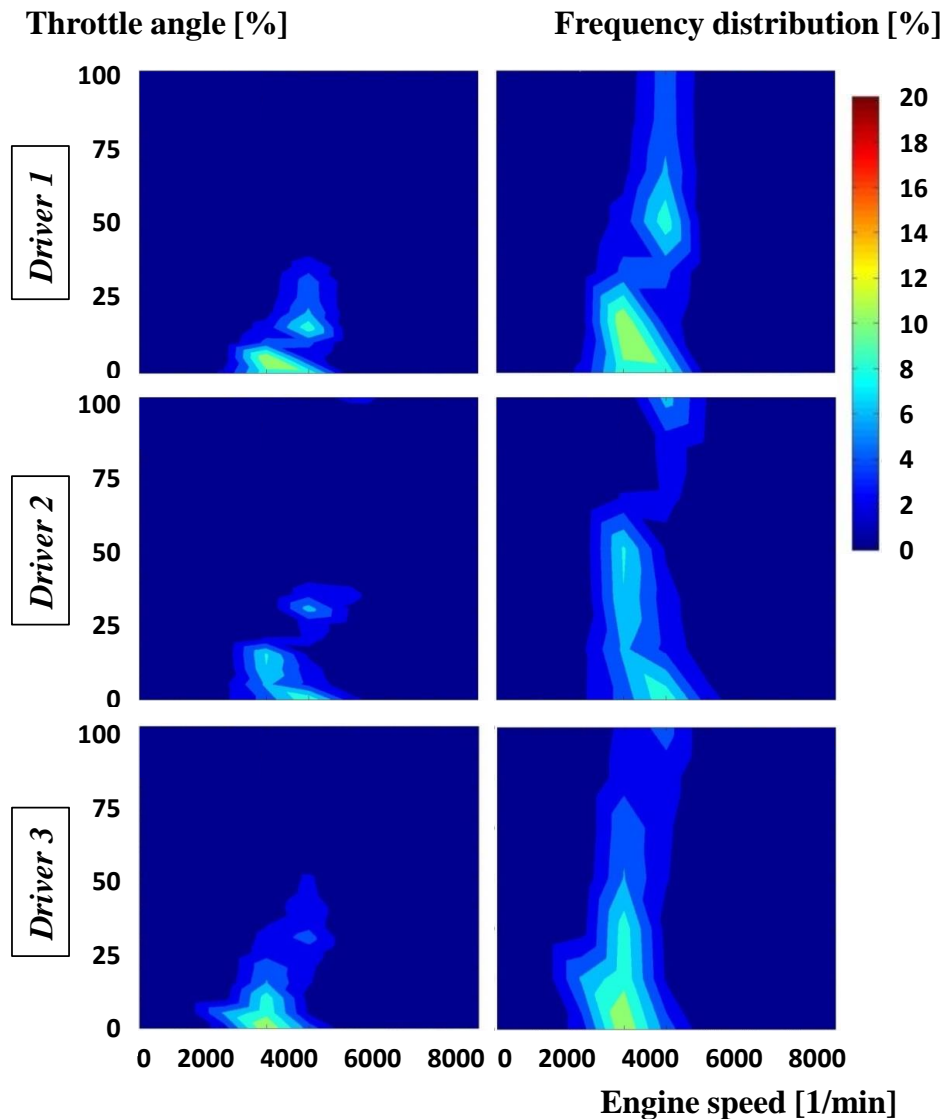


Figure 38. Frequency distribution of n/α -classification for different driving pattern: cruise (left) vs. ambitious (right).

Another influence factor on the evaluated trip indicators is the traffic flow, which was differentiated in the categories free, bounded, and jams, like illustrated in Table 8. Drivers assessed the traffic situation subjectively during the trip and documented it.

The influence of both mentioned factors, the driving pattern and the traffic situation, can be illustrated by plotting and comparing trip indicators like it is done exemplarily in Figure 39 to Figure 41 and Figure 42. To minimize the influence of subjective perception, three drivers rode each on-road route (each micro-trip respectively; see Table 8) for several times and on different day times.

2.5.6 Evaluation of the single micro-trips

The prescribed single on-road micro-trips (see section 2.5.2) were evaluated and compared against multiple automotive RDE tests with an Audi Q7. Figure 39 to Figure 41 illustrate the results of all three evaluated speed ranges, namely urban, rural and motorway. The grey dotted

data illustrate the measurements with an Audi Q7. The test data from the passenger car was taken for comparison as this vehicle allows relatively dynamic driving with its available 85 W/kg. The transparent circles show the results for the described single micro-trips out of Table 8, each positioned by the mean value of RPA and VA_{pos} over all data per micro-trip (see legend). The diameter of a circle marks a weighted factor for standard deviation of the scattered data. Hence, the bigger circle in the diagram illustrates data that are more scattered.

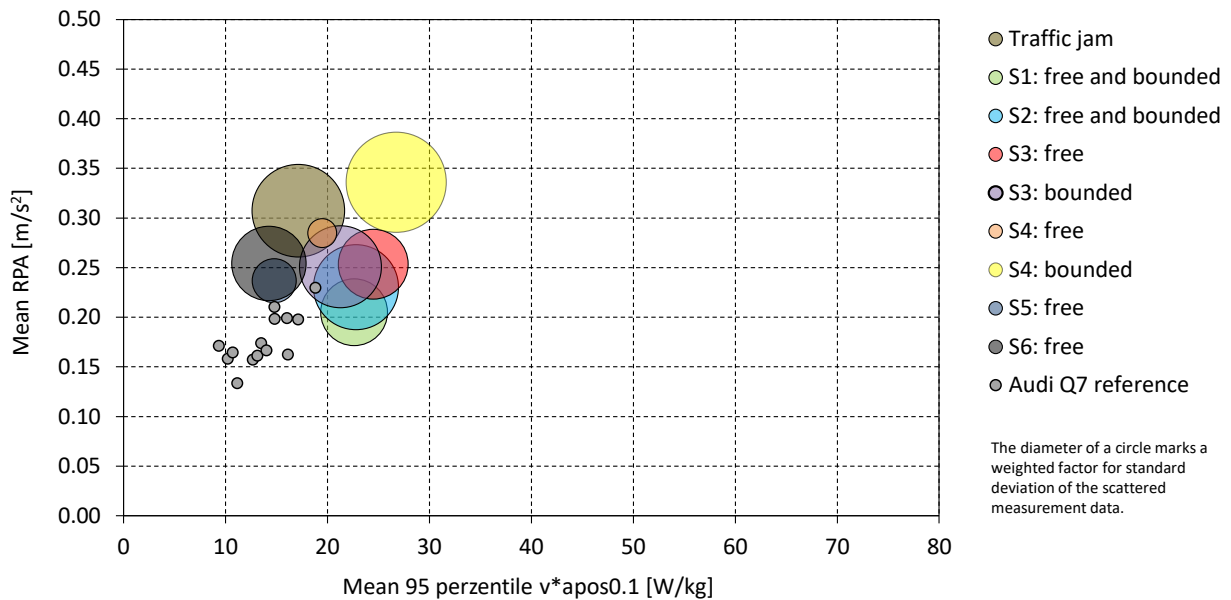


Figure 39: Trip indicators RPA and VA_{pos} for urban on-road motorcycle micro-trips.

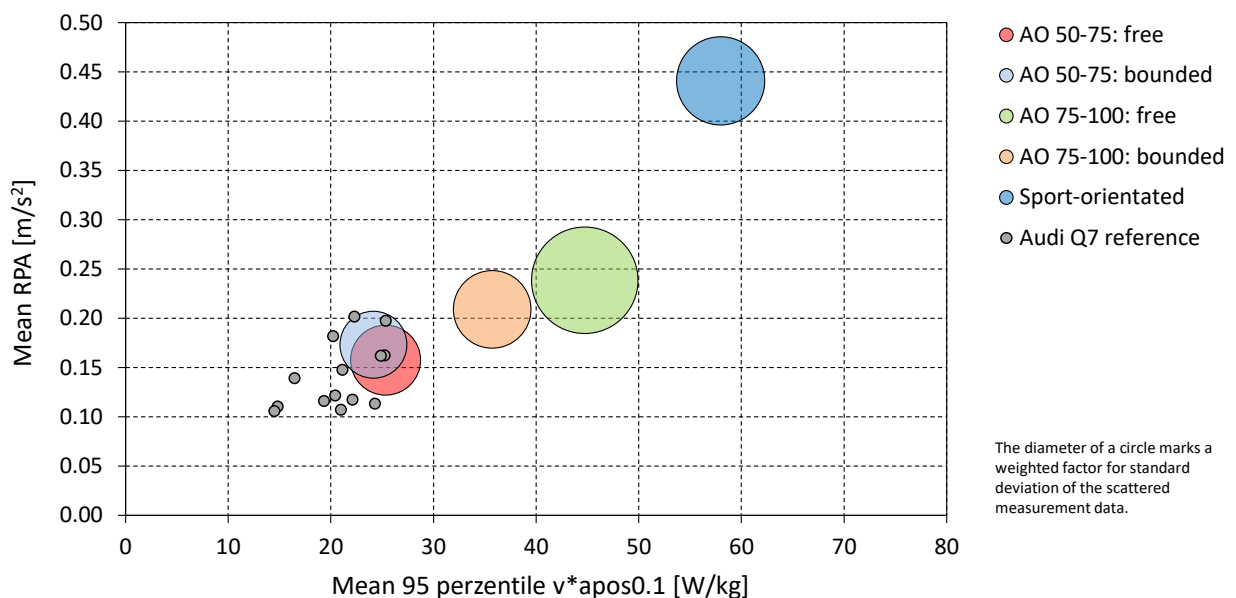


Figure 40: Trip indicators RPA and VA_{pos} for rural on-road motorcycle micro-trips.

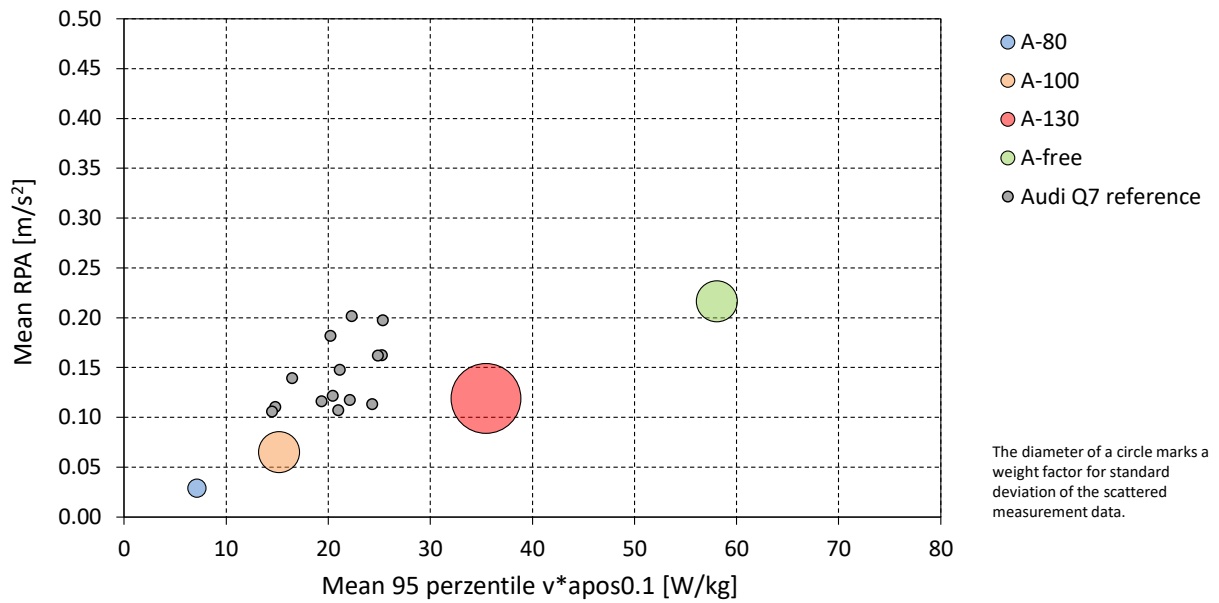


Figure 41: Trip indicators RPA and VA_{pos} for motorway on-road motorcycle micro-trips.

All three diagrams show the same trend towards a higher driving dynamic for motorcycles. Especially when it comes to sport-oriented driving, as illustrated in Figure 40 by the blue circle, the values for all trip indicators reflecting driving dynamics are exceeding common established limits by far (compare to section 2.5.3.2 and Figure 42).

The following Figure 42 sums up the trip indicators RPA and VA_{pos} and their corresponding borders for passenger cars and light commercial vehicles for all measured micro-trips and traffic situations (Table 8) in accordance to [14]. The values are plotted over the respective mean velocity \bar{v}_k of an evaluated micro-trip k (urban marked in green, rural in blue, and motorway in orange). The dashed line illustrates the regulatory limits wherein the RPA value ensures a minimum of driving dynamic and the VA_{pos} value confines the maximum driving dynamic, as described above. According to schematic Figure 35 and Table 10 and Table 11, the overall validity of a test is given when the mean value of a trip appears between these boundary conditions in the diagram.

Once again, this illustration clearly shows the higher driving dynamic of motorcycles. Measurement data of automotive RDE test routes (Arzberg and Ries) and type approval test WMTC, driven with the test objects, are illustrated with yellow and magenta dots as reference. One can see, that the automotive RDE test tracks result in higher values for driving dynamic than the type approval test. These automotive RDE test routes reflect the investigated on-road micro-trips with good correlation if one compares its values with the scattered data and its mean values in Figure 39 to Figure 41.

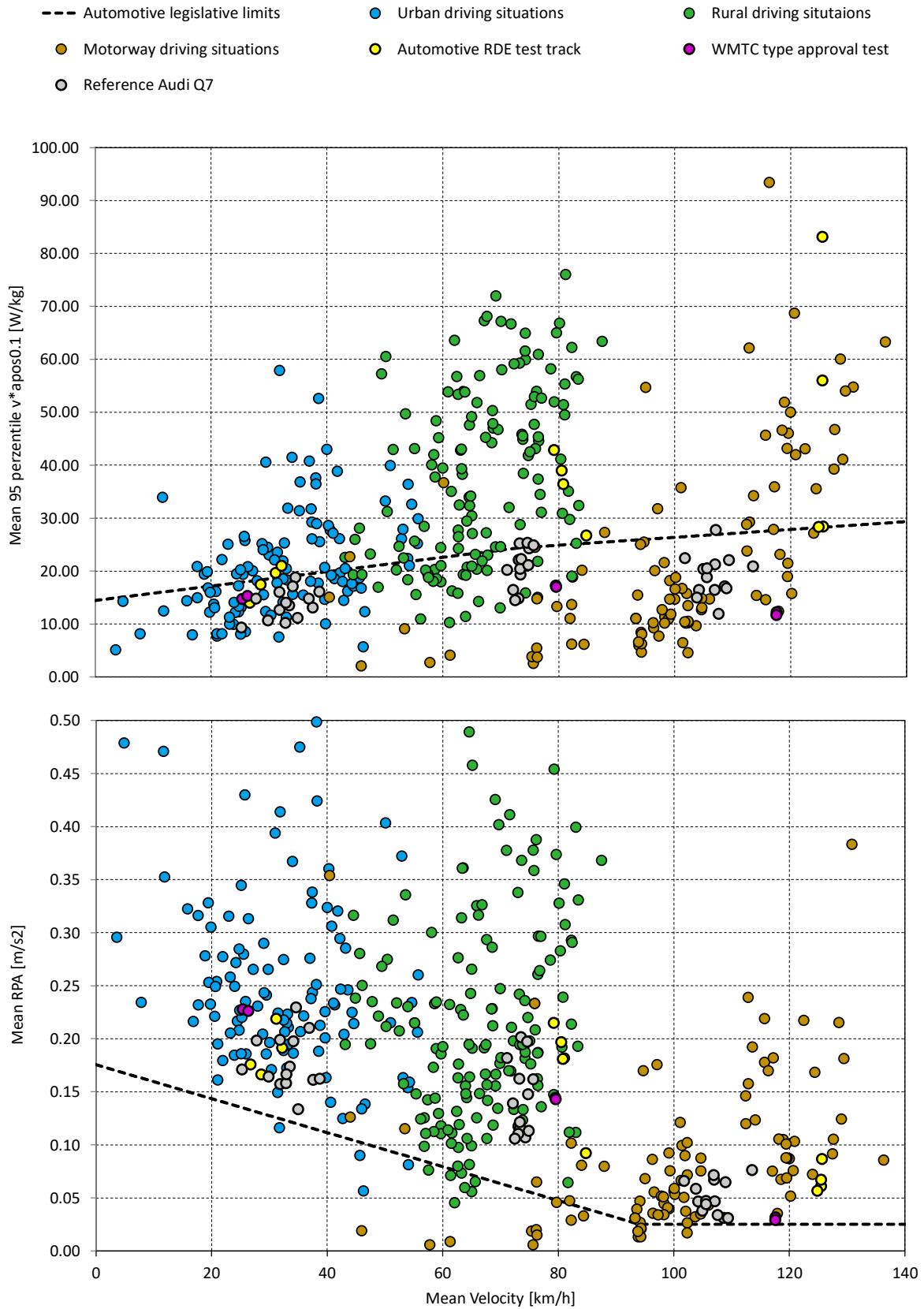


Figure 42: Trip indicators RPA and VA_{pos} for on-road motorcycle tests on defined on-road micro-trips with marked regulatory limits according to [14].

However, these results indicate that the type approval test is not reflecting real world driving behavior of motorcycles. To expand on this, the following Figure 43 and Figure 44 illustrate engine maps with engine torque over engine speed for a WMTC test on chassis dynamometer and one of the RDE tests with a BMW F800GT motorcycle. The blue dots represent the utilization of the engine map. The different engine load conditions over a full test trip are obvious. In particular, Figure 44 shows a shift of the engine operation towards higher loads and even full load conditions are present for the investigated automotive RDE test route.

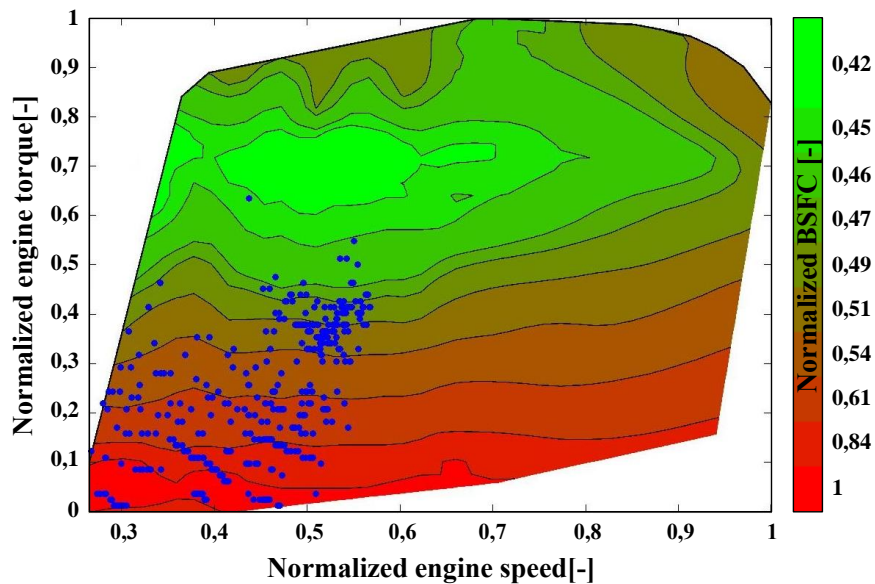


Figure 43: Engine map with engine torque over engine speed for a WMTC test on chassis dynamometer with a BMW F800GT motorcycle.

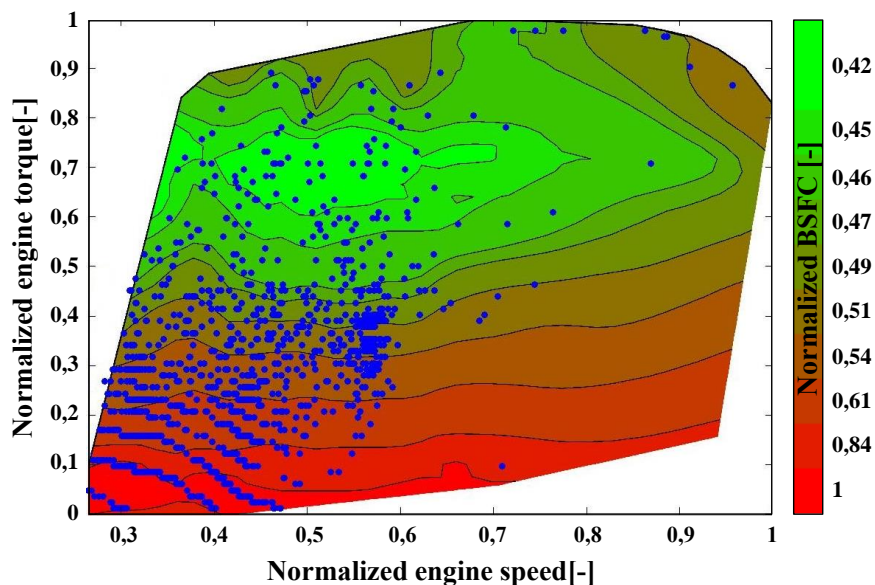


Figure 44: Engine map with engine torque over engine speed for the on-road RDE test "Arzberg" with a BMW F800GT motorcycle.

It can be concluded that driving dynamic of motorcycles significantly differs from other vehicles, whereby existing legislative provisions cannot be taken similar for driving dynamic

assessment. Moreover, type approval tests are not representing real world operation conditions adequately even if established automotive RDE test routes are driven and sport-orientated driving pattern are tuned out so far.

2.5.7 Deliberation on additional or changed trip indicators for motorcycles

Deliberations on including some sport-orientated micro-trips were made as described above and illustrated in Figure 34. This was done in consideration of the fact that most of motorcyclists also ride for the sake of pleasure and not only to get from one location to another. So this additional trip for sport-orientated uphill driving pattern for motorcycles was selected to meet the pleasure of riding aside the standard driving behavior deduced from passenger cars. The micro-trip is well known by motorcycleists in Styria as the “Gaberl” and commonly driven.

In this context, considerations of how to separately evaluate this sport-oriented trips aside the existing ones for urban, rural and motorway driving, were taken into account. Moreover, the idea of possible additional trip indicators for dynamic driving behavior was revised, to better represent the more dynamic behavior for motorcycles. The mentioned speed limits in Table 9 were one first step. It was also considered to separate the overall routes by geographical means, as it is exemplarily illustrated in Figure 45. It actually means that an urban micro-trip ends when the city is left (not when speed exceeds 60 [km/h] for a few seconds) but also that a rural micro-trip includes all urban access rides when the vehicle speed falls below 60 [km/h]. Particularly with regard to the evaluation of real world cycles as described in Regulation (EC) No 692/2008 and to keep it simple, this was not pursued yet.

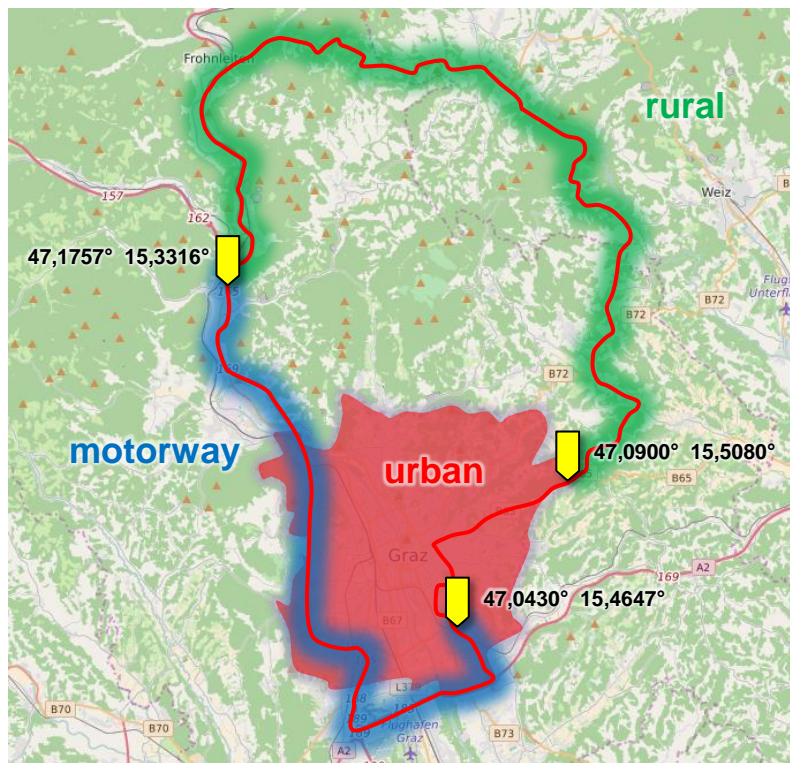


Figure 45: Exemplary separation of real world test route "Arzberg" by geographical means.

Moreover, considerations were made of introducing additional trip indicators as to capture a relative amount of trip duration to sport-orientated uphill driving patterns. For the sake of this investigation, different driving styles at the “Gaberl” with different drivers were evaluated in terms of dynamic trip indicators but also comparing emissions and fuel consumption.

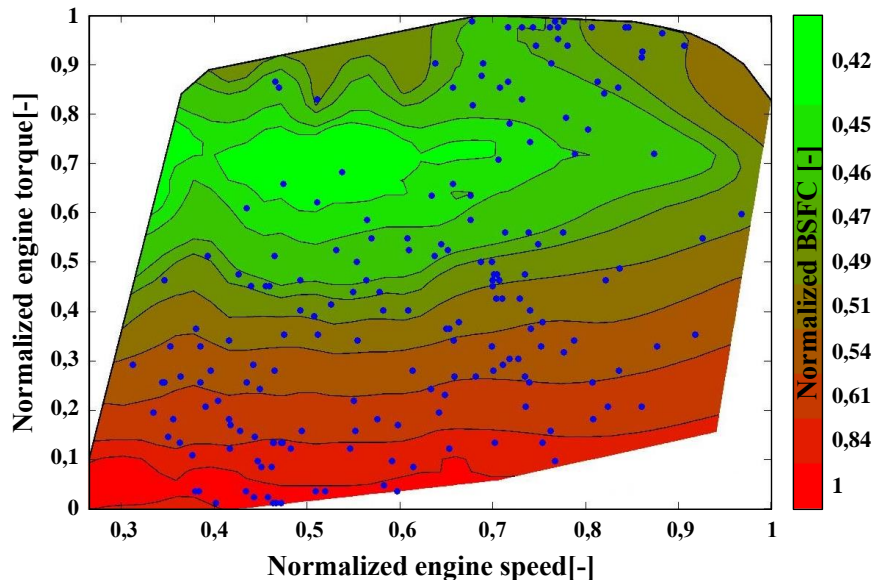


Figure 46: Engine map with engine torque over engine speed of the sport-orientated uphill route “Gaberl”, driven with a BMW F800GT motorcycle.

As to illustrate the influence on an engine map of this sport-orientated route, Figure 46 depicts the engine map of the BMW F800GT motorcycle. The blue dots symbolize the load points plotted as normalized engine torque over normalized engine speed. In comparison to the WMTC test cycle, illustrated in Figure 43, a significant difference between these engine maps can be seen which cannot be neglected in terms of assessing and evaluating real driving cycles for RDE measurements. Incidentally, the coherence to the trip indicators, shown in Figure 39 to Figure 42, should be marked out. In Figure 40 the averaged data for the uphill micro-trip “Gaberl” is marked by a blue circle at the very right of the diagram.

In order to consider these occurring sport-orientated trips, one idea was to evaluate an indicator similar to VA_{pos} . Therefore, a so-called dynamic slope factor was established, which is the product of vertical velocity (the vertical movement of the vehicle, calculated from geodetic altitude difference) times positive acceleration and its 95-percentile interval $(v_{vert} \cdot a_{pos})_{95}$. This factor can be calculated out of the common data sets used for calculating all other trip indicators. It respects not only sport-orientated driving patterns on an uphill road but also just curvy roads due to the greater impact of a_{pos} in the multiplication. It was calibrated with different on-road measurements. Table 13 sums up calculated dynamic slope factors for tests on “Gaberl” in comparison to the automotive RDE test track measurement on “Arzberg” with and without an uphill micro-trip, driven with a BMW F800GT motorcycle.

Table 13: Additionally evaluated trip indicator for sport-orientated uphill driving with motorcycles.

Test cycle	$(v_{vert} \cdot a_{pos})_{95}$
Gaberl	5.463
Arzberg	2.380
Arzberg without uphill micro-trip	1.384

By observing several data sets of on-road real driving cycles, it can be derived that a factor of at least 3 [W/kg] classifies a dynamic slope factor that indicates the pleasure of riding for motorcyclists or a so-called sport-orientated driving pattern. The height profile of mentioned automotive real world test cycle is illustrated in Figure 47 with the marked uphill driving trip “Rechberg”.

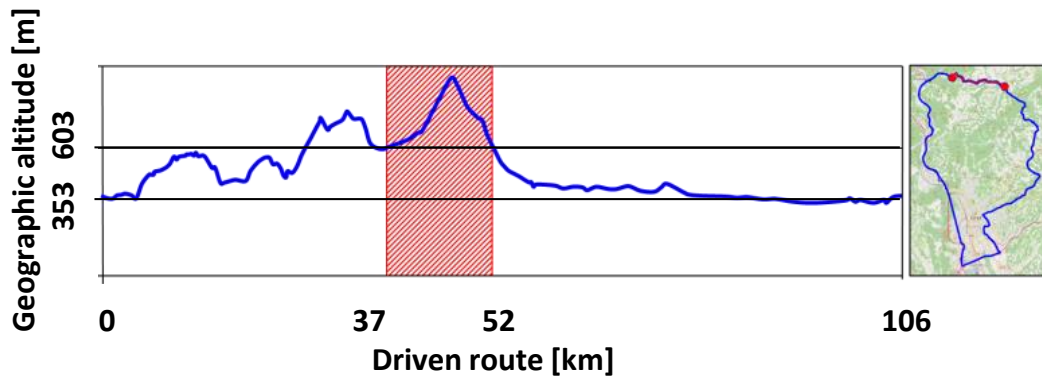


Figure 47: Geographic location and altitude over longitude of the real world cycle “Arzberg” with marked uphill micro-trip “Rechberg”.

Pursuing the thoughts on such an exemplary additional trip indicator, classifications may also use the evaluation by percentile borders for different cubic capacity classes or specific engine power. This can be used to meet a higher number of vehicles. This thought also leads to more influencing factors, as the overall vehicle weight, as engine power corresponds to total weight of a motorcycle [17]; and by the nature of PTWs, the diversity of engine classes and vehicle classes is by far greater than it is in the sector of passenger cars.

2.6 Real drive test cycles for chassis dynamometer

A synthetic real driving cycle for chassis dynamometer was compiled from the tests on the above mentioned representative single micro-rips, to investigate its usability as test cycle to evaluate and assess RDE and fuel consumption aside on-road measurements. As to respect all measurement areas (urban, rural, motorway) with the same weight, the time slices of each area were chosen with a third of total cycle time. Moreover, each measured micro-trip, e.g. the

micro-trips S1 to S6 for different traffic situations each (see Table 8), were integrated in the synthetic RDC with around 100 seconds for each micro-trip category to respect each road category and driving situation with a minimum duration. As by the nature of the above described measurement campaign and the processing of the data, the length of a measured trip is not 100 seconds. Hence, a Matlab function was built to cut and select the appropriate parts of a micro-trip. The requirement for the selection of such a 100 second part was the smallest deviation of the mean value of the selected 100 second part to the overall mean value of all measured micro-trips of one area/road/traffic ART combination. For example, to select a 100 second long part of the ART combination S1-free (S1_f), the overall mean value over all S1-free measurements was calculated for VA_{pos} , RPA, and the mean velocity. Furthermore, the mean values for all possible 100-second-long parts of all measured S1-free micro-trips were calculated for VA_{pos} , RPA, and the mean velocity. As to find the best suitable and representative 100 second part of all micro-trips of one ART combination, the one with minimum deviation from the overall mean value for each trip indicator VA_{pos} , RPA, and mean velocity was chosen. Figure 48 illustrates the computational scheme.

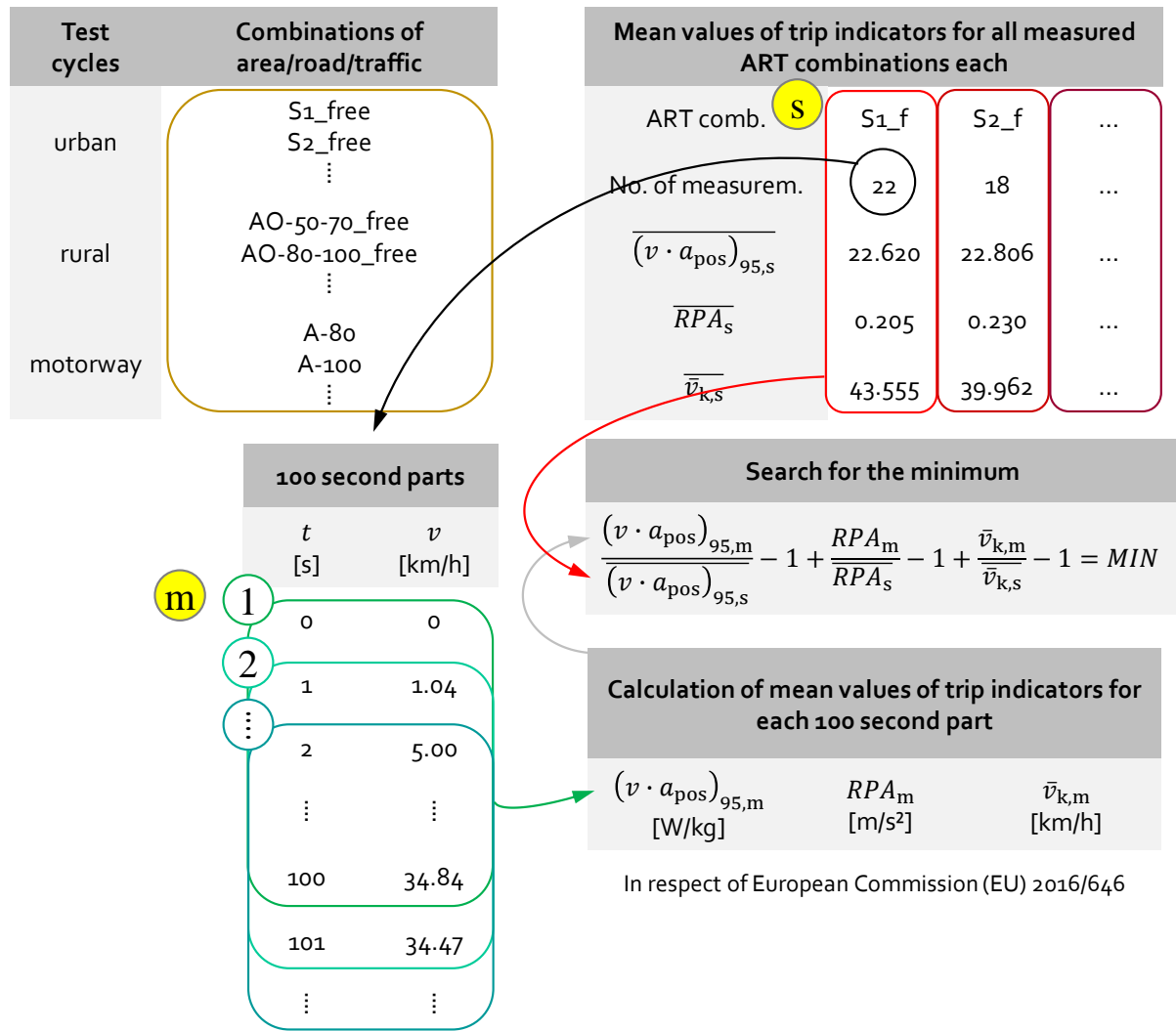


Figure 48: Calculation and selection scheme for representative 100 second parts of measured on-road micro-trips for single ART combinations.

- m – Index for sub-cycle measured in a micro-trip; e.g. a 100 [s] long segment of one measurement within micro-trip S1-free
- RPA_m – Relative positive acceleration of one segment m in [m/s²]
- \overline{RPA}_s – Mean value of the relative positive acceleration of all measured sections s of one ART combination in [m/s²]
- s – Part of an micro-trip with one ART combination
- $\overline{v}_{k,m}$ – Mean vehicle velocity of one segment m in [km/h]
- $\overline{v}_{k,s}$ – Mean value of vehicle velocity of all measured sections s of one ART combination in [km/h]
- $(v \cdot a_{pos})_{95,m}$ – 95th percentile interval of velocity times positive acceleration of one segment m in [W/kg]
- $\overline{(v \cdot a_{pos})_{95,s}}$ – Mean value of 95th percentile interval of velocity times positive acceleration of all measured sections s of one ART combination in [W/kg]

The orange frame sums up all possible ART combinations. The red frames indicate the calculation of the mean values of trip indicators for all measurements for one ART combination. The green frames mark the calculation of mean values of trip indicators for all possible 100 second parts for all measurements for an ART combination. Thereof, the one with minimum deviation according to following Equation 4 is selected in order to be integrated in an RDC.

Equation 4

$$\frac{(v \cdot a_{\text{pos}})_{95,m}}{(v \cdot a_{\text{pos}})_{95,s}} - 1 + \frac{RPA_m}{RPA_s} - 1 + \frac{\bar{v}_{k,m}}{\bar{v}_{k,s}} - 1 = MIN$$

As the used velocity profiles are GPS raw data, measured with 1Hz, a moving three second average of the velocity profiles was performed to increase usability for the chassis dynamometer tests. Moreover, values smaller than 0.2 km/h in the velocity profile were set to zero. It has to be kept in mind that this modification slightly changes the calculated trip indicators.

Gear shift rules for the resulting test cycles were adapted velocity-dependent from WMTC legislation. The tolerance range for the velocity profile was also adapted from WMTC legislation.

A realistic transition was inserted between all 100 second parts like illustrated in Figure 49.

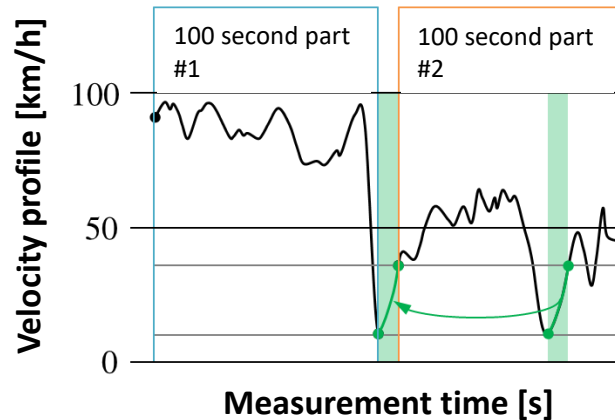


Figure 49: Method to connect single 100 second parts of representative road segments.

Different real drive cycles were compiled for motorcycles and mopeds with the above described method. An exemplary comparison of RDC1 with WMTC is given in Table 14. The corresponding velocity profiles of some other real drive cycles, including real world cold start test cycles, are illustrated in Figure 51 to Figure 55.

Table 14: Comparison of main parameters of RDC1 and WMTC chassis dynamometer test cycles.

		WMTC	RDC1
Mean velocity	urban	24.54 km/h	28.68 km/h
	rural	54.72 km/h	67.68 km/h
	motorway	94.32 km/h	97.17 km/h
Test duration	urban	600 s	979 s
	rural	600 s	928 s
	motorway	600 s	927 s
Test distance	urban	4.09 km	7.80 km
	rural	9.12 km	17.29 km
	motorway	15.72 km	25.02 km
VApos	urban	14.7 W/kg	17.2 W/kg
	rural	17.1 W/kg	37.9 W/kg
	motorway	12.3 W/kg	20.8 W/kg
RPA	urban	0.19 m/s ²	0.205 m/s ²
	rural	0.143 m/s ²	0.176 m/s ²
	motorway	0.029 m/s ²	0.048 m/s ²

RDC1, as illustrated in Figure 51, has integrated a three-minute sport-orientated part of a segment that is based on the above described measurements on the “Gaberl” test route. To reproduce this sport-orientated part on the chassis dynamometer, the corresponding slope has to be adjusted during testing. This part of the test cycle has a constant slope of 6.97%.

RDC2, as illustrated in Figure 52, is a shorter test cycle with duration of around 30 minutes and without a sport-orientated uphill part.

An arbitrary variety of real drive cycles can be compiled with this workflow. The mentioned RDC1 and RDC2 tended to be the most useful to cover real world driving behavior of motorcycles on the chassis dynamometer so far.

Figure 50 illustrates the engine map with plotted normalized engine torque over normalized engine speed for a driven WMTC in black and a RDC1 in blue with a BMW F800GT motorcycle. It can be seen that the coverage of the engine map is more extensive for the real driving cycle. Moreover, the marked areas 1 to 3 are identified as follows: *Area 1* can be assigned to the highly dynamic parts of the rural third of the test cycle. The *area 2* and *area 3* are dedicated to motorway parts where the velocity is high but acceleration phases have relatively low values. The following section 2.6.1 expands on the assessment of these real drive cycles.

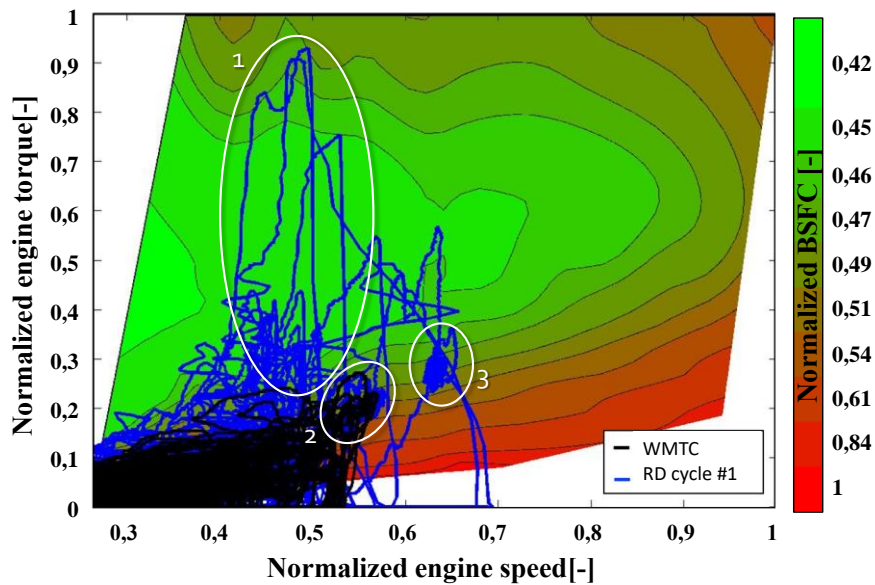


Figure 50. Comparison of load points of a driven WMTC and an RDC1 in an engine map of a BMW F800GT motorcycle.

The RDC investigations were carried out to clarify whether these measurements are sufficient for RDE and fuel consumption assessment for a broad variety of PTWs or not. It can be shown that emission levels are similar to RDE measurements but, of course, numerous test cycles for chassis dynamometer are available and all of them are considered broadly representative for driving conditions [35]. RDCs reflect local driving conditions, but even though they are fixed test cycles that will never suit for all kinds of PTWs, especially when thinking of the broad variability of engine capacities and concepts in this vehicle sector [17] [36]. The results of RDE and fuel consumption measurements on-road and also compared to RDCs will be discussed further on in chapter 3.

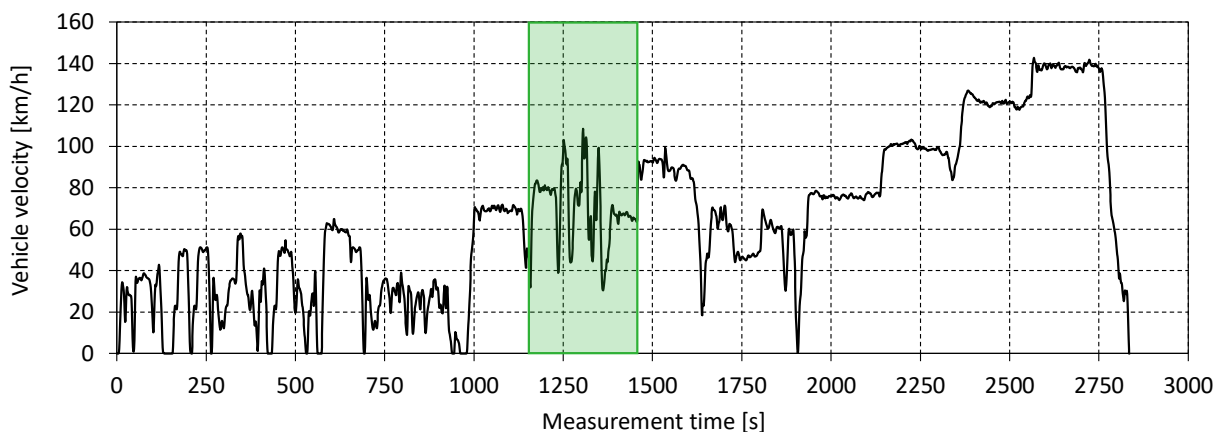


Figure 51: Velocity profile over time for real drive cycle RDC1 for motorcycles with marked sport-orientated uphill section.

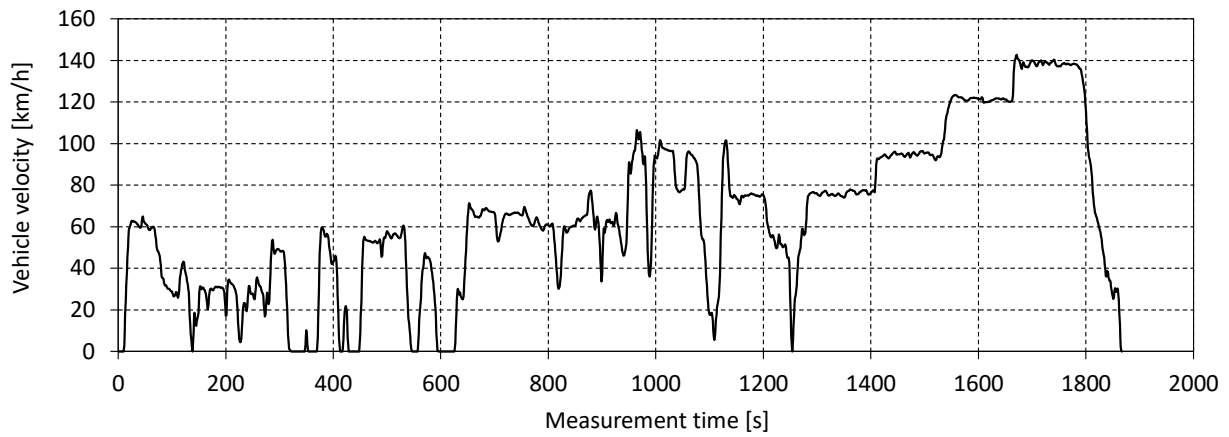


Figure 52: Velocity profile over time for real drive cycle RDC2 for motorcycles.

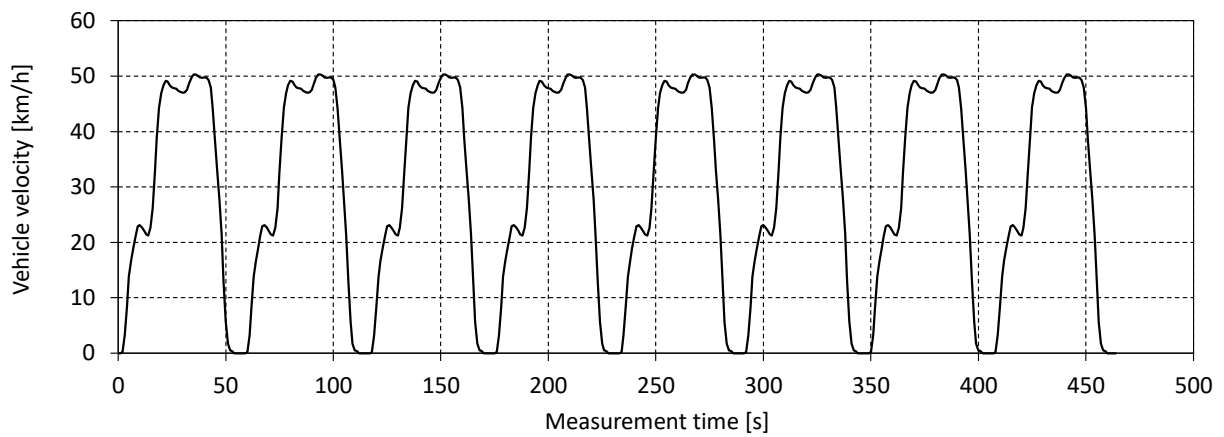


Figure 53: Velocity profile over time for real drive cold start test cycle for motorcycles.

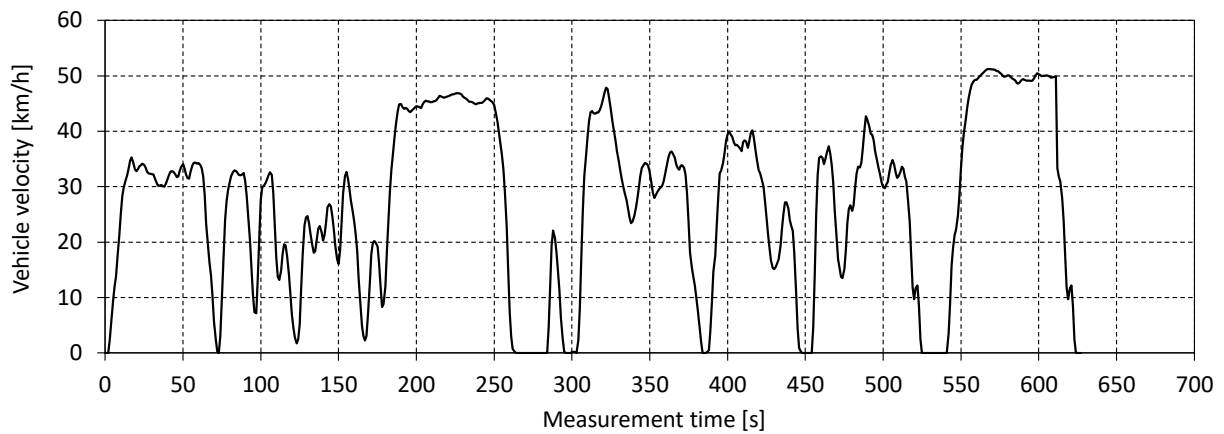


Figure 54: Velocity profile over time for real drive cycle RDM for mopeds.

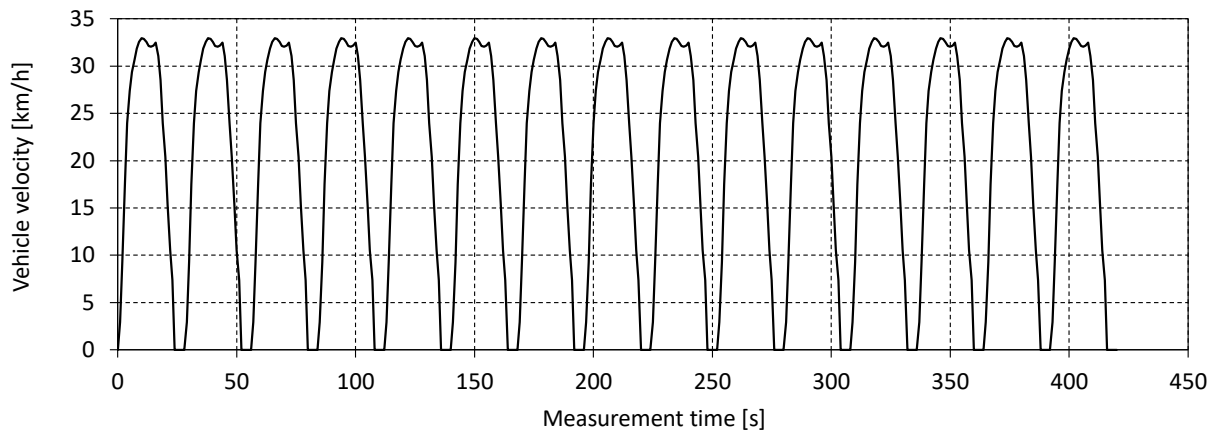


Figure 55: Velocity profile over time for real drive cold start test cycle for mopeds.

2.6.1 Assessment of Real Drive Cycles

The above described synthetic real drive cycles RDC have been evaluated in terms of their validity to reflect real world driving operation. Therefore, Figure 56 shows normalized engine power over normalized engine speed for different chassis dynamometer and on-road tests with a BMW F800GT motorcycle. The gold reference points indicate the engine map utilization for the type approval test WMTC, whereas the green points display operation points for the described real drive cycle RDC1. Moreover, blue points reflect the on-road test at the test track “Arzberg”. Figure 56 clearly shows the inadequate testing of the motorcycle with its type approval test in comparison to on-road driving. Furthermore, one can see that the RDC1 test cycle covers the same area of the engine map as the on-road test. The coverage is slightly thinner which is mainly due to test duration in this case. Nevertheless, the engine map utilization of the synthetic real drive cycle can be classified as sufficient.

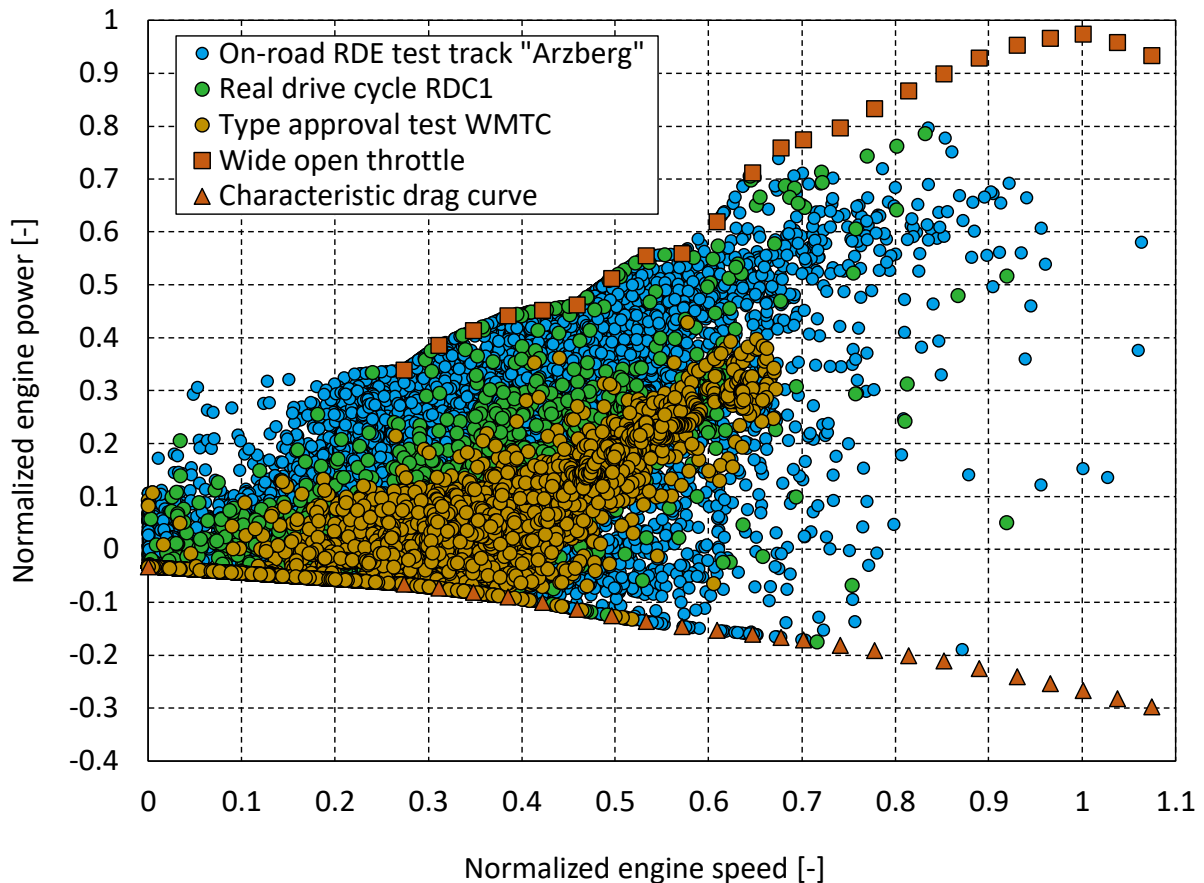


Figure 56: Normalized engine power over normalized engine speed for different chassis dynamometer and on-road tests with a BMW F800GT motorcycle.

The following illustrations Figure 57 and Figure 58 expand on this analysis. The first picture shows the appearance ratio for overall test duration over engine speed and throttle angle for the type approval test on the left-hand side and for the RDC1 test on the right-hand side. Figure 58 shows the corresponding diagram for the on-road test track “Arzberg”. The better coverage of the engine map of the RDC1 test can be seen as well as a clear shift of the main operation points in terms of their appearance ratio for overall test duration. Exemplarily, a major operation area around 25 [%] throttle angle position and 6000 [rpm] can be seen in RDE tests which is not covered by WMTC but by RDC1 tests. This analysis is extended by the corresponding emission test results – what adds the major significance to that shift – in the following chapters 3 and 4.1.4.

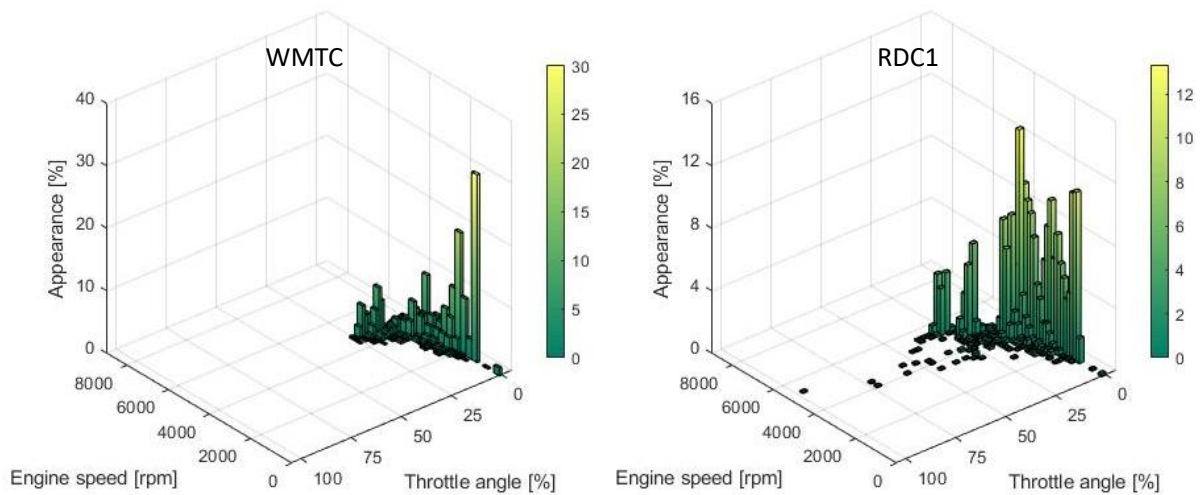


Figure 57: Time shares for overall test duration over engine speed and throttle angle for type approval test WMTC on the left side and real drive cycle RDC1 on the right side for a BMW F800GT motorcycle.

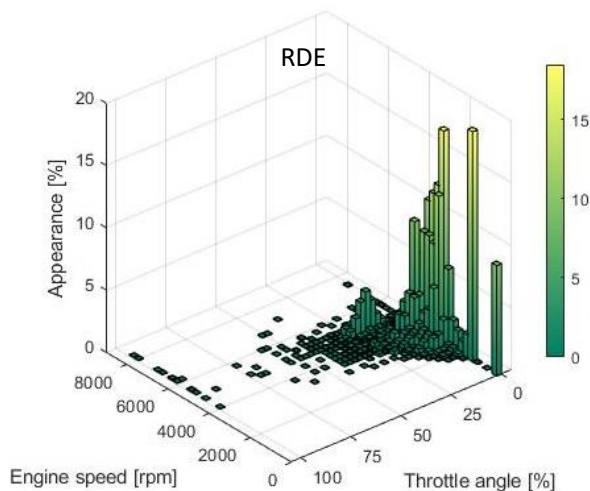


Figure 58: Time shares for overall test duration over engine speed and throttle angle for the on-road test track “Arzberg” for a BMW F800GT motorcycle.

Further analysis was made concerning the trip indicators for these different motorcycle tests. Figure 59 illustrates the trip indicators VA_{pos} and RPA over mean velocity for the type approval test WMTC with gold dots, the RDC1 test with green dots and a mix of on-road RDE tests with blue dots. The dashed black line describes automotive boundaries as described above. This illustration clearly shows that real world dynamic behavior of motorcycles is met in a better way with the generated real drive cycles than with the type approval test WMTC. It was also shown that more realistic driving dynamic can be represented by chassis dynamometer tests, keeping in mind the above discussed limits of the test rig (see section 2.2.1).

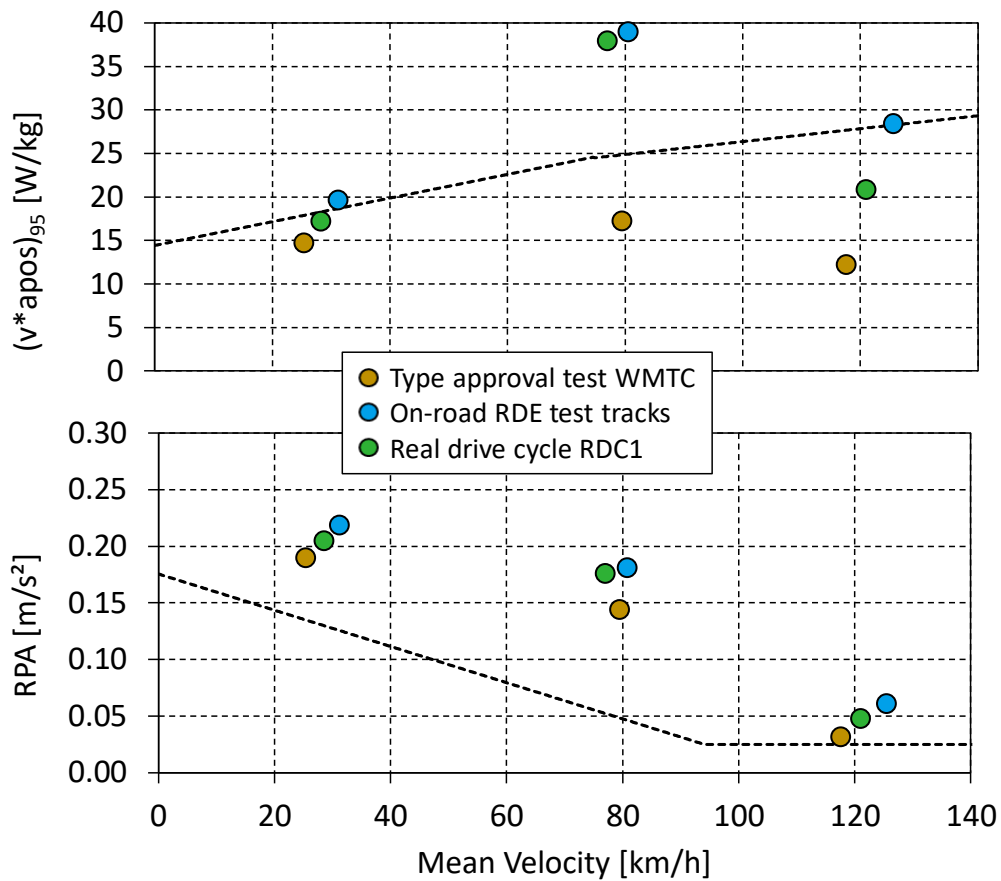


Figure 59: Dynamic trip indicators VA_{pos} and RPA over mean velocity for type approval test WMTC, real drive cycle RDC1 and a mix of on-road RDE tests.

Further on, the RDC test cycles were used for detailed emission analysis of different PTWs. Moreover, these chassis dynamometer tests could be used as learning input for the real drive emission simulation of motorcycles which will be described in chapter 0.

3 Results of the RDE measurement methodology

A huge amount of on-road test data was collected to analyze and to better understand real drive behavior in terms of RDE and fuel consumption of motorcycles. The state-of-the-art measurement equipment delivered reliable emission data and it can be shown that on-road driving behavior and therefore emission and fuel consumption values considerably differ from values of current chassis dynamometer test cycles [18].

This chapter sums up the emission measurement results of on-road RDE measurements as well as of chassis dynamometer measurements including the real drive cycle tests to fully cover all investigated possibilities and to pave the way for the development of a so-called RDE measurement methodology. This term is introduced to describe a possible comprehensive assessment approach for RDE for all the introduced test objects as the state-of-the-art measurement equipment for on-board tests is not sufficiently applicable on all vehicle classes. An extended discussion and the possible and particular form and description of the RDE measurement methodology will be given in section 5.1

The results of the main test objects of this study will be presented further on, which have been a BMW F800GT Euro 3 motorcycle as well as two more Euro 4 motorcycles, explicitly a BMW F800R and a BMW G1200GS motorcycle.

At first, on-road measurement results will be presented, followed by emission measurement results of chassis dynamometer tests. Moreover, special measurement results of non-regulated pollutant emissions are shown in section 3.3. Finally, section 3.4 gives a consolidating discussion of the emission results and leads over to a short discussion of further possible use of RDE measurements or real drive cycle measurements.

3.1 On-road measurement results

This section introduces to the results of RDE measurements for a Euro 3 motorcycle and expands on comparative results for Euro 4 motorcycles. The following Table 15 sums up a comparison of the “Arzberg” RDE test track measurement with on-board measurement equipment and a WMTC for the BMW F800GT Euro 3 motorcycle. The emission results in Table 15 are weighted according to [15]. All other presented emission results are not weighted but just average results per test. It can be shown that the real world test results in higher emissions than the type approval test. Nitric oxides raised about 56 [%] and carbon monoxide raised about 22 [%]. CO₂ emissions and fuel consumption respectively are not significantly higher than in the type approval test.

Figure 60 illustrates the full RDE measurement trace over time for the “Arzberg” test track for the most relevant parameters. The first diagram shows vehicle velocity and geodetic altitude, followed by engine speed and throttle angle in the next diagram. There are plotted temperatures before and after catalyst in the third diagram and the final two illustrations show the emission components CO₂, CO and NO_x. As said before, HC emissions could not be measured with this PEMS.

Table 15: Emissions and further characteristic parameters of type approval test WMTC compared to the RDE measurement at the test track “Arzberg”.

	WMTC ^(a)	RDE test
CO ₂	143.917 g/km	122.690 g/km
CO	0.914 g/km	1.114 g/km
NO	0.169 g/km	0.262 g/km
NO ₂	0.001 g/km	0.003 g/km
NO _x	0.170 g/km	0.265 g/km
Fuel consumption ^(b)	6.40 l/100km	5.59 l/100km
Mean velocity.	57.18 km/h	74.92 km/h
Mean engine speed	2991.82 rpm	3078.54 rpm
Duration	1840.00 s ^(c)	6168.00 s
Driven distance	29.08 km	128.17 km
Temperature ^(d)	24.4 °C	32.37 °C
Mean ambient pressure ^(d)	974.5 hPa	974.6 hPa
Relative air humidity ^(d)	38.0 %	44.87 %

(a) 350 kg tare weight which corresponds to a measurement with mounted PEMS.

(b) Calculated by carbon balance.

(c) The type approval test WMTC has a standard duration of 1800 [s]; the additional 40 [s] are because of additional measurement time before and after the test.

(d) Ambient conditions at measurement start

Figure 61 and Figure 62 illustrate the cold start phase and the rural part of the same test in more detail. The engine warm-up until catalyst light-off can be determined after about 110 [s] for this test object and corresponds to type approval tests. The first phase until catalyst light-off causes high emissions, especially for carbon monoxide and also for hydrocarbons. The light-off can be determined by the lowering of the carbon monoxide emissions or this moment can be set by the temperature after CAT. Exemplarily, the temperature diagram in Figure 61 illustrates that the temperature after catalyst raises above the temperature before catalyst after around 180 [s]. This indicated that the catalyst is fully working as the summed catalytic reactions are exothermic. The time duration before light-off is very critical as during this first phase a significant amount of pollutants are emitted which is relevant for overall emission level and for reaching legislative limits respectively. It will be shown that Euro 4 motorcycles comprise high improvements in this field.

Moreover, Figure 62 illustrates the rural route section of the “Arzberg” test. In comparison to the type approval test, where CO peaks are mainly occurring during engine warm-up and overall peaks do not exceed 400 [ppm] for this motorcycle, the RDE test shows many high peaks in carbon monoxide emissions. Especially high accelerations in combination with a positive road gradient cause high CO emission – and, therefore, probably also HC emissions – due to richer mixture for drivability purpose during accelerations. An exemplary phase is illustrated between 2200 [s] and 2300 [s] measurement time in Figure 62. Acceleration enrichment for this motorcycle is depending on throttle angle gradient and on values above 90 [%] throttle angle. Also, NO_x emissions can be determined as very high between 2100 [s] and 2200 [s] measurement time in Figure 62. The reason for this is the higher engine load during the hilly section of the “Gollersattel” (see geodetic altitude). Additionally, Figure 63 illustrates cumulated emissions for the whole RDE test. Four specific areas, where high gradients in emission level occur, are marked. The area (3) corresponds to the before mentioned section “Ries” and also the abruptly increase of carbon monoxides between 2200 [s] and 2300 [s] in Figure 62 can be seen in this area.

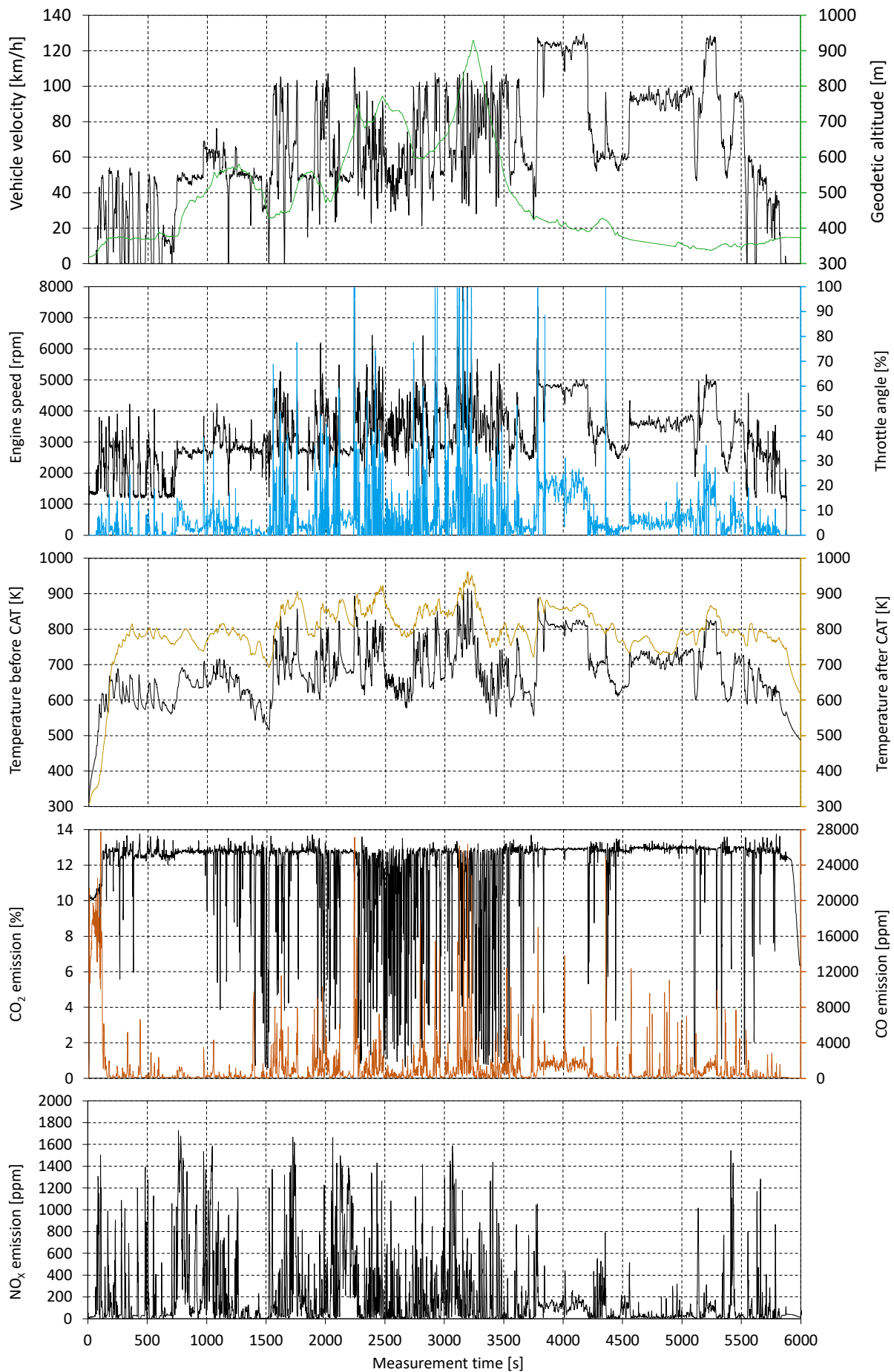


Figure 60: Measurement result of RDE route “Arzberg” with BMW F800 Euro 3 motorcycle.

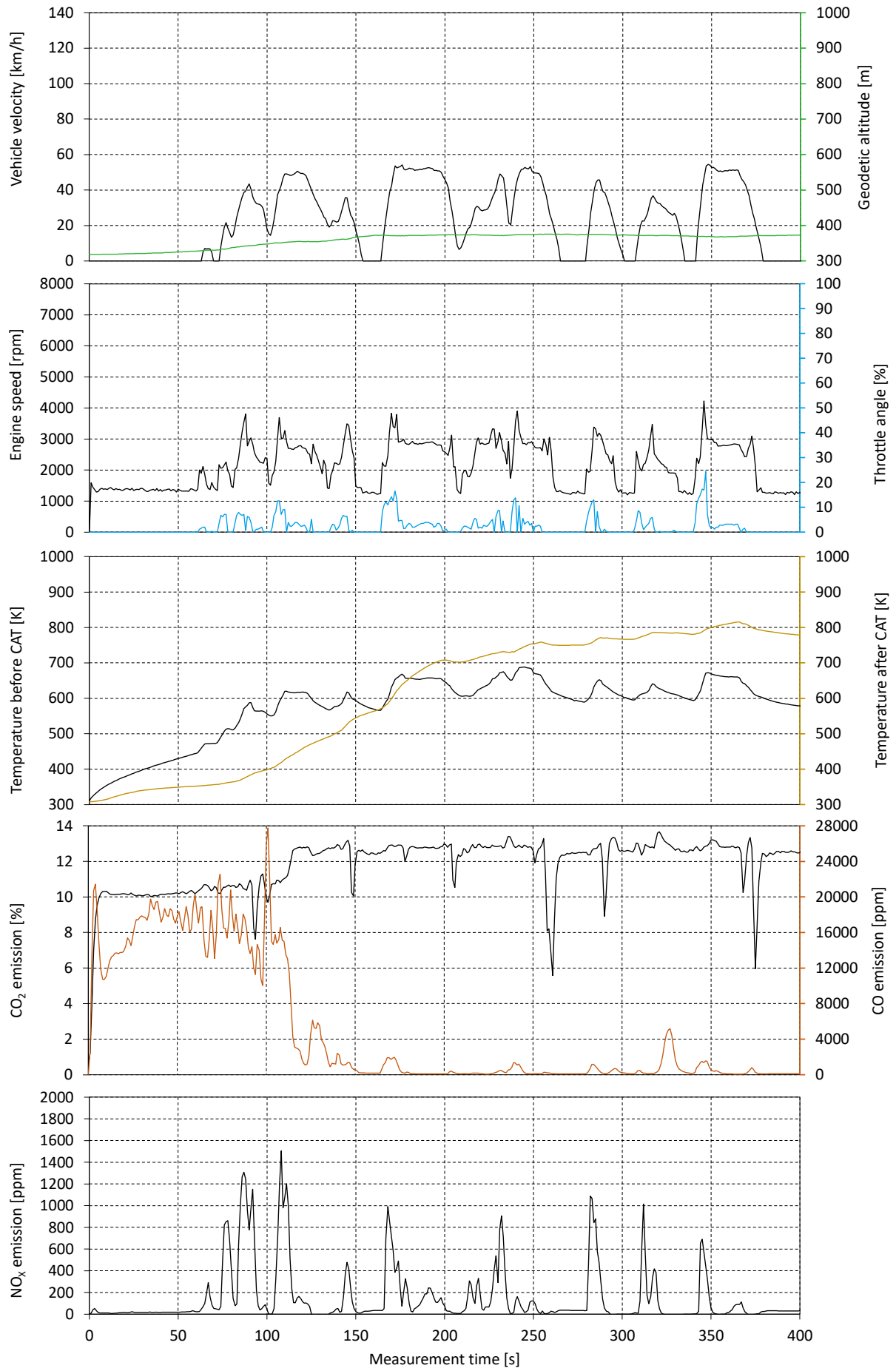


Figure 61: Detailed (out of Figure 60) RDE measurement result for the cold start phase.

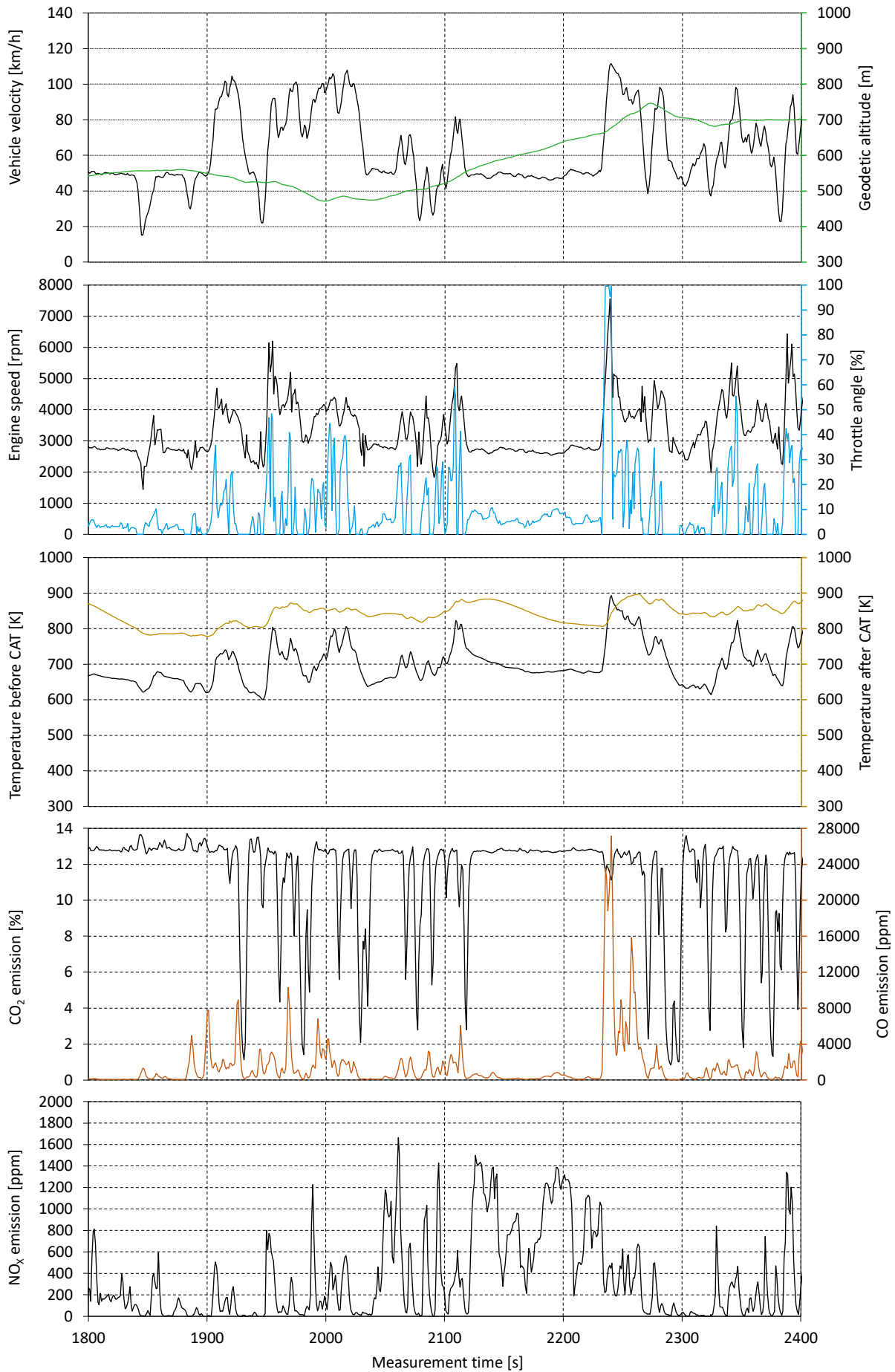


Figure 62: Detailed RDE measurement result for the rural part of the „Arzberg“ test track.

The first area (1) in Figure 63 marks the cold start phase until the catalyst light-off as described above. The second area (2) can be ascribed to a city access road which has a very high road gradient. This section is driven with almost stationary engine load conditions but it lasts for about six minutes which causes a high thermal load and therefore a high gradient in nitric oxide emissions. The above-mentioned driving scenario “Gollersattel” between 2100 [s] and 2200 [s] measurement time in Figure 62 has a similar cause.

The third (3) and fourth area (4) can be ascribed to a highly dynamic driving pattern. The road has sharp bends and a high road gradient in this area of the test track which causes high accelerations up to 4 [m/s²] and high engine loads. Moreover, many short but steep throttle angle gradients appear in this road section and additionally cause richer mixture in many cases. The result is a carbon monoxide emission of around 18 [%] of the whole test cycle just for the marked area four (4) in Figure 63. The area three (3) is very similar to (4) and is illustrated more detailed in Figure 62 between 2200 [s] and 2300 [s] measurement time and described above.

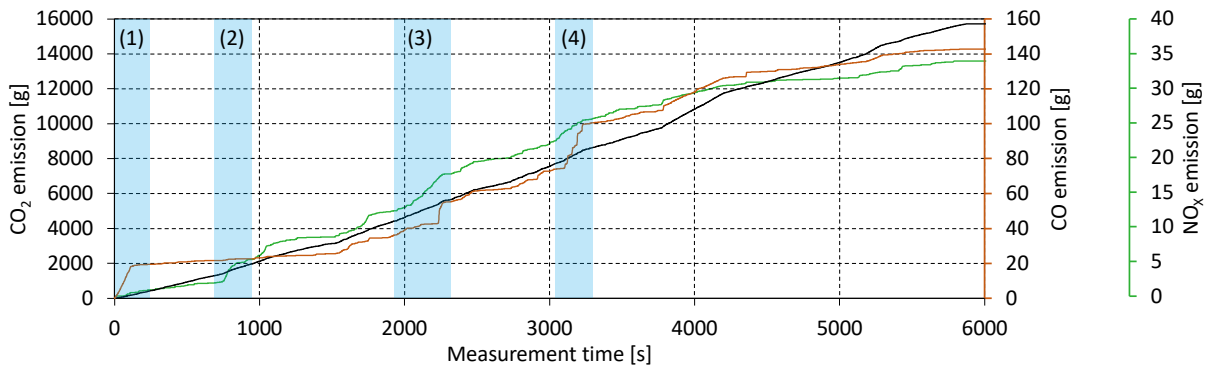


Figure 63: Cumulated emissions for the RDE test track „Arzberg“ with marked areas of high gradients in cumulated emission level.

Figure 63 clearly illustrates the above described emission relevant driving scenarios for RDE measurements. The marked areas (3) and (4) are not covered by any type approval test so far, but these driving scenarios are real world scenarios and even those are not sport-orientated driven at all. Thus, the WMTC as type approval test can be classified as not dynamic and not fully representative for real world driving. Even for this specific test object the throttle angle position will never exceed 30 [%] in its type approval test.

Figure 64 and Figure 65 summarize real drive emission RDE test results for a BMW F800R Euro 4 and a BMW G1200GS Euro 4 motorcycle divided in test segments and including legislative limits, but for type approval test. The first group of bars shows the overall test result. The following groups illustrate the emission results for the test segments urban, rural and motorway.

The higher amount of carbon monoxide emissions in the urban part in Figure 64 can be mainly ascribed to the cold start emissions, whereas the relatively high share of NO_x emissions in the motorway part is caused by a high specific engine load during this test section. Nevertheless, all emission components are in-between legislative limits (for type approval tests) which is a very positive result if one thinks about conformity factors for RDE in passenger car legislation Euro 6d.

Comparing the NO_x emissions in Figure 64 and Figure 65 for the motorway part, it is even more obvious that the higher NO_x emissions are dependent on specific engine load as the values for

the BMW G1200GS are relatively low due to its additional 40 [%] engine capacity. However, carbon monoxide emissions result in relatively high values in the urban part for this motorcycle. This could be ascribed to a lot of phases where vehicle velocity is low and the engine is operated in part load or idling due to its high engine capacity and the very low loads during stop-and-go traffic situations in the urban section.

Of course, additional differences arise from the engine concepts and applications. Exemplarily, the F800 engines emissions are inter alia controlled by one lambda probe for two cylinders which can cause higher raw emissions in some operation points and must be compensated by a given capacity of the catalyst. By contrast, the 1200 engine is a two cylinder boxer engine with two separate lambda probes and a totally different engine application.

Nevertheless, the RDE measurement results of these motorcycles are very gratifying as both overall emission levels are in-between legislative limits for the investigated on-road tests.

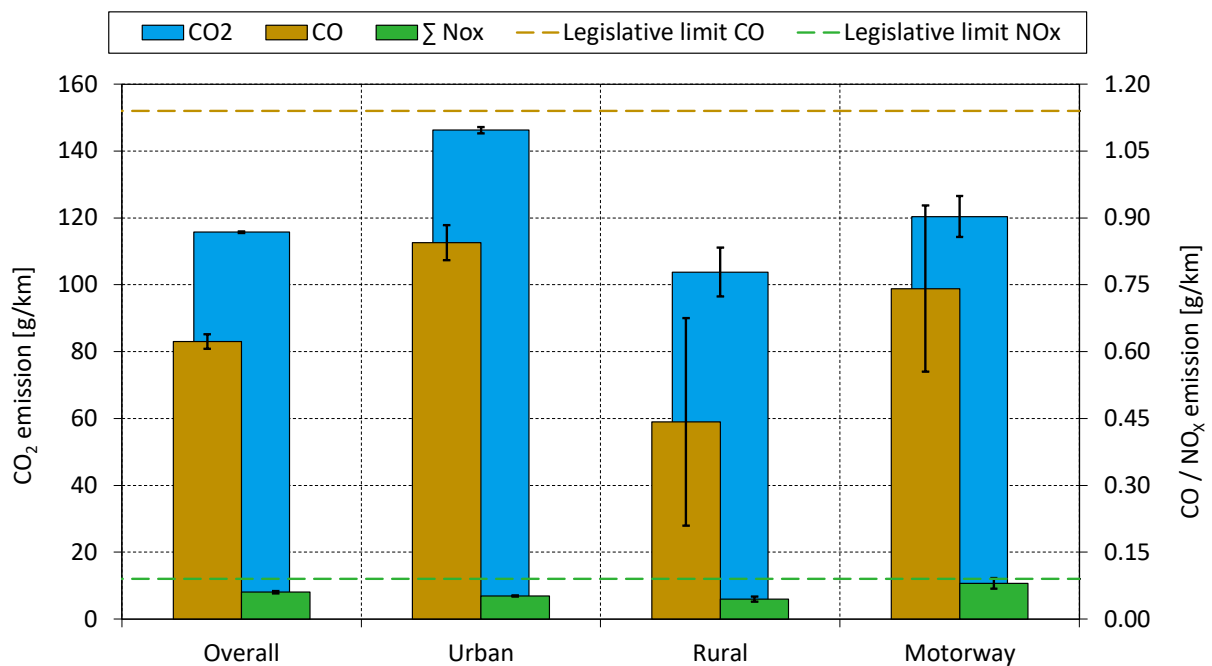


Figure 64: On-board real drive emission RDE test results (summed emissions over test or part of test) for a BMW F800R Euro 4 motorcycle divided in test parts and including legislative limits of type approval test.

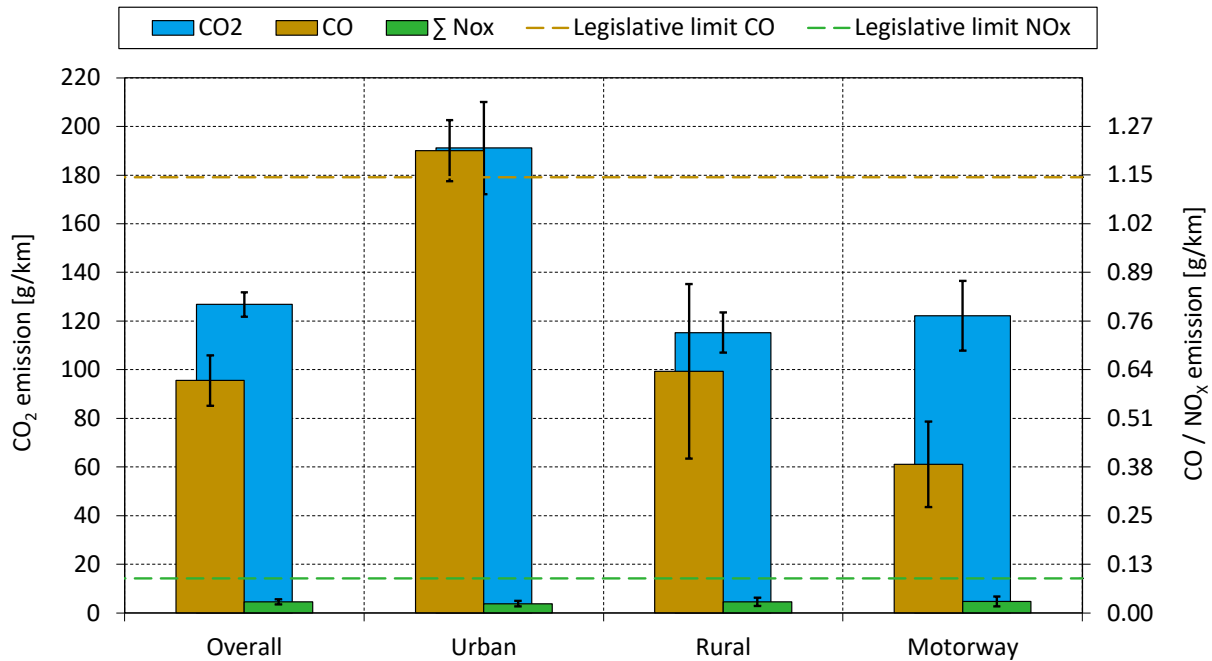


Figure 65: On-board real drive emission RDE test results (summed emissions over test or part of test) for a BMW 1200GS Euro 4 motorcycle divided in test parts and including legislative limits of type approval test.

Further on-board RDE measurement results will be shown in section 3.4 for a comparison of chassis dynamometer tests and on-road test and for the final discussions in chapter 0.

3.2 Chassis dynamometer measurements

This section introduces detailed emission measurement results on chassis dynamometer, once again for the three main test objects BMW F800GT Euro 3, BMW F800R Euro 4 and BMW G1200GS Euro 4. Therefore, Figure 66, Figure 67 and Figure 68 expand on the discussion about influences of additional mass on the BMW F800GT Euro 3 motorcycle (see section 2.4.1.1). Further on, real drive cycle RDC measurements are presented for the Euro 4 motorcycles. A comprehensive comparison of all emission tests is given in section 3.4, wherein the chassis dynamometer emission measurement results are extended.

Figure 66 and Figure 67 illustrate HC, CO and NO_x emissions separated for urban, rural and motorway sections for type approval tests WMTC and RDC tests with differently adjusted overall vehicle weight. The vehicle weight of 350 [kg] corresponds to the tare weight of the test object including a full PEMS as described above. Two main influences for emission formation can be derived from these figures.

Firstly, CO emissions are clearly influenced by cold start emissions and driving dynamic. The right-hand sided diagram in Figure 66 illustrates with blue bars that the cold start emissions are more relevant for WMTC than for RDC, which is caused by test duration and catalyst light-off, triggered by engine load during the cold start phase respectively. Moreover, the orange bars for the RDC tests compared to WMTC test in the same diagram indicate a clear dependency of CO emissions on driving dynamic. Richer mixture in acceleration phases and for engine protection as well as throttle angle positions larger than 90 [%] are triggering these results. Especially richer mixture, due to the same reasons, is also causing the disproportionate increase of CO

emissions for the RDC test with 350 [kg] in the rural part. The HC emissions are very much linked to carbon monoxide emissions in their variation over the test cycles.

Secondly, the NO_x emissions are significantly deteriorated by overall vehicle weight and driving dynamic. This could be affiliated to the higher loads in the engine map. One has to keep in mind that the engine load is higher for the more transient real world test cycles RDC and therefore the raising of emission component, especially for NO_x , might be even enforced. This clear trend can be seen in the rural part in Figure 67, wherein the emissions rise with weight for one to the next WMTC and again with driving dynamic from WMTC to RDC.

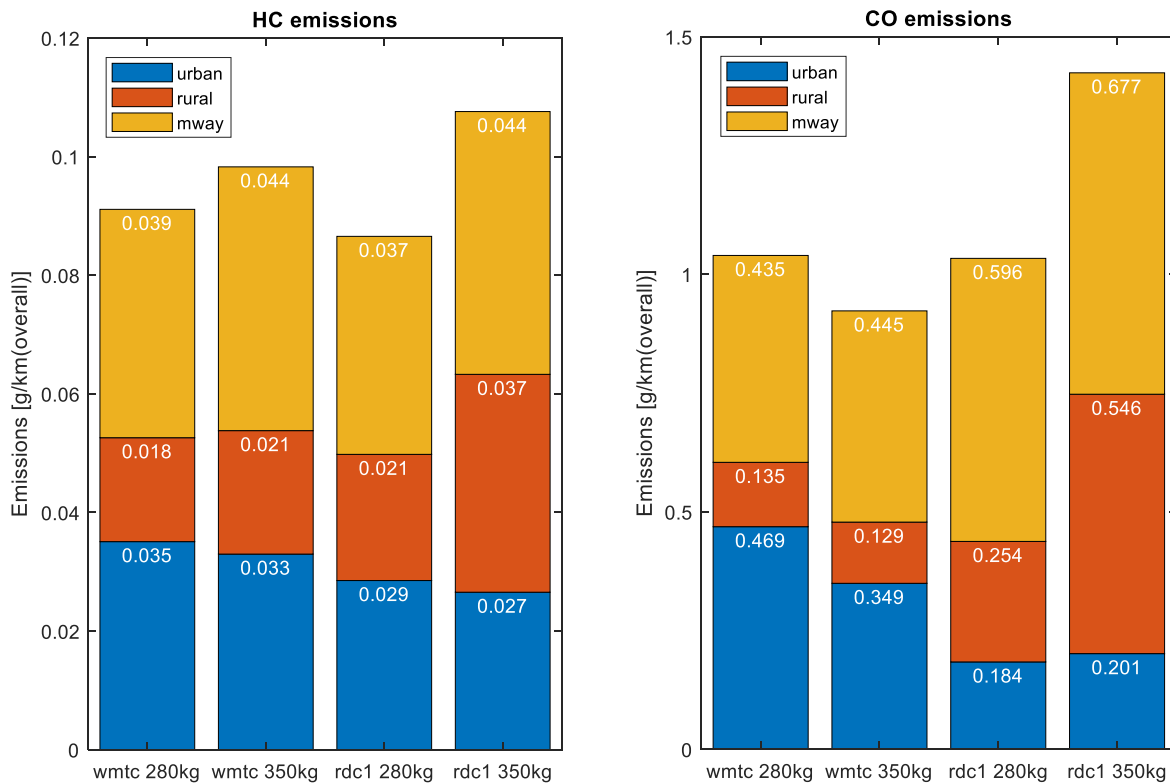


Figure 66: HC and CO emissions for urban, rural and motorway sections for type approval tests WMTC and RDC tests with different adjusted overall vehicle weight for BMW F800 Euro 3 motorcycle.

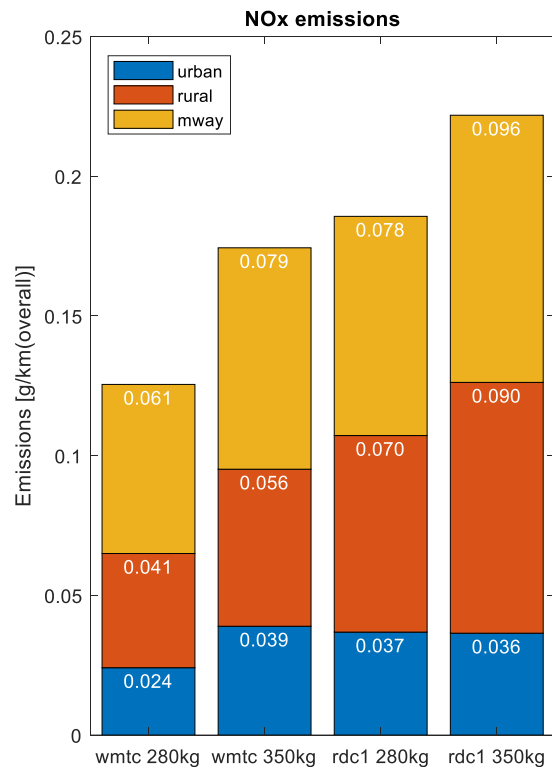


Figure 67: NO_x emissions for urban, rural and motorway sections for type approval tests WMTC and RDC tests with different adjusted overall vehicle weight for BMW F800 Euro 3 motorcycle.

Further analysis of the above described tests with the BMW F800GT Euro 3 motorcycle included the evaluation of carbon monoxide and NO_x emissions for influenced of driving dynamic indicators. Figure 68 illustrates the emissions over the dynamic trip indicator VA_{pos} . In this diagram, especially the carbon monoxide emissions show a significant increase for higher driving dynamic. This underlines the influences on emission formation discussed above. Furthermore, the lack of engine operation points in the type approval tests for higher VA_{pos} values (for the groups 500 [W/s] and 600 [W/s]) are reminding of above discussed representation of on-road driving pattern. Another interesting issue are the missing bars for WMTC test in the groups of 400, 450 and 550 [W/kg]. The lack of these peaks can only be a reason (aside inaccuracy in the measurement trace) of different acceleration behaviors of the motorcycle with PEMS for the same predefined velocity profile compared to the test without PEMS.

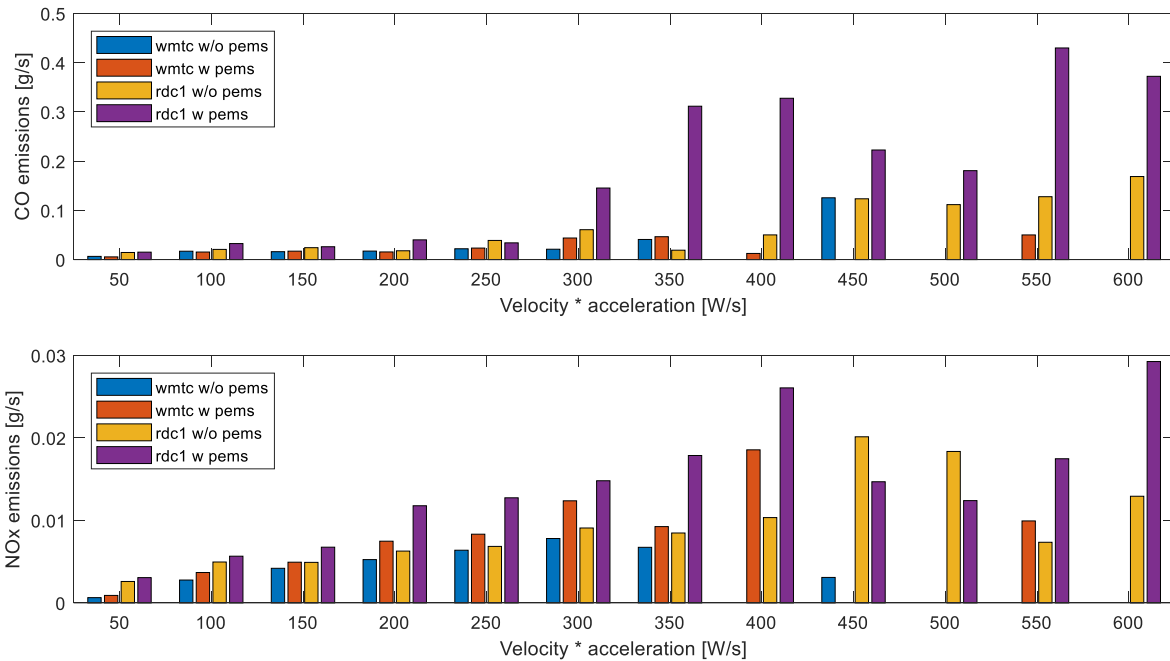


Figure 68: CO and NO_x emissions for type approval tests WMTC and real drive cycle RDC tests with different vehicle weight over dynamic trip indicator VA_{pos} measured with a BMW F800GT Euro 3 motorcycle.

The following illustrations expand on real drive cycle RDC1 measurements but for the Euro 4 test objects. Real drive cycle chassis dynamometer emission test results divided in test segments and including legislative limits are presented in Figure 69 for the BMW F800R motorcycle and for the BMW G1200GS motorcycle in Figure 70. Both results are similar to the above presented RDE measurement results (compare to Figure 64 and Figure 65 and its discussion) in terms of relative assignment to the other emission components. But differences appear in terms of their absolute values.

Figure 69 illustrates around half the carbon monoxide emission output for the BMW F800R motorcycle compared to Figure 64 and Figure 65. By contrast, the NO_x emissions are even higher for each driving part compared to Figure 64. For the BMW G1200GS motorcycle both emission components, CO and NO_x, are far below the RDE emissions compared to Figure 65.

These results lead to the remaining need for on-road emission tests to adequately and reliably assess real drive emissions RDE for motorcycles. The presented real drive cycles RDC can serve as estimations but will not substitute any real world measurement with its vast variability of driving scenarios, route options, road parameters and driving pattern possibilities.

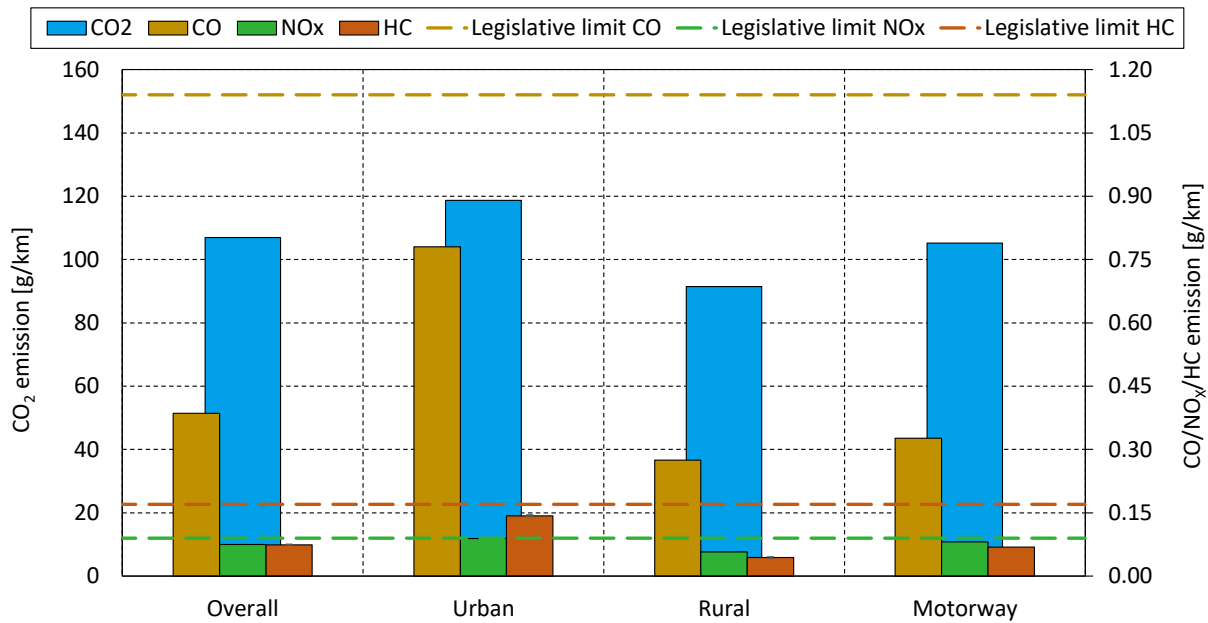


Figure 69: Real drive cycle RDC1 chassis dynamometer emission test results for a BMW F800R Euro 4 motorcycle divided in test segments and including legislative limits.

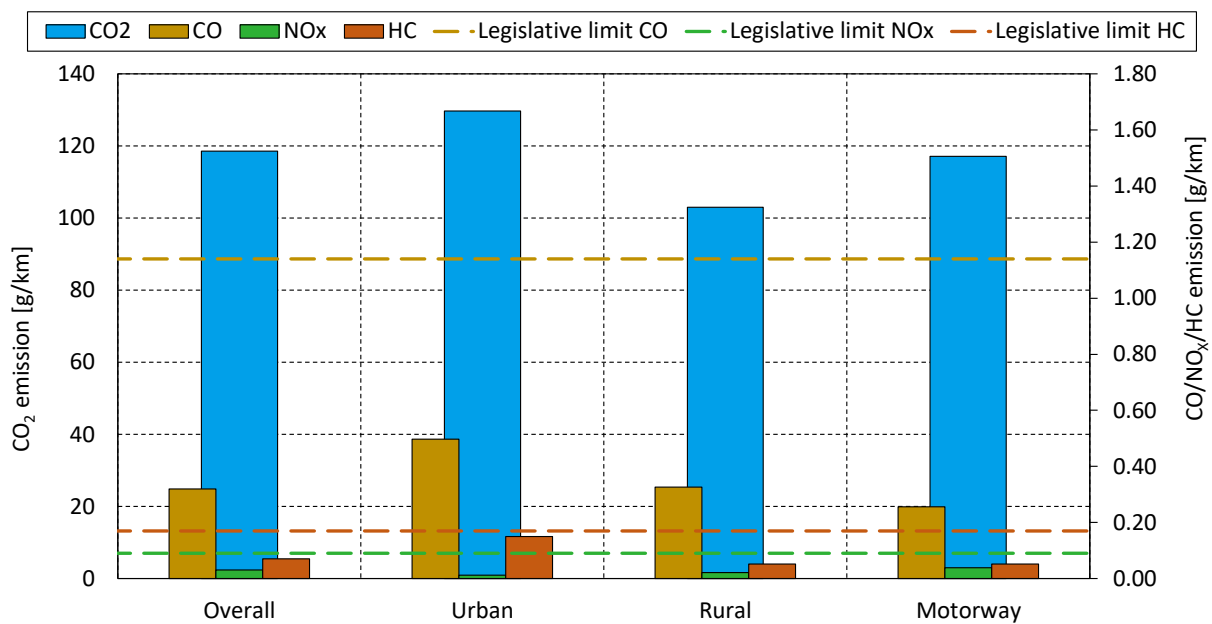


Figure 70: Real drive cycle RDC1 chassis dynamometer emission test results for a BMW G1200GS Euro 4 motorcycle divided in test segments and including legislative limits.

The usability and relevance for real drive cycle RDC tests in comparison to type approval tests was shown. Especially, case studies like the presented weight variation for the more dynamic RDC tests served deeper insights into emission relevant driving scenarios and parameters. Moreover, the use of additional laboratory measurement technologies at the chassis dynamometer in combination with real drive cycles is another benefit when it comes to RDE evaluations of non-regulated emissions. The following section expands on this topic.

3.3 Non-Regulated gaseous emissions

For many measurements at the chassis dynamometer, a Fourier transform infrared spectroscopy FTIR measurement system was used for additionally detecting not legislatively limited gaseous emissions. This measurement gauge can analyze the exhaust gas for a lot of emission components. Hence, a selection of the most relevant substances has to be made first. The following Table 16 and Table 17 sum up the assessment of a selection of substances and a short description of their impact on human and environmental health. With a BMW F800GT Euro 3 motorcycle, 23 test cycles, type approval tests and real drive cycles, were driven including the FTIR analyzer. These tests were included in the weight factors for assessing the relevance of substances in Table 16.

The assessment criteria for Table 16 were set between 0 and 4, whereby a value of 0 means that there is no relevant risk caused by the substance. Firstly, the impact on climate change and the hazardous effect on human and environmental health were evaluated and summed up as environmental impact reference number in the column (C). Table 17 gives a short overview of some relevant components and their potential danger. Secondly, the occurrence of the substances was evaluated using an analysis of the whole measurement data and summed up in column (G) as a concentration reference number. Herein, the column (D) describes a ranking factor for the mean value of the concentration. The column (E) describes an assessment factor for the time course of the concentrations (e.g. if there occur spiky peaks etc.) and the column (F) shows a factor for the assessment of the sum of emissions over a test cycle. Finally, column (H) sums up all criteria in an overall assessment. A high number means serious threat for human and environmental health and simultaneously a relevant emission concentration in the evaluated measurements.

Table 16: Assessment criteria and evaluation of importance for measurement of not legislatively limited gaseous emissions.

	Weight	C2H2	CH4	C2H6	C6H6	CH3OH	NH3	C3H6	SO2	N2O	C4H6	HCHO
A	0.5	0	4	0	0	0	0	0	0	4	0	0
B	0.5	1	1	1	4	2	3	1	4	1	4	4
C		0.5	2.5	0.5	2	1	1.5	0.5	2	2.5	2	2
D	0.25	2	4	1	2	1	3	1	1	0	0	1
E	0.25	0	3	1	1	0	1	0	2	2	0	1
F	0.5	1	3	2	4	1	3	2	1	1	1	1
G		1	3.25	1.5	2.75	0.75	2.5	1.25	1.25	1	0.5	1
H		0.75	2.87	1	2.37	0.87	2	0.87	1.62	1.75	1.25	1.5

- A Impact on climate change
- B Hazardous effect on human and environmental health
- C Environmental impact reference number
- D Ranking factor for the mean value of the concentration
- E Assessment factor for the time course of the concentration
- F Assessment of the sum of emissions over the test cycles
- G Concentration reference number
- H Overall assessment

Table 17: Assessment of hazardous impact on human and environmental health of selected not legislatively emission components.

C ₂ H ₂ Acetylene	1	Non-toxic; anesthetic effects
C ₆ H ₆ Benzene	4	Carcinogenic and toxic; harming of the central nervous system and of the hematopoietic system for chronic toxicity;
HCHO Formaldehyde	4	Carcinogenic; trigger allergies; causing skin, respiratory and eye irritations; TLW: 0.37 [mg/m ³];
C ₂ H ₆ Ethane	1	Weak anesthetic effects;
CH ₃ OH Methanol	2	Harm of the central nervous system, however lower risk of ingestion via the respiratory tract; TLW: 270 [mg/m ³];
SO ₂ Sulfuric acid	4	Highly toxic; symptoms of poisoning after very low dose; environmental harm caused by acid rain; involvement in smog forming; TLW: 2.7 [mg/m ³];
C ₃ H ₆ Propane	1	Not toxic; acts as a mild anesthetic with high dose; TLW: 1800 [mg/m ³];
CH ₄ Methane	1	Not toxic; acts as a mild anesthetic with high dose;
NH ₃ Ammonia	3	NH ₃ vapors are irritating and caustic; TLW: 14 [mg/m ³];
N ₂ O Nitrous oxide	1	Anesthetic with high dose; danger of suffocation; TLW: 180 [mg/m ³]; very high greenhouse gas effect;
C ₄ H ₅ (1,3-Butadiene)	4	Carcinogenic and toxic; TLV: 11 [mg/m ³];

- TLV Threshold limit values of carcinogenic and mutagenic substances
- TLW Threshold limit value at work places

Table 16 and Table 17 already include the most relevant substances. For all test objects, presented in section 2.1, multiple repetitions of type approval tests and real drive cycle tests were measured. Figure 71 and Figure 72 illustrate the measurement results, divided in three vehicle categories. Especially the benzene emissions, as well as methane and ammonia emissions occur in relevant amounts. Exemplarily, the test results of benzene are correlating to published values for Euro 4 passenger cars, which are considered between 0.5 [mg/km] and 60 [mg/km] for the Artemis test cycle [49] [50] [51].

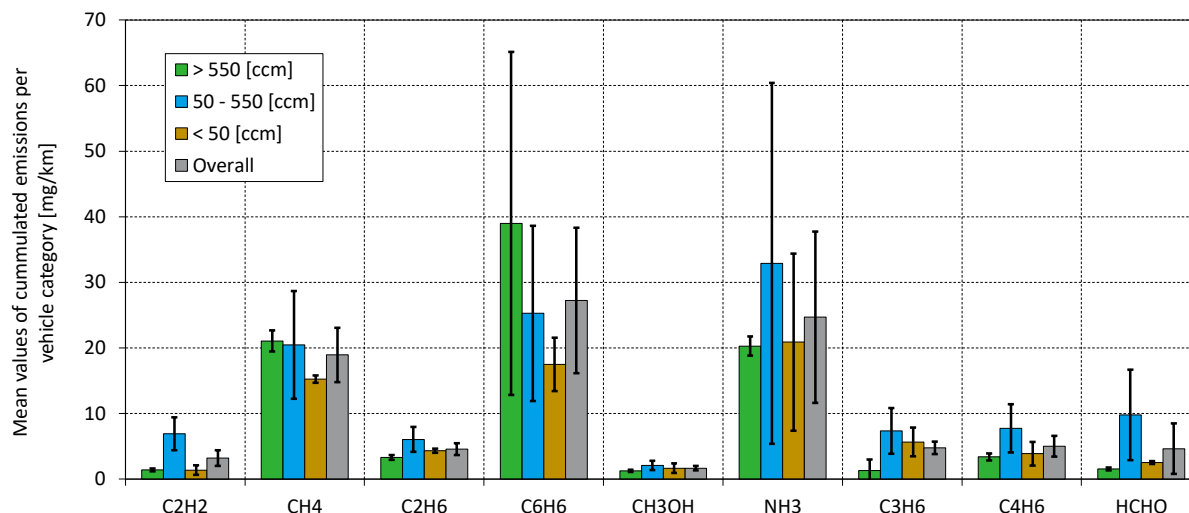


Figure 71: Mean values of cumulated not legislatively limited emissions per vehicle category and overall mean values in [mg/km] for Euro 3 motorcycles.

Figure 72 additionally illustrates carbon monoxide and nitric oxide on the right-hand side to illustrate the order of magnitude of the measured substances. Even if the emitted amount of not legislatively limited substances seems to be low, their impact on the environment is evident and with more stringent legislative limits their contribution will even rise. Moreover, with smarter detection gauges for these emitted substances, it is more likely that highly hazardous components like benzene will be regulated in the future [49].

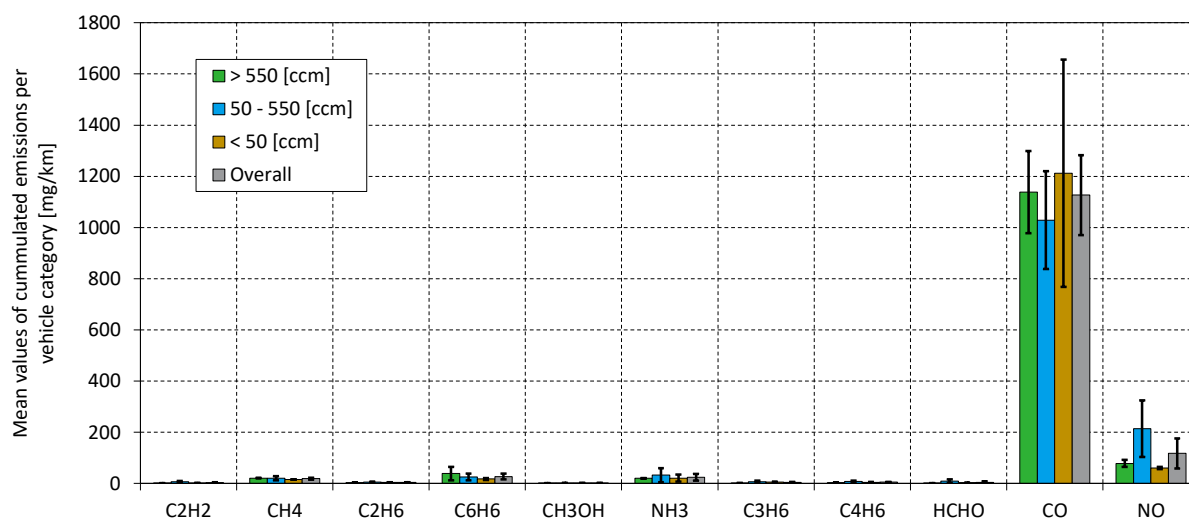


Figure 72: Mean values of cumulated not legislatively limited emissions per vehicle category and overall mean values in [mg/km], including CO and NO emissions.

Moreover, an assessment of not legislatively limited emissions was made including the evaluation of dynamic trip indicators. Figure 73 illustrates the above described substances over the dynamic trip indicator VA_{pos} for multiple chassis dynamometer measurements with a BMW F800GT Euro 3 motorcycle. Multiple type approval tests WMTC as well as multiple real drive cycles have been evaluated.

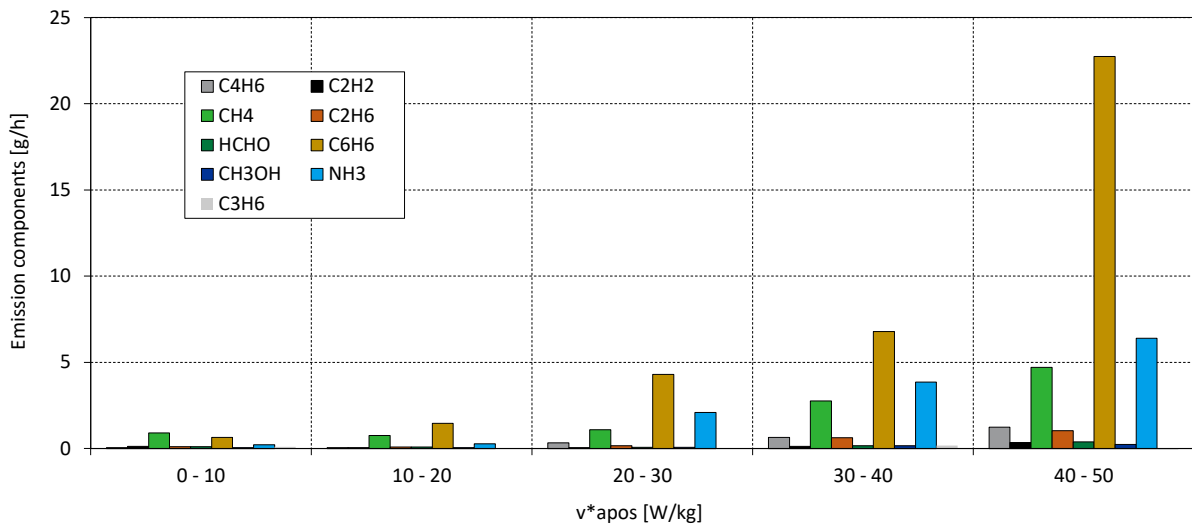


Figure 73: Not legislatively limited emission components in [g/h] over dynamic trip indicator VA_{pos} in [W/kg] for a BMW F800GT motorcycle.

In comparison to Figure 71, this illustration shows a disproportionate increase of benzene emissions with increasing driving dynamic compared to ammonia and methane, which are the second most relevant components. This phenomenon was also detected for the vehicle class between 50 [ccm] and 550 [ccm] engine displacement where the disproportionate increase of benzene was even more glaring.

In summary, relevant concentrations for benzene, ammonia and methane were detected for the investigated test objects and chassis dynamometer test cycles. Moreover, some substances like nitrous oxide occur in relevant concentrations due to its highly toxic and/or environmentally harmful properties. The testing of not legislatively limited emission by real drive cycle serves a great tool for estimating RDE. Exemplarily, above introduced Figure 68 in comparison to Figure 73 shows that the type approval test WMTC is not sufficiently covering on-road behavior of motorcycles. Hence, the combination of a measurement gauge for those substances and the real drive cycles give more representative results for these emission components.

3.4 Consolidating discussion of the emission results

Figure 74 to Figure 76 consolidate the emission measurement results for the three main test objects as described in the beginning of chapter 3. Emission components are illustrated as mean values for the measured test cycles WMTC, RDC and RDE-on-board-tests. HC emissions were not measured on-road as described above.

For all emission components and test objects a clear trend to higher emissions for the more dynamic test cycles can be identified. Carbon dioxide emissions vary in some cases what can be inter alia linked to the shift in operation points and the utilization of areas with better BSFC in the engine map as discussed in section 2.4.1.1.

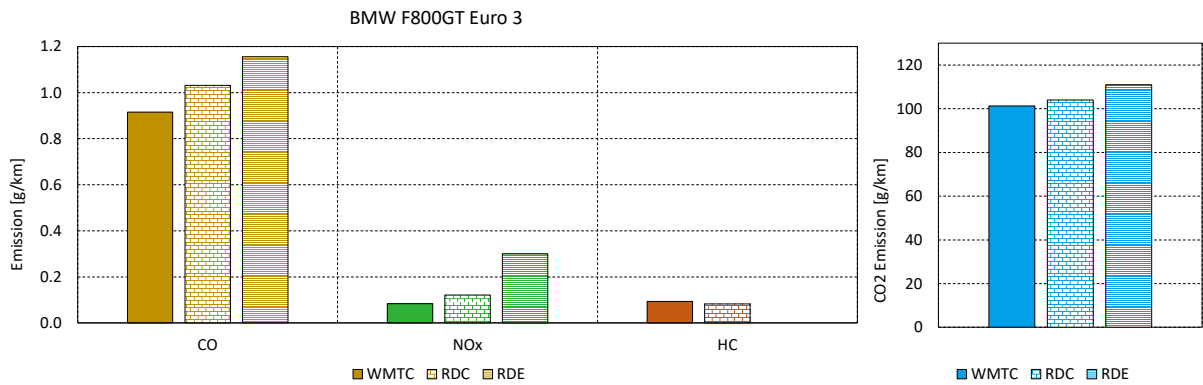


Figure 74: Comparison of WMTC, RDC and RDE measurement results for the BMW F800GT Euro 3 motorcycle.

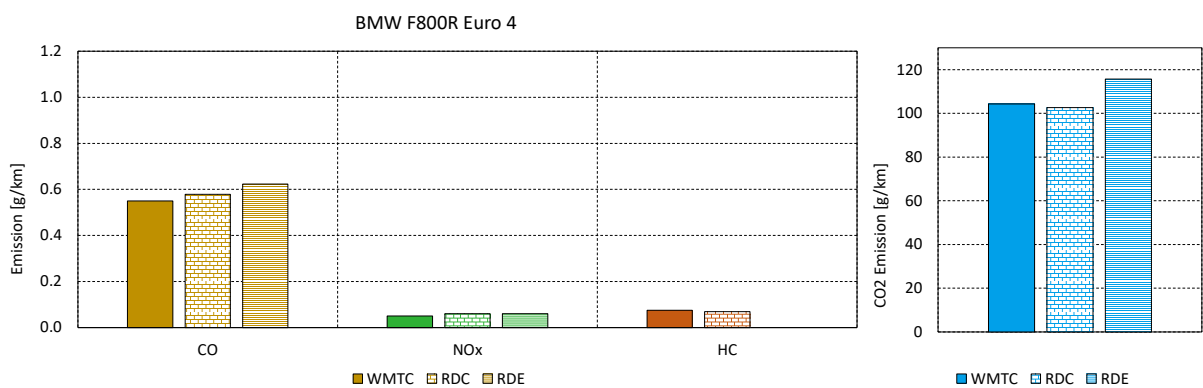


Figure 75: Comparison of WMTC, RDC and RDE measurement results for the BMW F800R Euro 4 motorcycle.

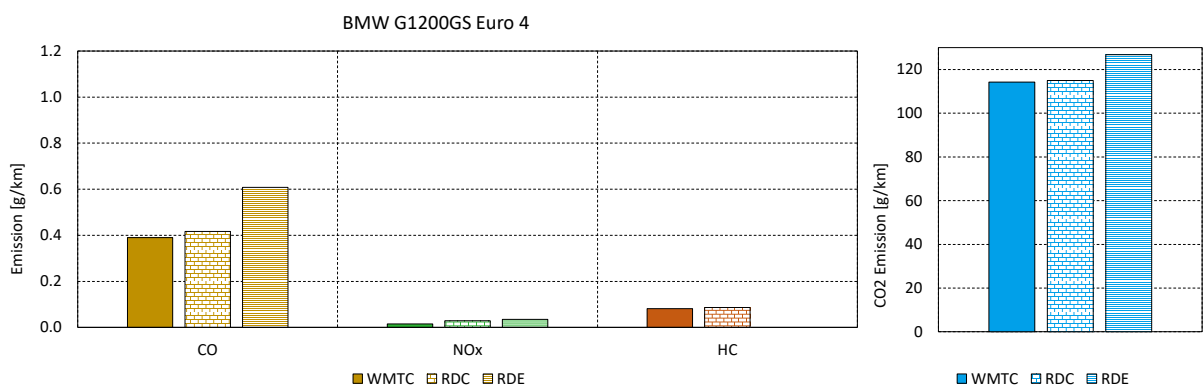


Figure 76: Comparison of WMTC, RDC and RDE measurement results for the BMW G1200GS Euro 4 motorcycle.

Figure 77 to Figure 80 illustrate cross comparisons of the emission measurement results for different test cycles. The bars in the diagram cannot be summed up for their values in [g/km] because these values are calculated for the different test sections urban, rural and motorway separately. The stacked bars were chosen for better illustration and discussion but in fact the mean value over a whole test cycle will be much lower than the top of each bar implies. Therefore no legislative limits or axis values are added in these diagrams.

Figure 77 and Figure 78 sum up the measurement results for both BMW F800 motorcycles by comparing the Euro 3 and Euro 4 vehicles. The development from Euro 3 to Euro 4 emission levels can be seen very well in the results for the WMTC test cycles. Emissions are higher for the real drive cycle test and also RDE are higher than type approval test results. Moreover, a shift to higher emission levels toward the rural test sections can be seen for the more dynamic test cycles especially for RDE results.

Figure 79 and Figure 80 sum up the measurement results for the Euro 4 motorcycles, namely the BMW F800R and the BMW G1200GS. Once again a clear shift toward higher emission levels for higher driving dynamic can be seen. Furthermore, as discussed above, the higher specific loads of the F800 engine for similar driven velocity profiles results in significantly higher NO_x emissions as illustrated in Figure 80.

Surprisingly, HC emissions result in higher values for type approval tests compared to the real drive cycle tests. Unfortunately it was not possible to measure hydro carbons on-road with the used PEMS. Moreover, another interesting issue are the carbon monoxide emissions for the BMW G1200GS in the urban section of the RDE test track as illustrated in Figure 80. The measurement trace was investigated more carefully to find the reason of this phenomenon. In fact, the higher values were caused by a higher volume of traffic and a lot of traffic jam situation during the tests. Obviously, this led to higher emissions per driven distance what is especially critical when the exhaust gas after treatment system is still cold.

The analysis of the emission measurement data can be expanded with modal measurement traces and detailed analysis of single emission relevant driving scenarios as exemplarily discussed in section 3.1. Moreover, further beneficial analysis can be made for emission relevant driving scenarios related to their temporary appearance during the test cycle. These results will be introduced in section 4.1.4 (see Figure 95 to Figure 100) in combination with RDE simulation results.

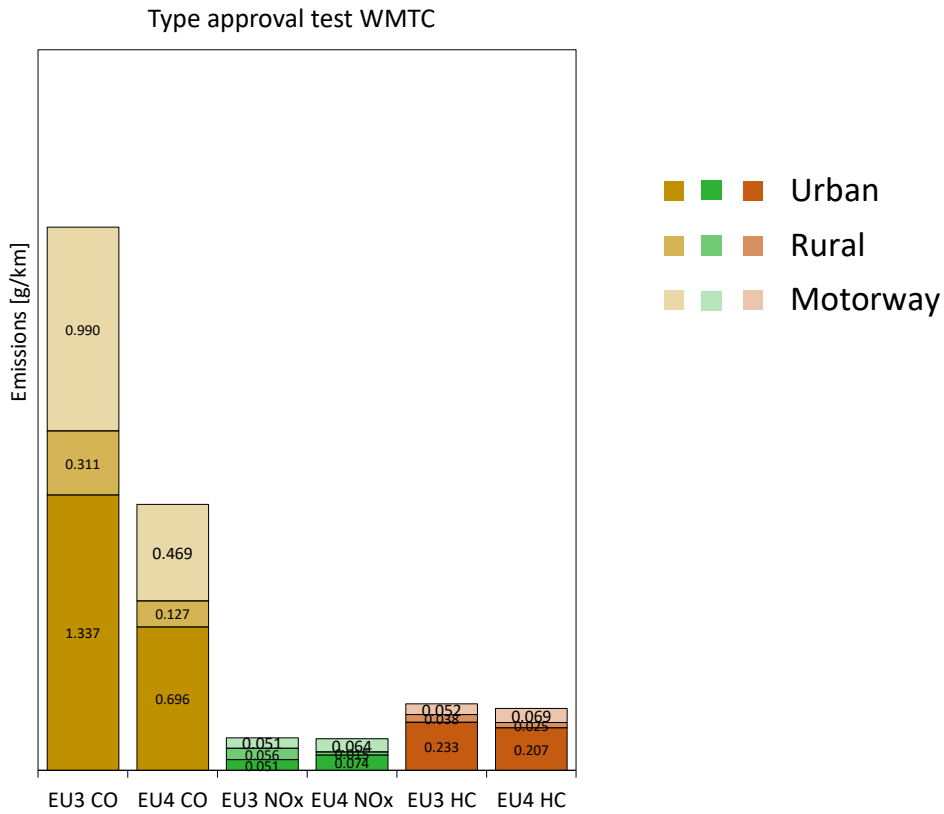


Figure 77: Comparison of WMTc emission measurement results per substance and per test cycle section (urban, rural, motorway) for BMW F800 Euro 3 and Euro 4 motorcycles.

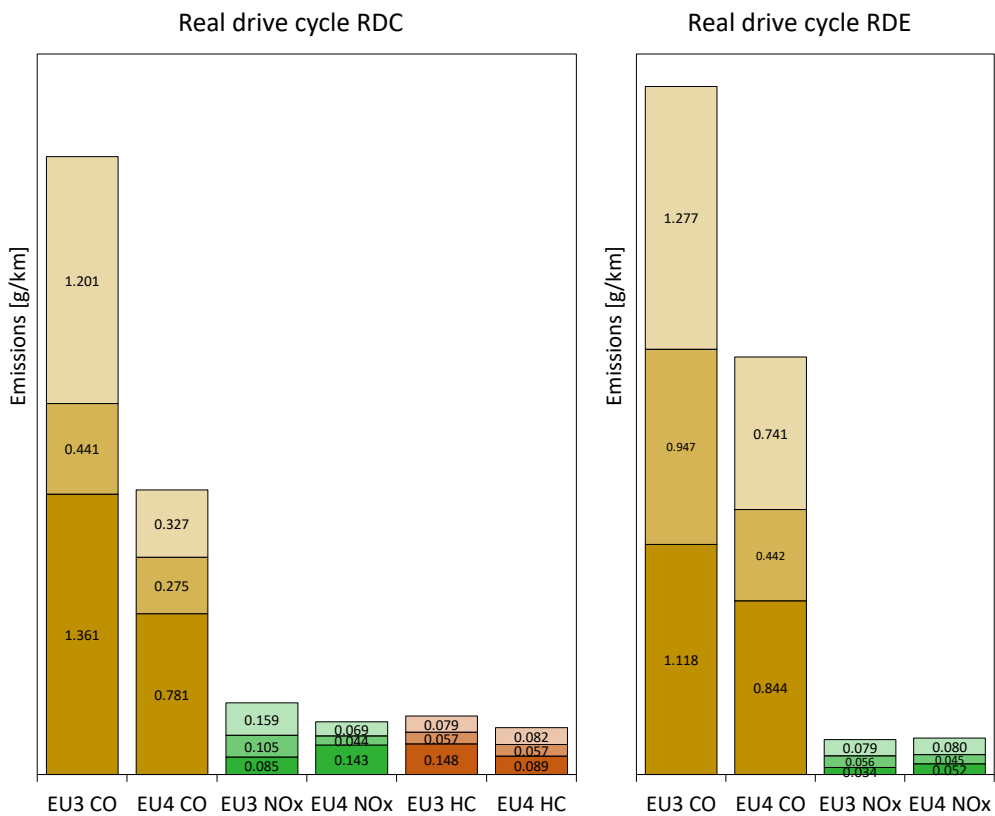


Figure 78: Comparison of RDC and RDE emission measurement results per substance and per test cycle section (urban, rural, motorway) for BMW F800 Euro 3 and Euro 4 motorcycles.

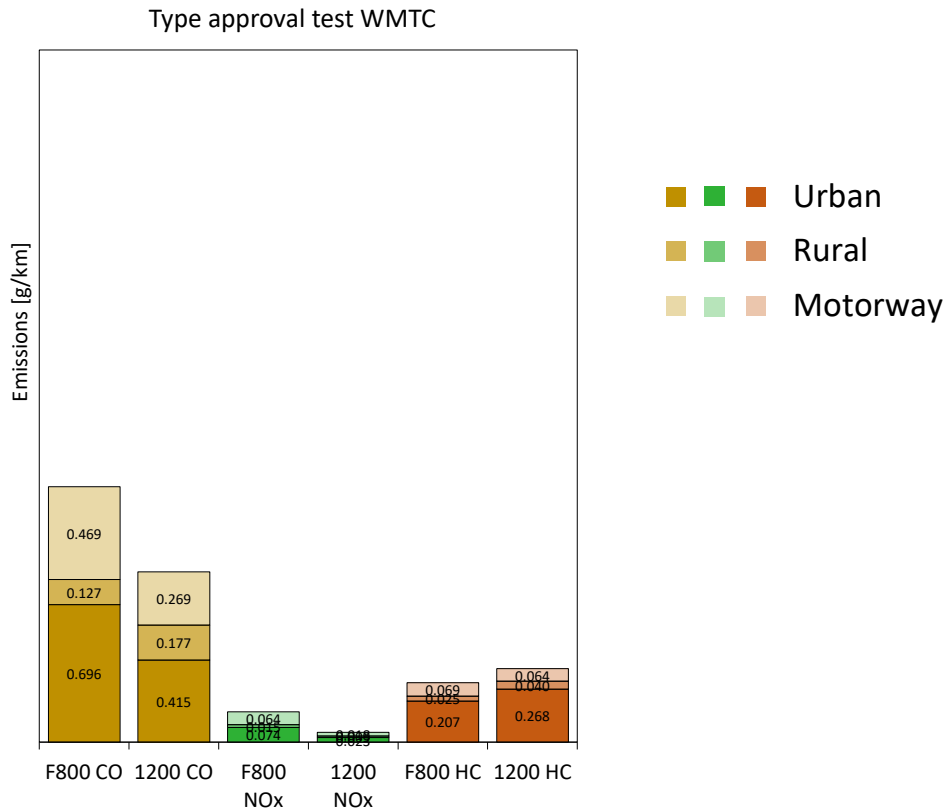


Figure 79: Comparison of WMTC emission measurement results per substance and per test cycle section (urban, rural, motorway) for BMW F800R and BMW G1200GS Euro 4 motorcycles.

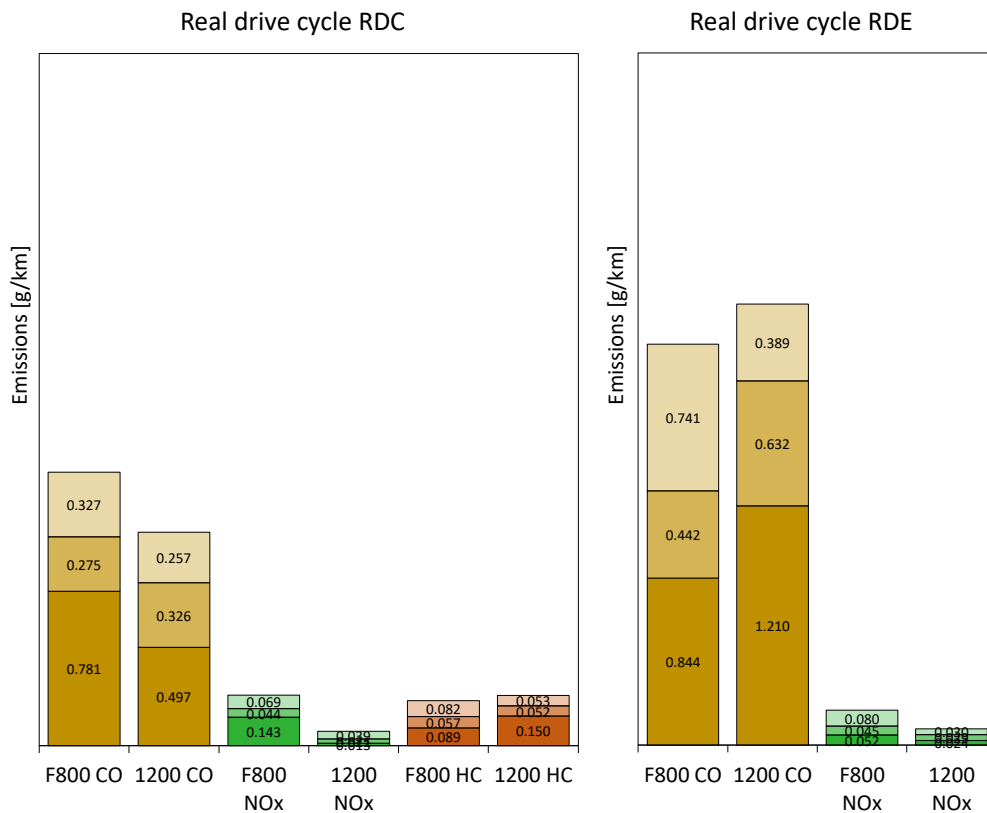


Figure 80: Comparison of RDC and RDE emission measurement results per substance and per test cycle section (urban, rural, motorway) for BMW F800R and BMW G1200GS Euro 4 motorcycles.

4 Methodology for real drive emission simulation

Based on above presented insights into driving dynamics, emission measurement methodologies and emission results for motorcycles, the following chapter introduces a simple and adaptive methodology for real drive emission RDE simulation model. The investigations were carried out with a BMW F800GT motorcycle as a feasibility study for further applications with other test objects. The goal is to estimate the potential of a tool which results in sufficiently accurate emission and fuel consumption levels with a minimum of measurement effort to prepare input data for the simulation model. So, this tool can serve as an additional assessment criterion for a comprehensive RDE evaluation methodology, exemplarily including a small number of chassis dynamometer measurements in combination with the simulation model and possibly additional on-road measurement for adjustment and matching.

Hence, the simulation model expands on the previously presented measurement methodologies for real drive emissions for motorcycles to minimize the effort in estimating real world effects and to serve as a tool for further improvement towards upcoming more stringent emission limits. Therefore, the applicability of the software will be shown with three examples.

4.1 Simulation model description

As the number of different engine and vehicle concepts for powered-two wheelers is very high and will even rise with hybridization, the simulation of emissions and fuel consumption is indispensable for further development towards more environmentally friendly mobility. Hence, an adaptive artificial neural network based predictive model for emission and fuel consumption simulation of motorcycles operated in real world conditions is presented. The model is developed in Matlab and Simulink and is integrated into a longitudinal vehicle dynamic simulation whereby it is possible to simulate various and not yet measured test cycles. Subsequently, it is possible to predict real drive emissions RDE and on-road fuel consumption by a minimum of previous measurement effort. The modelling approach is adaptive in terms of usability for different engine and exhaust gas treatment systems as the model does not require specific knowledge of technical vehicle parameters, which might be unknown due to manufacturers' concealment. Backpropagation is used as supervised learning technique for training the neural networks and various learning inputs are investigated and evaluated.

The following section introduces shortly the longitudinal vehicle simulation model in which the emission model will be embedded. Subsequently, section 4.1.2 gives an overview on machine learning in general and some work related to emission simulation in this field. Section 4.1.3 introduces the artificial neural network modelling and steps into detail for the developed emission simulation model. Finally, simulation results are presented in section 4.1.4.

4.1.1 Longitudinal vehicle simulation model

The use of complete vehicle simulations gains in importance during the research and the development phase of motorcycles. The reasons lie in a reduction of development time and costs while taking into account the increasing system complexity. The simulation target is the description of complex complete systems by connecting simulation modules of system parts (engine, gear box, e-motor, cooling circuit, etc.) [52] [53] [54] [55] [56] [57] [58].

In this research project, a dynamic forward simulation built up is used, as it starts with the driving cycle as target value for the vehicle speed. The driver module in this simulation acts like a PID-controller or virtual driver, which tries to follow the prescribed driving cycle. This simulation is based on a detailed mathematical description of the vehicle and component behavior using differential equations and characteristic maps which are previously investigated on test rig. With this approach, the transient behavior can be described well and statements concerning drivability, control strategies, fuel consumptions and emission behavior are possible [52] [56]. Figure 81 illustrates a simplified scheme of a forward simulation [59].

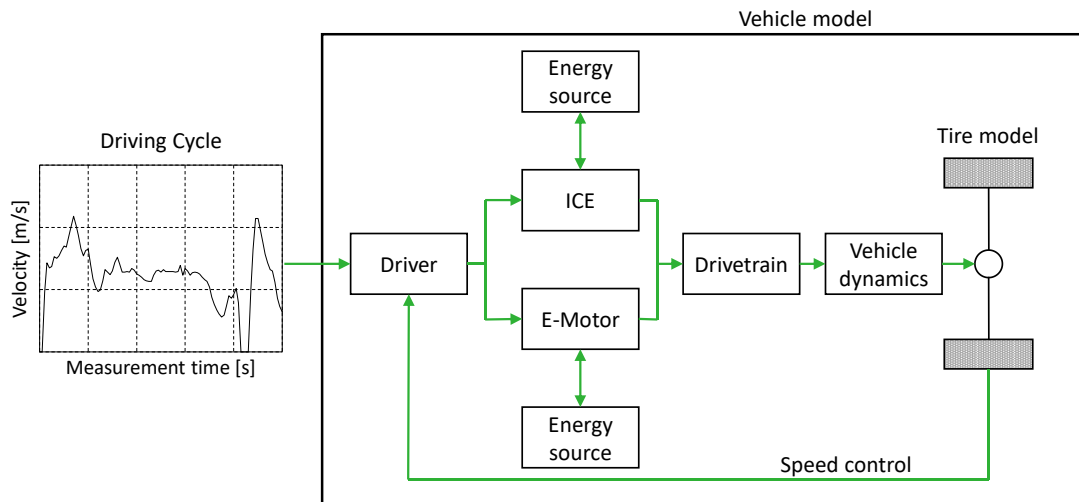


Figure 81: Simplified scheme of a forward vehicle simulation model.

The used platform is set up within the simulation framework Matlab and Simulink [60] as dynamic forward simulation model. Within Matlab and Simulink it is possible to generate C-codes for the use in ECUs and further for the setup of hardware in the loop HIL platforms [53] [52] [56] [61]. Therefore, all modules must achieve real time capability in the complete vehicle simulation [59].

The emission and fuel consumption model was built into the longitudinal vehicle simulation model as a standalone module (see section 4.1.3.1). Its simulation technique is based on machine learning and will be introduced in the following section to lead towards the specific modelling approach for emission and fuel consumption simulation.

4.1.2 Introduction to machine learning and related work

Artificial neural network (ANN) technology originates from computational models which are inspired by networks of biological neurons, wherein the neurons compute output values from input values. In fact, it is a computational model that is based on a machine learning technique and it works like a human brain neuron system [62] [63]. The application of ANN is widely spread nowadays. It is used for process controlling, real time control applications, statistics, data processing, scenario prediction modeling and other apps spreading from the field of medical and pharmaceutical engineering over agricultural, biological and geophysical processes to more fields of research and application. Due to its simple and fast modeling approach, utilization and adaption to different problems, ANN technology is used for performance, emission and fuel economy simulation of engines. As hybridization and the different vehicle and engine concepts rise, it would be a never-ending effort to develop precise

physically based models for further development in this field; and this approach, to meet the requirement of performance data gathering, is very costly and time consuming as well as a comprehensive testing study for different engine concepts for so many different possible operation scenarios. Nevertheless, this modelling approach cannot be used for developments from scratch as training data can be gathered for existing things only. However, the ANN approach allows a faster way of modelling physical phenomena in complex systems without requiring explicit mathematical representations or in depth knowledge of physical phenomena [64] [65] [66]. This modeling technique is also very fast in adaption to changed systems or changed system parameters which additionally allows fast forward case studies. Furthermore, predictive models could act as virtual emission sensor in the future to replace costly hardware [67] which is already done for numerous vehicle components that incorporate learning controllers to improve performance and adapt to component wear or driving behavior [68] [69].

Hence, the motivation of the presented research is to use the advantages of ANN to present an emission model for motorcycles that predicts real drive emissions based on the minimum possible measurement effort. Test rig measurements should be used as base for training the ANNs to subsequently simulate on-road emissions. Therefore, the specific modeling approach and different learning inputs (for training the neural network) will be presented and evaluated. To reach sufficient accuracy of e.g. $\pm 10\%$ of CO emission level over the whole test cycle with the used approach, it is required to employ an accurate model to identify the relationship between the controlling and output parameters of the used ANN [70]. Therefore, a key concept is the modeling of dynamic parameters which determine driving dynamic, driver's pattern and engine operation in combination.

Many projects have been elaborated to determine vehicles emission levels in real world condition under dynamic operation scenarios. A lot of them rely on a large number of measurements and a broad data base to determine the expected effects [71]. A goal of the presented work is to minimize the measurement effort by simultaneously reaching good correlations for emission prediction in a modal way for real driving scenarios. Studies have been carried out to do these simulations in a map-based way like presented in [72], [73] or [74]. But in this thesis rather the above described advantages of ANN will be used than extending measurement effort for reaching good simulation results. ANN based approaches are used in a significant number of studies to predict engine emissions. Investigations are stated in [65] where correlation coefficients in the range of 0.98 to 0.996 were found for predictions of engine performance and exhaust emissions. But as additionally presented in [72], a lot of predicting models rely on steady-state engine measurements and are expanded by some correction functions if transient behavior is requested. Furthermore, very accurate models were already investigated for diesel engines for predicting NO_x and smoke which rely on engine test bed measurement and data covering most of the engine operating range [75]. Moreover, efforts have been made to predict emissions of diesel engines with ANNs by implementing the emission models into a complete vehicle simulation to subsequently predict emissions and dynamic performance of the simulated engines during transient maneuvers like occurring in type approval test cycles [76]. Optimization algorithms are also presented in [70] to improve emission predicting models. The neural network based emission simulation is a very interesting tool for all kind of combustion engines like dual fuel engines [77] or also for predicting emissions of hydrogen powered vehicles [78] where physically and chemically based prediction models can become highly complicated too. Furthermore, the simulation of hybrid vehicles is an upcoming scope of application for ANN emission simulation [66] as addressed above.

A lot of research work found in this field relied on steady state engine behavior, data covering most of the engine operating range or approached the simulation of type approval tests or other tests that can be done on test rig. The herein presented modelling approach reaches a step further. Very little test data from chassis dynamometer is used as input for the ANN modelling

process to subsequently simulate not afore tested real drive emissions RDE.

In the following section the herein used artificial neural network modelling approach will be presented and neural structures are introduced. Training approaches for the ANN are subsequently shown as the learning performance is a key for good simulation results. Finally, the applicability of the software will be shown with three examples: The engine adaption to stoichiometric condition, the impact of start-stop control and the impact of additional mass are presented. In conclusion, some limitations of the used approach are discussed and future ideas will be stated.

4.1.3 Artificial neural network modelling

The following section provides a short introduction to artificial neural network modelling in general and subsequently leads to ANN emission modelling in particular. The approach for the catalyst model is discussed further on and, finally, the learning input and training data sets are discussed as this is the key for good simulation performance. The fitting and generating of all neural nets was made with Matlab Neural Network Fitting toolbox.

An ANN is an information processing paradigm that is inspired by the way biological nervous systems, such as the brain, learn and process information [67] [79]. The structure of a neuronal network consists of multiple single neurons for multiple layers as depicted in Figure 82. There is an input layer where the network is fed with data, a single hidden layer or multiple hidden layers with neurons that follow a specific transfer function algorithm for their learning paradigm and there is an output layer where the output parameter(s) is (are) provided by the network. A transfer function in the hidden layers' neurons is used for processing the data that is fed forward to the neuron. Usually four different transfer functions are used which are called Sigmoid, Log-Sigmoid, Sinuous and Linear. Multiple hidden layers with nonlinear transfer functions allow the network to learn nonlinear relationships between input and output [60].

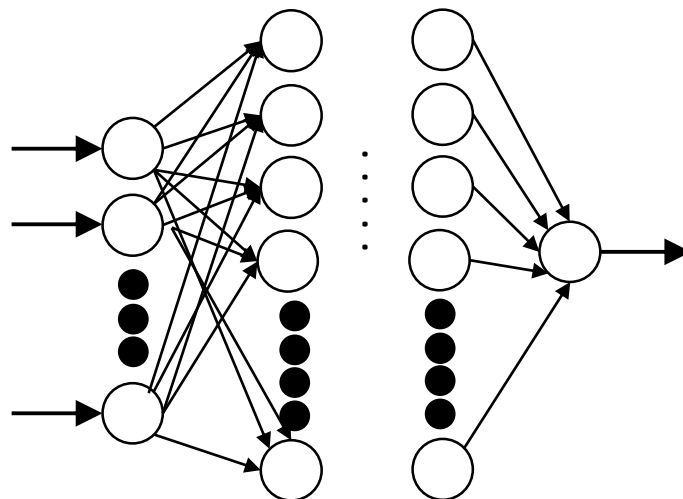


Figure 82: Schematic illustration of an artificial neural network structure with input, hidden and output layers and neurons.

The neurons are processing the input data by the transfer function [79]. The processing of the data depends on the effectiveness between two attuned neurons called as weight and bias which enclose the information gained through training, testing and validation. Learning has been gained by adjustment of weights and bias with reference to input blueprints [80]; weights and

bias are the only learnable parameters of the model and its values' starts are initialized randomly and adjusted by training towards values that are followed by a correct output of the network. So, the knowledge of the mapped system to simulate is stored in ANNs as a set of connection weights and biases [65].

Different training algorithms can be used for the overall learning process of a neuronal network. Such an algorithm optimizes the network weights and biases in the direction in which a predefined performance function converges most rapidly. In general, two different algorithms can be used; supervised and unsupervised learning algorithms. The first one is dependent on a set of training data whereas the second one is not. Furthermore, the neural network structure can be fed forward or with an enclosed loop for re-feeding the input with the output signal of the network. The presented emission neural network is a multi-layer feed forward network with the supervised training method called backward propagation of errors. The ANN uses the Levenberg-Marquardt algorithm. This training function works very stable for most function optimization networks.

In fact, an ANN can handle very complex real-life problems in a nonparallel and distributive way like a biological neural network [62]. The mathematical description of a neural network can be understood by the following equation:

Equation 5: Mathematical description of a neural network.

$$Y = F * \left\{ \sum_{i=1}^n (X_i * W_i + c) \right\}$$

Herein \mathbf{Y} is the target vector, \mathbf{F} is the transfer function, \mathbf{X}_i is the training or input vector for the neurons, \mathbf{W}_i is the weight vector for the neurons and \mathbf{c} is the bias. The single neurons form the sum of the weighted inputs given by the expression in the brackets. The sum of the weighted inputs with a bias is processed through a transfer function and subsequently the output \mathbf{Y} is computed [65]. The training function optimizes the network by that equation towards specific parameters like the root mean square error or any performance indicator. The trained ANN is now capable of simulating the system outputs for the inputs which have not been introduced before.

The following section introduces the emission and fuel consumption modelling with Matlab and Simulink and expands on the used neural network modelling.

4.1.3.1 ANN emission modelling

The goal is a simulation model that is applicable for real world driving scenarios to determine RDE without testing on-road. Therefore, a minimum of measurement effort was carried out that includes the motorcycle test cycle WMTC and one additional real drive cycle RDC which is a derivative of multiple on-road dynamic investigations as described above. Here, the chassis dynamometer measurement results of RDC1 and WMTC are used in 1 [Hz] measurement traces for training input of the artificial neural network. Based on the simulation results, it should be possible to follow trends in emissions for real world driving scenarios.

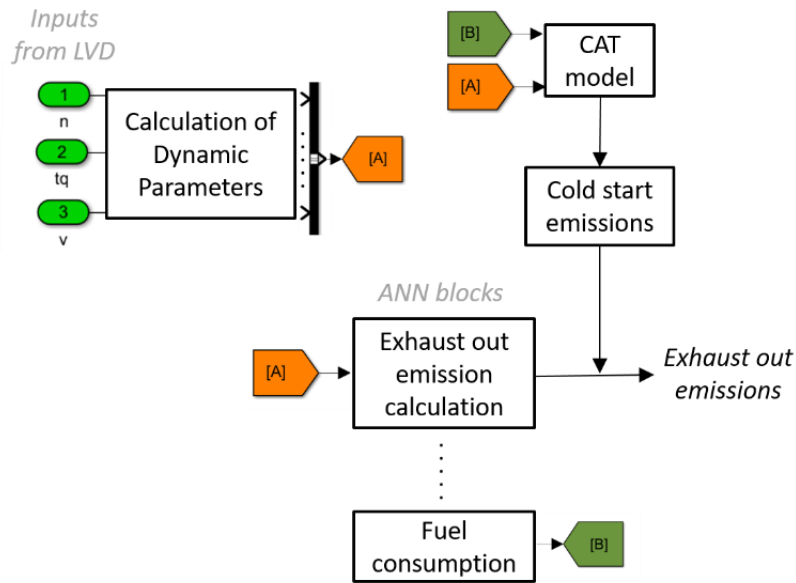


Figure 83: Schematic illustration of the emission simulation model.

Therefore, Figure 83 illustrates the schematic structure of the simulation model. As afore said, the model is embedded in a longitudinal vehicle dynamic simulation (LVD) and, therewith, the only input parameters for the emission model are the engine speed n , the engine torque tq and the vehicle velocity v . Chassis dynamometer measurements did not contain engine torque measurement. Hence, this parameter was calculated separately as engine test bed measurements have also been carried out for the F800 engine on which base the model was built at first. So-called dynamic parameters are calculated further on with the three input parameters to be fed forward to the ANNs. These dynamic parameters, e.g. the positive power gradient ΔP_{pos} , the throttle angle gradient $\Delta \alpha$ etc., ensure the link between engine or driving behavior to the occurring emission scenario and, therefore, represent the physical connection for emission formation. All these parameters are fed forward as input parameters to the emission ANN blocks. Each emission component and the fuel consumption have a neural net and its output signals are provided in grams per second. Emissions are calculated as exhaust out emissions and, subsequently, the CAT model is inversely modeled so that it increases the emission level during cold start operation until the exhaust gas after treatment is operating. The CAT model additionally uses the actual fuel consumption as an input parameter. Further on, this is described in more detail followed by a section about learning input and training of neural nets. A summary of input and output parameters for every used ANN is given in Table 18.

4.1.3.2 Catalyst modelling

As a result of the above-mentioned goal to directly simulate exhaust out emissions based on exhaust out emission measurements, a suitable structure of a model for this catalyst is difficult to implement. The purpose of the catalyst model is to integrate the warm-up phase of the after-treatment system and, therewith, the un-converted exhaust gas until the light-off of the catalyst. A model based on the already converted exhaust out emissions as input parameter would be working with an inversely calculated conversion rate. This system must be solely developed for each gaseous emission component and quantified by a factor in each case due to the need for normalization of the training data (see section 4.1.3.3). Hence this catalyst model is also not adaptable for investigations concerning better or different catalytic converters.

Subsequently, the herein used catalyst model is based on ANNs trained with raw emission measurements afore the light-off. Additionally, the catalyst model includes a block that simulates the temperature at the catalyst shell which determines the light-off. The emission model includes a switch function that changes the emission level in accordance to the catalyst shell temperature. Therefore, un-converted emissions are provided before the distinguished light-off point of the catalyst. Even though, to be able to calculate raw emissions before catalyst light-off, the measurement effort must not be extended because the cold start phase delivers sufficient data.

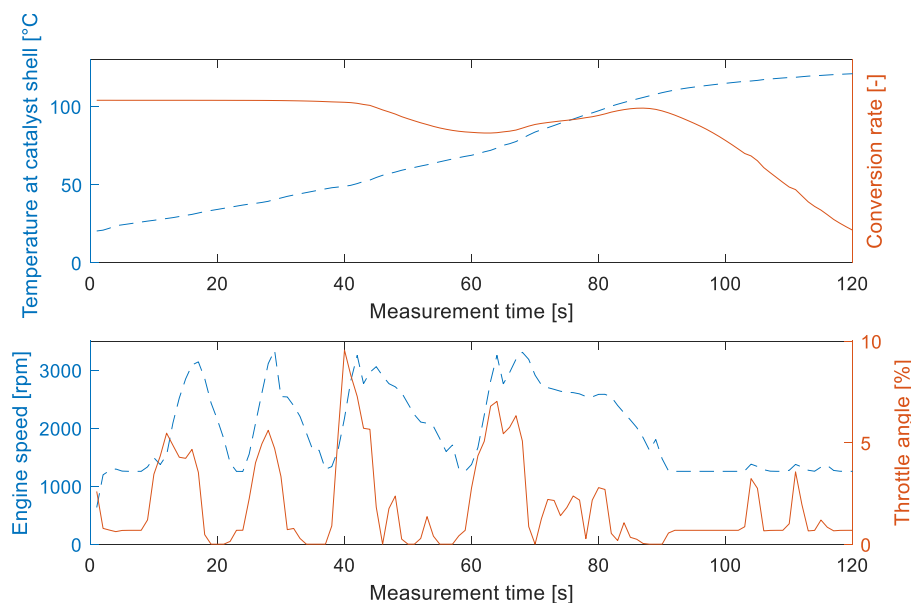


Figure 84: Temperature at catalyst shell and conversion rate out of the catalyst model with additionally displayed engine speed and throttle angle.

Figure 84 exemplarily illustrates the simulation result of the temperature at the catalyst shell and the inversely modeled conversion rate for a real driving scenario with additionally displayed velocity profile and throttle angle position. In fact, the conversion rate determines the switch function in the simulation model. As soon as the value drops under a specific value the light-off is assumed and the catalyst model is not valid anymore due to its limited training data set. The range of validity of the catalyst model was carried out by a comparison with measurement results. The temperature at the catalyst shell can be modelled even more detailed if the vehicles velocity is used as additional input parameter when the set of training data is extended. In this case, only the two above mentioned test cycles were used as input parameters and the use of additional input parameters would have disturbed the simulation results due to the little amount of training data. This effect is discussed in more detail in the next section 4.1.3.3 because it relies on learning functionality of the used ANNs. Moreover, the validation of the emission model is discussed in the end of the upcoming section.

4.1.3.3 Learning input

The following section can be separated in two different parts. A first part is covering the training data measurement, selection and preparation wherein raw data will be collected from PEMS measurements for CO, CO₂ and NO_x emissions and by CVS measurements for HC emissions,

all gauges used on the chassis dynamometer (see to *Figure 88*). A second part about training techniques including evaluation and validation. In fact, these parts are dependent to each other and the essential facts for these topics will be emphasized.

Various learning inputs were investigated and evaluated. The best learning input would be, of course, a similar set of measured data for training as it is used further on for simulation. This would not correspond with the above stated goal of the simulation. Hence, the learning input is not covering all relevant scenarios that will be simulated further on leading to the need of a precise analysis of how and with which dataset the neural networks are trained. In fact, just one WMTC and one RDC were used for training. The simplest exercise might be the training of a network and the subsequent simulation of the same set of training data. Unfortunately, there are a few issues that disturb that wish for simplicity. The first one is that a herein used modal measurement trace has no singular assignment. E.g. a specific emission scenario with a specific value can have multiple allocations in an engine map exemplarily consisting of throttle angle α and engine speed \mathbf{n} . Furthermore, the vehicles' velocity \mathbf{v} is another parameter that influences emission formation for the same \mathbf{n} - α combination, the gear shift respectively, as do all the other possible combinations of dynamic parameters. Moreover, not all input data can be used for learning because the algorithm needs additional parts for validating and testing itself. Consequently, a combination of dependencies for particular emission events, engine parameters, and dynamic parameters have to be found that rebuild the training data in the best possible way with sufficient generalization performance and avoided overfitting coincidentally [81].

Results can be improved by different approaches. As a network is initialized one more time, the network parameters are different each time and the training might produce a different solution. Another approach is the changing of the hidden layer. Larger numbers of neurons in the hidden layer give the network more flexibility because the network has more parameters to optimize. But the number must be increased gradually as one might cause the problem to be under-characterized and the network must optimize more parameters than there are data vectors to constrain these parameters [60] [81].

It was found to get the most accurate simulation output by a combination of the following simple set of parameters for input for all emission neural nets: throttle angle gradient $\Delta\alpha$, vehicle velocity \mathbf{v} , engine power \mathbf{P} , and engine speed \mathbf{n} ; but in combination with an additional training manipulation for vehicle speed ranges. Three different ANNs for each emission component for the speed ranges 0-60, 60-110 and above 110 km/h were trained. This was done in respect to the fraction of usage of training data for training, validation and testing, which is needed by the training algorithm and set to 70, 15 and 15 [%] by default for Levenberg-Marquardt algorithm. The selection of training, validation and testing data was chosen randomly for all input data.

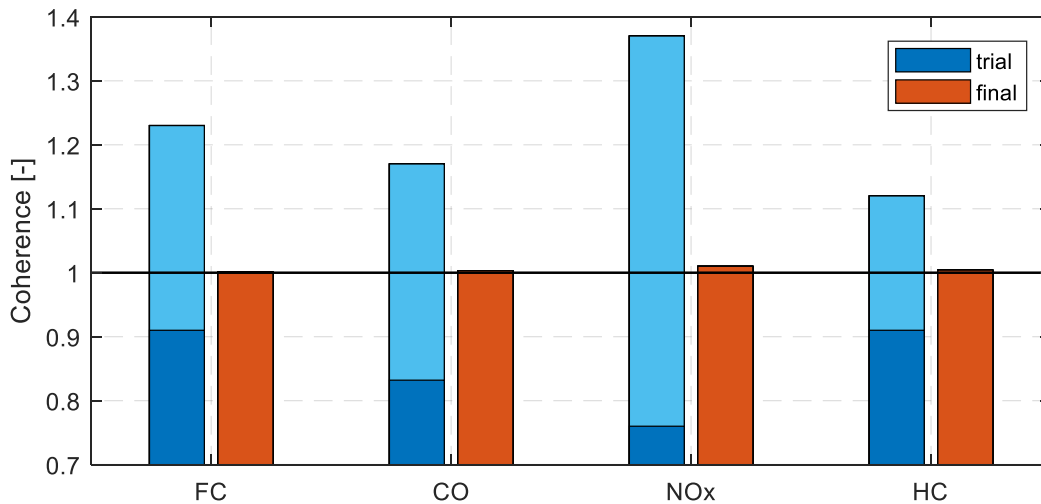


Figure 85: Coherence between simulation and training data for first trials and the final version of the neural nets.

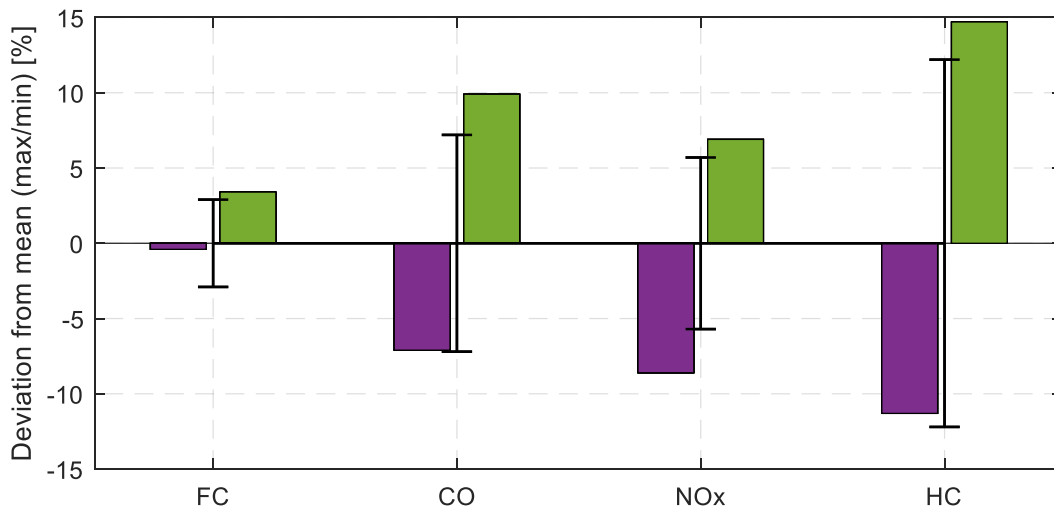


Figure 86: Occurring deviation and standard deviation of measurement data itself, with maximum (green) and minimum (purple) arisen deviation.

Figure 85 shows the maximum/minimum arisen deviation between simulation and training data (or coherence between simulation and training respectively) and the improvement through optimization of the network parameters and variation of dynamic parameters. In other words, the network parameters of each ANN were varied to get a minimum deviation between training data itself (the measured data) and a simulation test with the same input data as the training data (measured data again). After the simulation, measured emissions and simulated emissions were compared and the coherence was calculated as the difference between the summated measurement and summated simulation emission values divided by the summated measured emission values. All tested models have had coefficients of determination R^2 of at least 0.92, so one might expect that simulating the same values as trained should result in accurate results; but in fact this is not true for neural network modelling as long as the chosen training algorithm and network parameters are not adjusted to the nature of the fitting problem. There are recommendations of specific algorithms for different fitting problems, but the network parameters have to be optimized for each specific problem individually, what is presented in Figure 85. Hence, further assessment tools like monitoring error histograms,

validation performance and training state have been used as well as the above described coherence factor [60]. So, the orange bars in Figure 85 indicate the final version of the neural nets wherein the deviations between simulation and training data were found to be below 0.7 [%] for all ANNs in the final version. One has to keep in mind that the measured results are scattered as indicated by the lower graph in Figure 86 and just one measurement trace is used for training (from one test cycle measurement out of multiple for WMTC and RDC each).

For training multilayer feedforward networks, any standard numerical optimization algorithm can be used to optimize the performance function. These optimization methods use either the gradient of the network performance with respect to the network weights, or the Jacobian of the network errors with respect to the weights. The gradient and the Jacobian are calculated using a technique called the backpropagation algorithm, which involves performing computations backward through the network. It is very difficult to know which training algorithm will best fit to a given problem. It depends on whether the network is used for pattern recognition or linear regression models and also on parameters like the complexity of the stated problem and the amount and quality of the training data [60]. The present model is a nonlinear regression problem and therefore the quasi-Newton method, the Levenberg-Marquardt algorithm, was chosen. The performance function for this algorithm is mean square error as shown in the following equation.

Equation 6: Definition of mean square error.

$$mse = \frac{1}{n} \sum_{i=1}^n (x_i - y_i)^2$$

The average square error between the network output \mathbf{y} and the target \mathbf{x} determines the network performance. The network performance is increased by normalizing training data which was made by following equation for a given parameter \mathbf{X} .

Equation 7: Normalization of training data.

$$X_{norm} = \frac{X_{abs} - X_{min}}{X_{max} - X_{min}}$$

Table 18 sums up all relevant network parameters and the chosen input parameters for the ANNs that resulted in the best simulation performance. As NO_x emissions are generally on a very low level, their simulation is very sensitive. To meet that the best way possible a cascade-forward network architecture was chosen for this specific case. This structure includes a connection from the input and every previous layer to the following layers [82]. Furthermore, a regularization for the performance function for the NO_x nets was included to achieve better generalization of the network and to more likely avoid overfitting [81].

Table 18: Network parameters and chosen input parameters for all ANNs with best results in simulation performance.

	FC	CO	NO _x	HC	CAT temp.	CAT conv.
Input parameters	$\Delta\alpha, v, P, n$	$\Delta\alpha, v, P, n$	$(\Delta\alpha, v, P, n)^{(*)}$	$\Delta\alpha, v, P, n$	T, FC_{cum}, P_{pos}	T_{CAT}
Number of neurons	10	57	20 ^(**)	30	3	10
Data division	70/15/15	60/20/20	70/15/15	70/15/15	70/15/15	70/15/15

- (*) Including regularization²
- (**) Cascade forwarded net

The fit of the ANNs compared to the training data is very good as shown above. The training data itself has a wide variety in its modal measurement trace as shown in Figure 86. This variety results from three main issues.

First reason is the drivers' behavior and his capability to follow the predefined velocity profile and gear shifting table on the test rig. Second one is the chassis dynamometer setup. It is common to measure motorcycles on an open constant volume sampling system CVS which dilutes the exhaust gas with ambient air. This damps transient effects on the measured emission signal due to mixing up the exhaust volumes of consecutive time steps. Moreover, the length of the sample tubes, until the gas analyzers are reached, is a key parameter for an accurate measurement trace. The effects of variable gas transport times are well known to be a challenge for generating high quality test results from emission measurement [83] and not to lose all the information of a measured signal [84]. Figure 87 exemplarily illustrates the constant time delay for the CVS system for CO. Herein, the emission components are corrected with a first order low-pass filter for proper signal adjustment. The correction shown was made for the CVS measurements only as for PEMS measurements a certain evaluation software was used for post processing the measurement results. This software has implemented its own signal adjustment algorithm in correspondence to engine speed. Even if this delay is adjusted to fit the current engine event, its quantity is highly diminished. Furthermore, the time delay has an additional unsteady component which results from the engines transient operation. Gas transport times are different in idle and full load operation and can exemplarily differ from 0.3 up to 1.8 seconds for the investigated motorcycle with 800 [ccm] displacement and an idling speed of 1250 [rpm].

² Regularization is a mathematical method for improving generalization. This involves modifying the performance function (for training the network), which is normally chosen to be the sum of squares of the network errors on the training set [60].

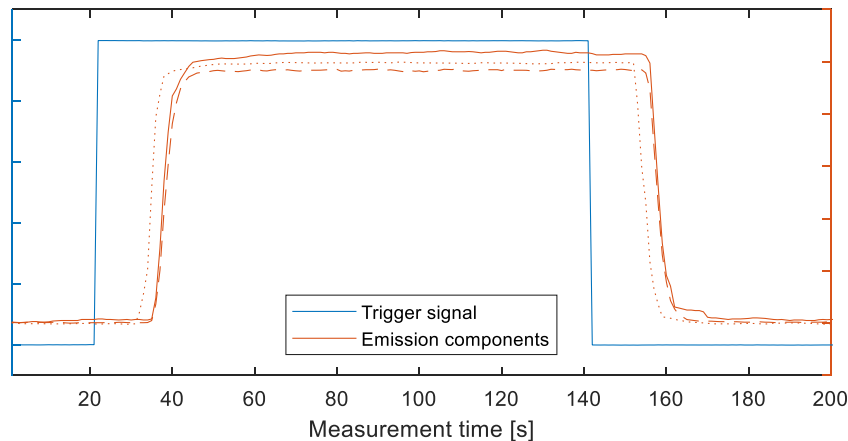


Figure 87: Constant time delay of emission scenario and sensor reaction for CO, NO_x and HC emissions.

The third reason is the measurement principle and calculation scheme of the exhaust gas mass flow and the emission components. The mass flow measurement highly determines accuracy. To be the most accurate as possible, herein a PEMS was used on test rig with the shortest possible tapping tubes for measuring the training data for CO, CO₂ and NO_x. For HC emissions, a test rig diluted CVS system with a subsequent flame ionization detector FID was used. The following Figure 88 illustrates above described exhaust gas tapping positions of the test rig setup.

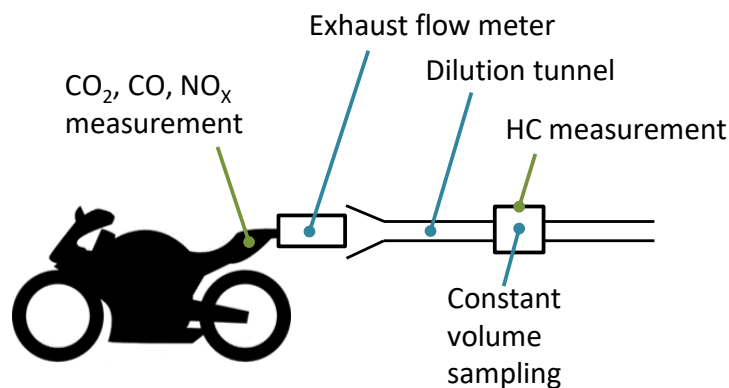


Figure 88: Schematic illustration of the exhaust gas tapping positions of the test rig setup.

Due to the nature of the measurement principle for hydro carbons, the modal measurement trace is not optimal as training input for an emission ANN as the exhaust gas is already mixed with dilution air and in combination with the delay time transient effects are already damped. Figure 89 shows the effect of damping that is reflected in the simulation. A 80 second section of a WMTC chassis dynamometer test is shown, wherein the simulated emission results relies on CVS measurements as afore mentioned. The emission level was additionally measured not diluted and directly after the exhaust pipe with a Fourier-transformation infrared spectroscopy FTIR emission measurement system for this investigation. Hence, this comparison shows the blurring of emission events due to the diluted analyzing method with CVS.

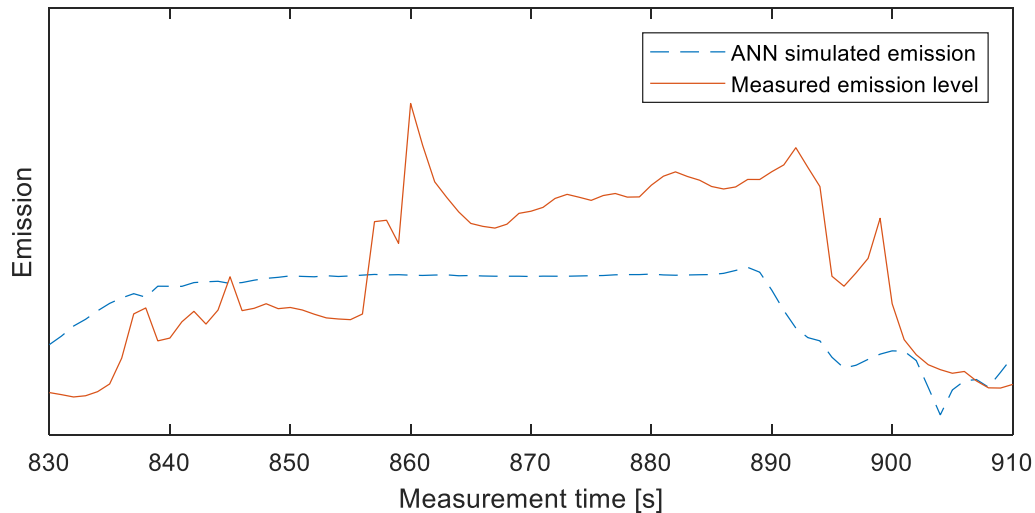


Figure 89: Transient damping effect due to emission measurement with diluted CVS system.

The above-mentioned issues concerning the variety in training data sets result in two main influencing parameters for the training input data and further on the optimization of the ANNs. First is the volatility of the modal measurement trace which has a direct impact on the output function of a trained ANN. Second is the resulting variety of the cumulated emission and fuel consumption values (see Figure 86). These sums are additionally used for the optimization and as the values for comparison are scattered, the optimization has its a priori limits. Nevertheless, the following illustration sums up the optimization result in values for emission levels.

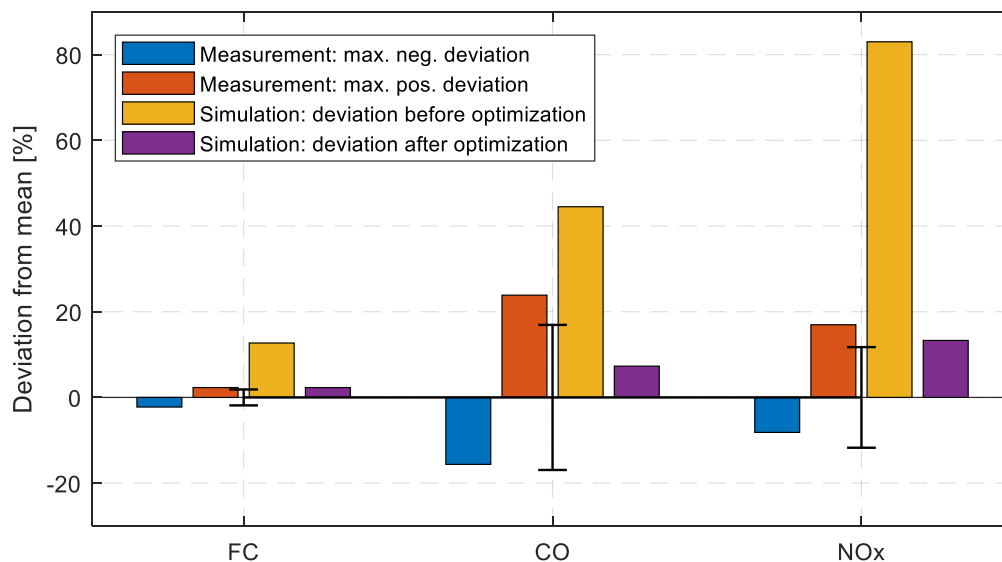


Figure 90: Improvement of summated emission results for simulated RDE routes throughout ANN optimization compared with measurement variability, shown by deviation from mean; standard deviation calculated from measurement results (not used for training of the ANN).

Figure 90 shows the improvement throughout the above-mentioned optimizations but already for RDE simulation. The validation of the emission model was carried out with reference simulations for the RDE test cycle “Arzberg” that also had been measured on-road multiple times with a PEMS. Maximum negative and positive deviation of multiple measurements of

the RDE test cycle are illustrated in blue and orange bars. Moreover, it can be seen that the emission results of the optimized ANNs fit quite well into the standard deviation of the measured results. NO_x emission simulation results in the highest deviation. This is due to very small mean values in NO_x emission level just about zero and spiky peaks up to $30 \cdot 10^{-3}$ [g/s] among other things. Hence, the variability of NO_x emissions for simulated RDE test cycles is very sensitive and will be discussed in more detail below.

As an additional assessment of the emission model, the following Figure 91 shows the linear regression relation between fuel consumption simulated by ANNs with LVD input parameters and fuel consumption simulated by ANNs with measurement data input parameters. There is plotted a second fit with y axis intercept shown orange dashed and the coefficients of determination R^2 for both fits are given in the legend. Despite the good simulation results for the final ANN versions, this comparison shows severe deviations compared to measurement input parameters what is mainly caused by the LVD model itself. Hence, the discussion about Figure 85 has to be kept in mind at this point, as the accuracy of simulation results is also determined by other assessment tools. Nevertheless, the following Figure 92 and Figure 93 additionally shows the possible cause for the result in Figure 91. The vehicle speed is followed by the LVDs driver model with very good accordance compared to the measurement (Figure 92). But in fact, the drivetrain and vehicle dynamic model as well as the internal combustion engine (ICE) model are already falsifying the simulated engine speed result in comparison to the measured engine speed for the same velocity profile.

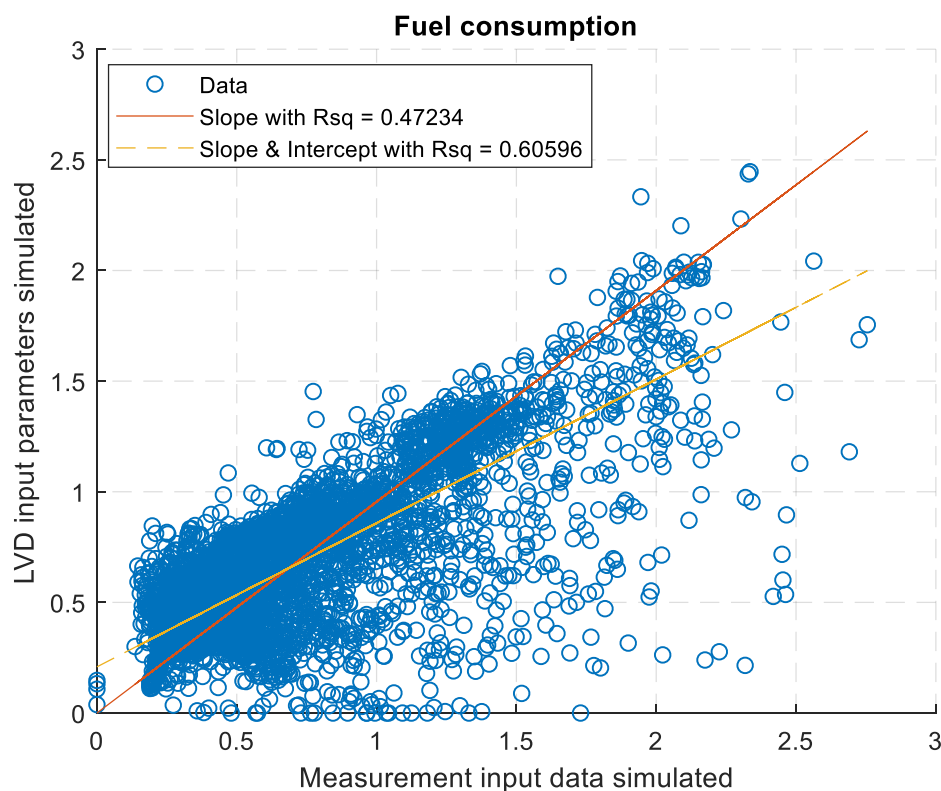


Figure 91: Linear regression relation between fuel consumption simulated by ANNs with LVD input parameters and fuel consumption simulated by ANNs with measurement data input parameters.

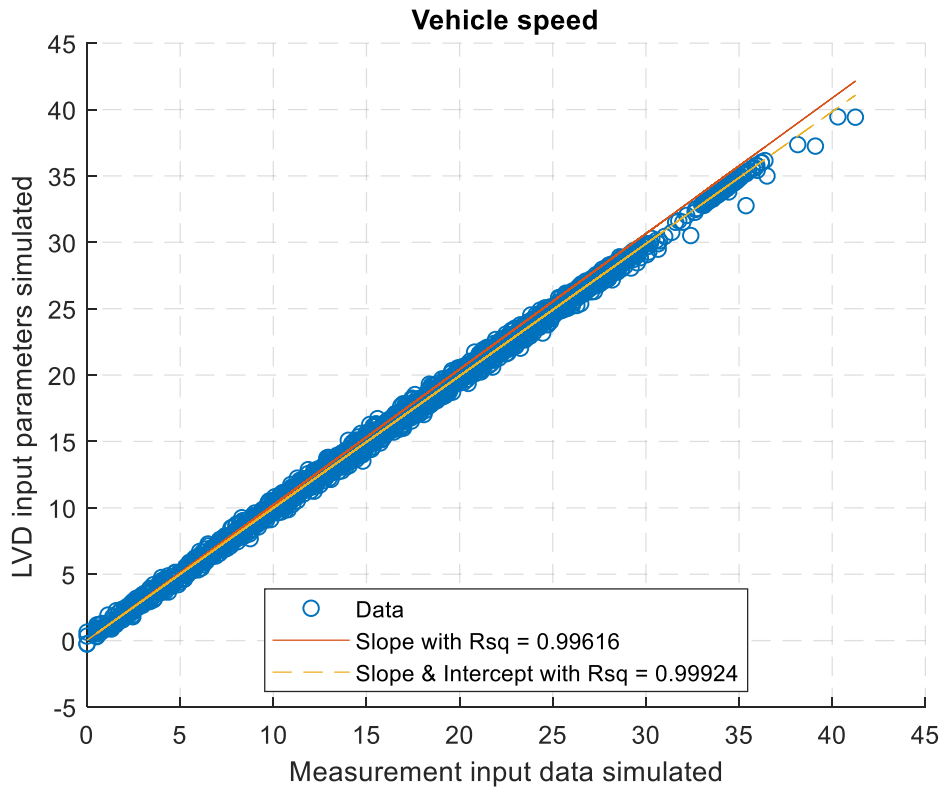


Figure 92: Linear regression relation between vehicle speed simulated by ANNs with LVD input parameters and vehicle speed simulated by ANNs with measurement data input parameters.

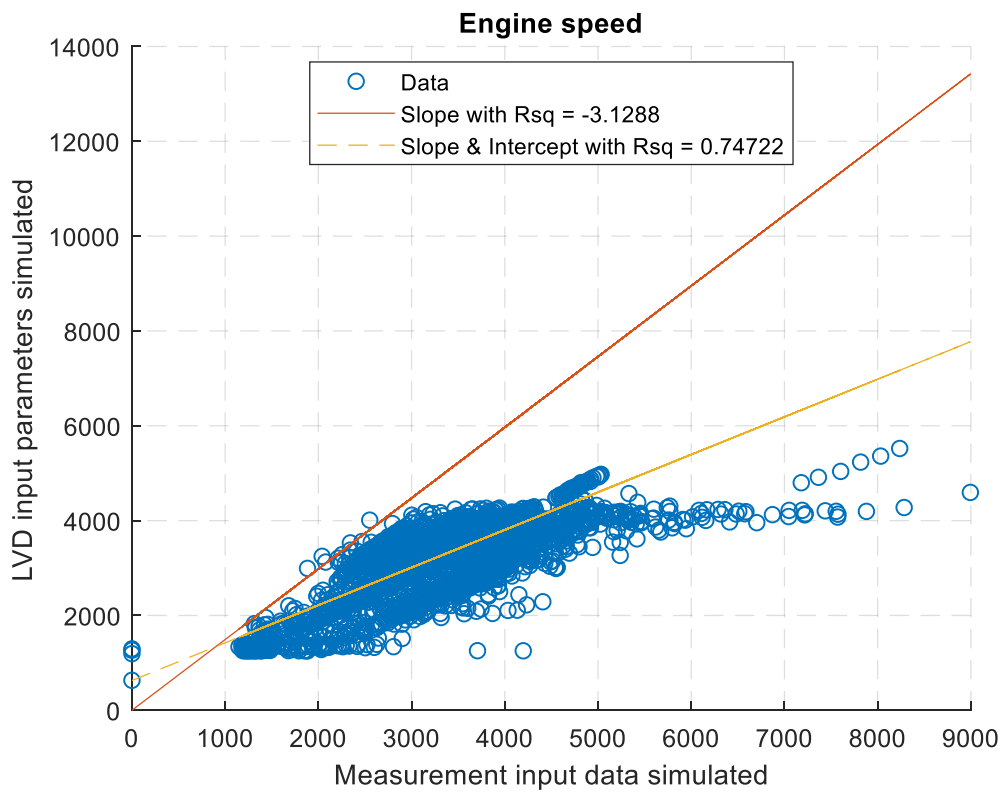


Figure 93: Linear regression relation between engine speed simulated by ANNs with LVD input parameters and engine speed simulated by ANNs with measurement data input parameters.

The adaption of the LVD towards more realistic on-road driving pattern was not part of this thesis as its claim is mainly the determination of applicability of ANNs for emission modelling. Nevertheless, possible and necessary adaptations of the LVD for further use of the emission model are discussed in chapter 4.1.5 and 5.2.

The following section steps into detail concerning emission and fuel economy simulation. More simulation results will be shown and discussed, further possibilities for the use of this simulation technique will be presented.

4.1.4 Emission and fuel economy simulation

An on-road RDE measurement test was simulated for validation of the performance of the above described ANN based emission and fuel consumption simulation method. The modal trace of fuel consumption has very good accordance to the measurement, even though headwind, inclined position of the motorcycle and the real gear shifting have not been included in the longitudinal vehicle dynamic (WMTC gear shifting scheme was used instead).

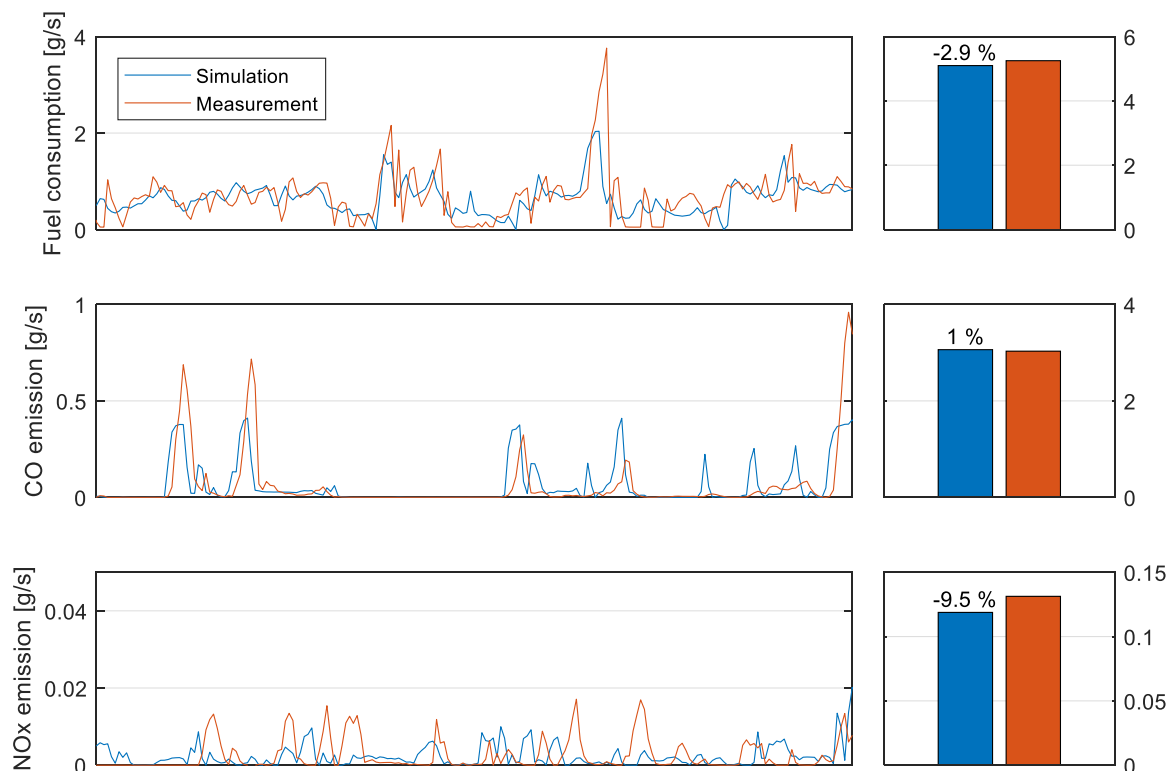


Figure 94: Modal simulation and measurement results of an RDE segment; fuel consumption is shown in l/100km, CO emissions in g/km and NO_x emissions in g/km; right side shows summated measurement results over the illustrated section of the test cycle on the left side with additional deviation from measurement result in percentage.

The modal trace of fuel consumption and CO emissions in Figure 94 shows good accordance in comparison to a measured RDE test cycle. The signal follows trends and, therefore, captures relevant emission scenarios so that it is suitable for further analysis of real drive emissions. Best accordance of the modal trace shows the fuel consumption measurement with a maximum

overall deviation compared to measurements of $\pm 3\%$, whereas emission level can differ up to $\pm 10\%$ depending on the observed segment.

Once again, the presented results in Figure 94 indicate the difficulty in simulating NO_x emissions in a modal way due to the broad learning data scatter. One reason for bad reproduction of this emission signal might be the conversion capacity of the catalyst. The NO_x conversion rate is highly dependent on the oxygen storage of the catalyst if one or multiple engine operation points have rich mixture a few seconds ahead of the considered moment. Due to the temporal singular assignment of engine operation points to emission scenarios, this effect cannot be mapped with the presented ANN learning scheme. An indicator for this phenomenon is the spikier measurement trace of NO_x emissions of the investigated Euro 3 engine compared to the same motorcycle with a Euro 4 engine. In general, the difficulty in reproducing NO_x emissions could be met if engine application parameters are mapped in the simulation model. As the emission model should be applicable for multiple motorcycles this could not be respected. Another solution might be the integrative simulation of all emission components in one ANN. This could not be done because of the specific training data gathering, as shown in Figure 88. Nevertheless, the presented NO_x model can be used for cumulated emission evaluation, as shown further on.

Another analysis of simulated emissions in real world operation scenarios is given below. The following figures illustrate the share of total emitted gaseous pollutants in accordance to its allocation to and its share of the engine map. This analysis is performed with a simulated RDE test cycle including cold start.

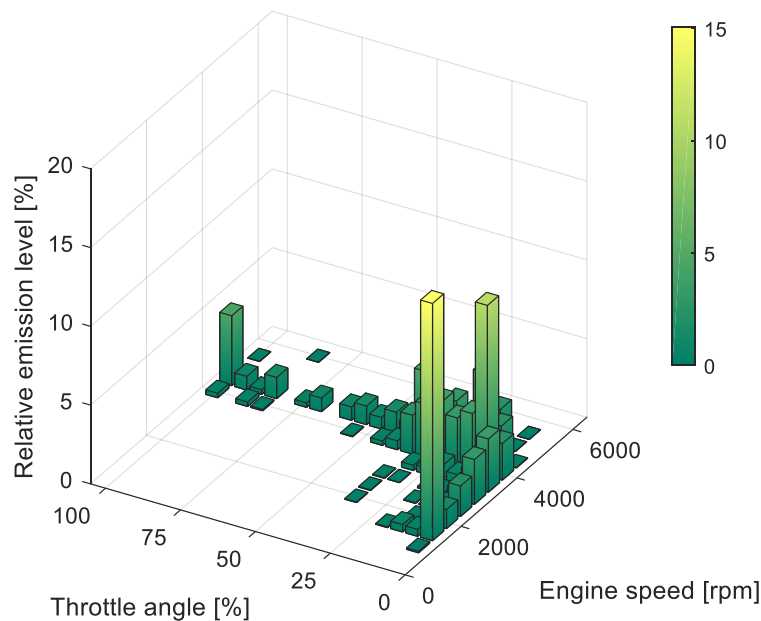


Figure 95: Relative share of CO emissions over throttle angle and engine speed out of RDE simulation in proportion to overall emitted CO during the simulated test cycle.

Figure 95 shows the relative share of CO emissions over throttle angle and engine speed. Additionally, Figure 98 indicates the relative share of engine speed and throttle angle combinations in proportion to the overall test cycle duration. It can be seen, that around 14 [%] of all emitted CO emissions are caused by driving scenarios that have a share of under 1 [%] on overall test duration. These emissions can be linked to operation points with richer mixture for throttle angle positions larger than 90 [%]. Furthermore, many peaks are visible in emission

levels in Figure 95 in-between 25 and 75 [%] throttle angle position that have very small corresponding shares on total test time according to Figure 98. This phenomenon could be linked to acceleration enrichment for drivability of the motorcycle.

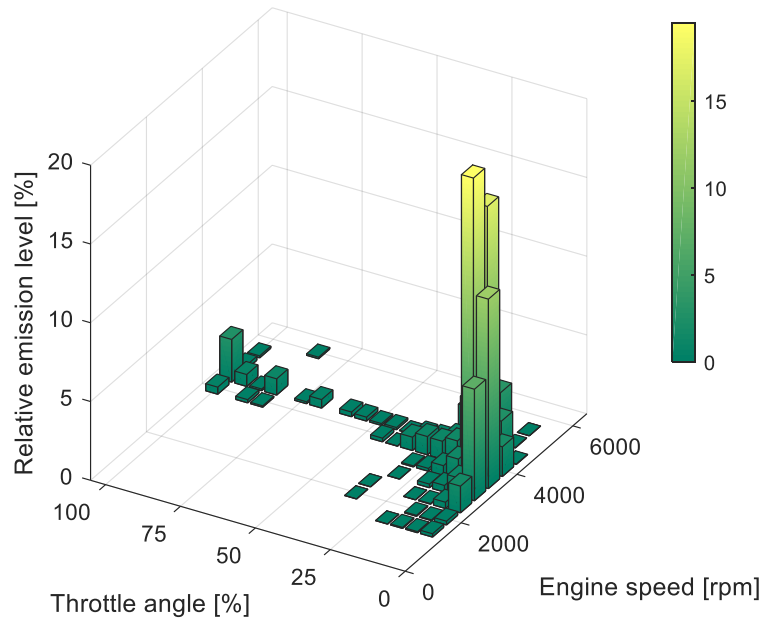


Figure 96: Relative share of NO_x emissions over throttle angle and engine speed out of RDE simulation in proportion to overall emitted NO_x during the test cycle.

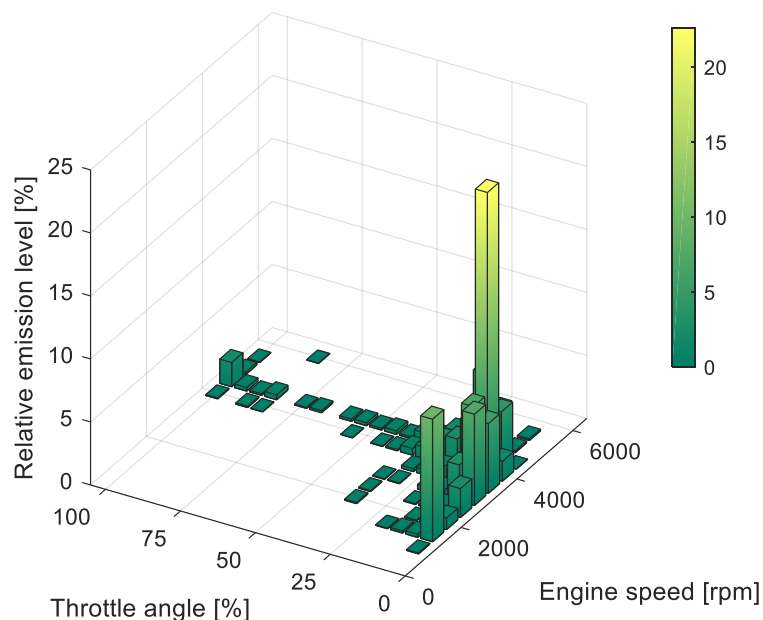


Figure 97: Relative share of HC emissions over throttle angle and engine speed out of RDE simulation in proportion to overall emitted HC during the test cycle.

A similar analysis is given in Figure 96 for the relative share of NO_x emissions proportional to overall emitted NO_x emissions during the test cycle. Once again, a high contribution of total NO_x emissions of some areas in the engine map which have little share on overall testing time can be associated. The analysis of HC emissions shows similar results, as illustrated in Figure

97. These are exemplary evaluations which can be derived by RDE simulations based on chassis dynamometer measurements with the herein presented emission model. Subsequent investigation and adaption of the emission relevant engine operation points based on the results can lead to lower emission values.

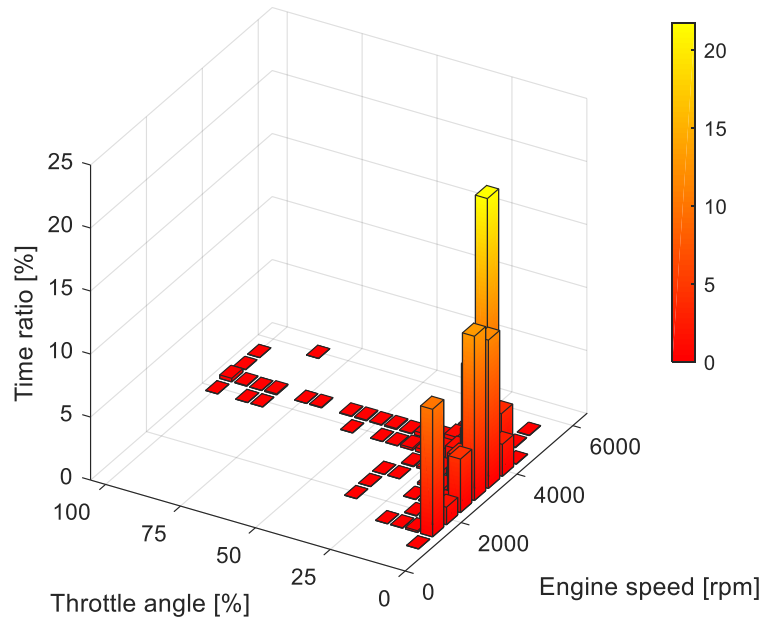


Figure 98. Relative share of engine speed and throttle angle pairs in proportion to test cycle duration from simulation.

The simulation results can be compared to on-road measurements of similar RDE test routes as simulated. Figure 99 shows the relative share of CO emissions over throttle angle and engine speed out of RDE test route measurement “Arzberg” in proportion to overall emitted CO during the test cycle. Compared to *Figure 96* differences in emissions can be seen. These may arise from slightly different driving pattern (on-road vs. simulated) as well as from general differences between simulated longitudinal vehicle dynamic compared to on-road behavior. Influencing parameters like drivers behavior (e.g. aggressiveness), inclined position, throttle angle gradient, etc. are relevant for the shown differences in emission results.

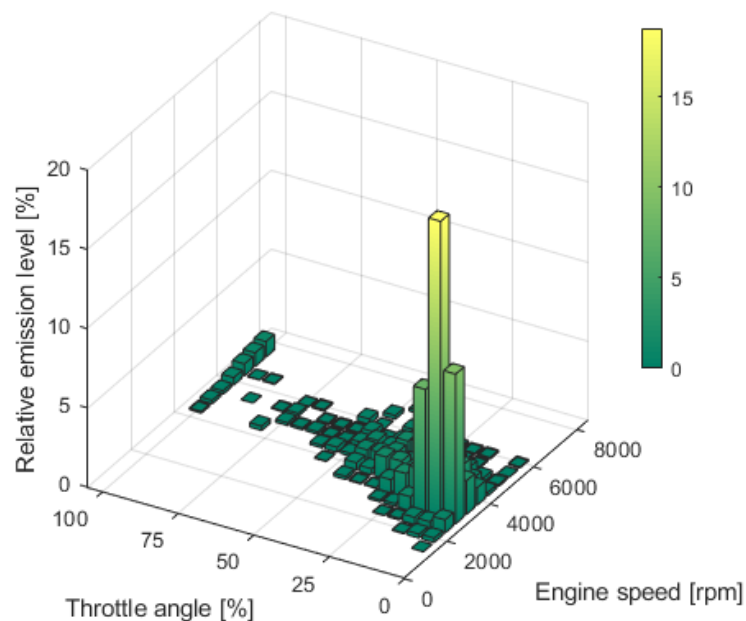


Figure 99: Relative share of CO emissions over throttle angle and engine speed out of RDE test route measurement “Arzberg” in proportion to overall emitted CO during the test cycle.

Hence, determination of real-world performance of motorcycles is also depending on driving dynamic [18] and, therefore, the correct simulation of vehicle driving dynamic. Figure 100 illustrates the relative share of engine speed and throttle angle pairs in proportion to overall test cycle duration for an on-road RDE measurement.

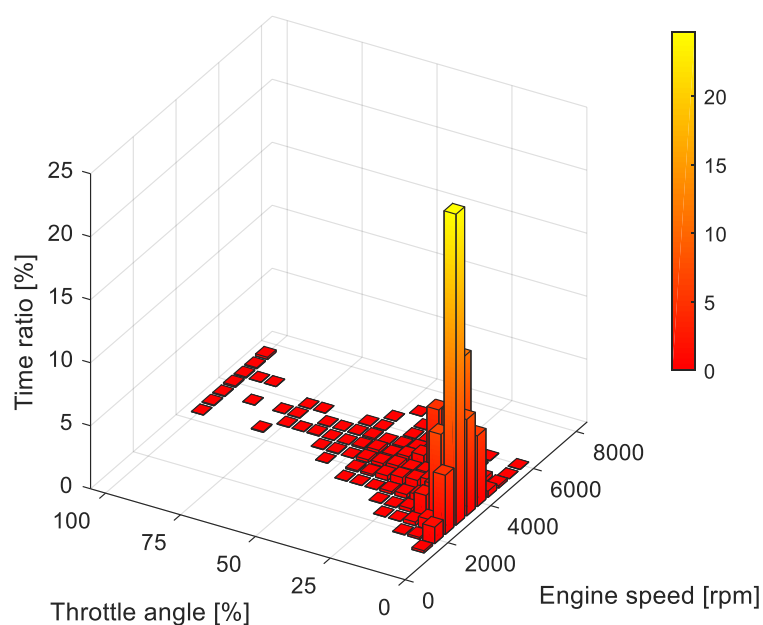


Figure 100: Relative share of engine speed and throttle angle pairs in proportion to test cycle duration out of on-road measurements.

The comparison with Figure 98 shows a clear deviation of the utilization of the engine map between simulation and real-world measurement. The following diagram enlarges upon this issue.

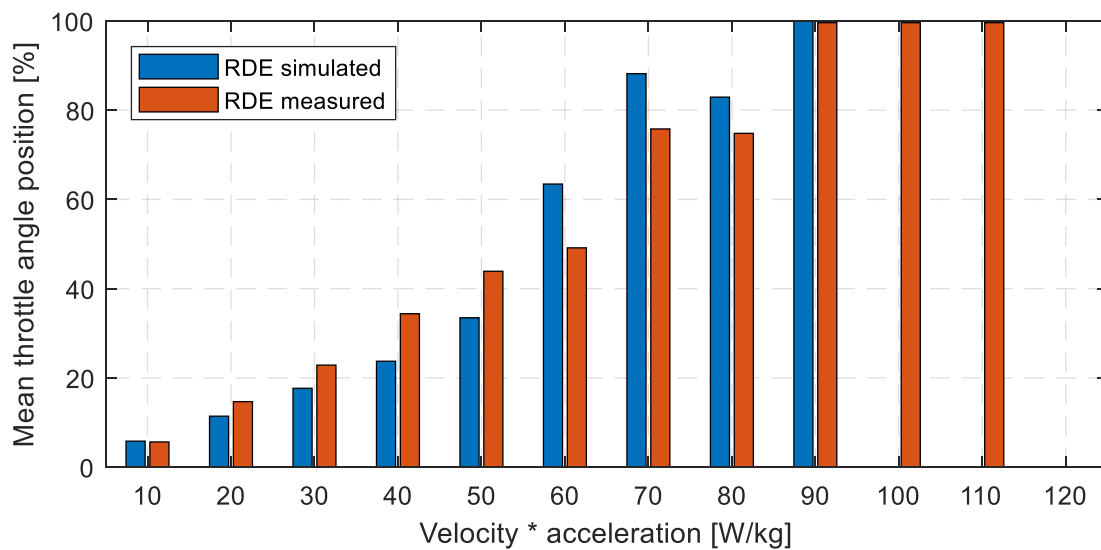


Figure 101: Comparison of mean throttle angle position per dynamic indicator (VA_{pos}) for simulated and measured RDE test cycles.

Figure 101 illustrates a comparison of mean throttle angle position over the dynamic indicator, velocity times positive acceleration VA_{pos} , for simulated and measured RDE test cycles. Higher values of the dynamic indicator result from higher driving dynamic of the motorcycle. The mean throttle angle position is rising in the same way as the driving dynamic increases. Moreover, it can be seen that the simulation is not covering the very right peaks of the driving indicator which is also reflected in the comparison between Figure 98 and Figure 100. This has an influence on emission simulation as the herein described driving scenarios are not covered at all.

Subsequently, gear shifting paradigm, throttle angle gradient, the drivers' aggressiveness in vehicle operation respectively and the resulting raise of engine speed gradients and overall engine speed level are the crucial parameters to fully display real world operation. Especially the gear shifting paradigm in on-road operation differs from the used WMTC scheme. As the used longitudinal vehicle dynamic was extended to on-road requirements but is still using the WMTC gear-shift rules, the emission simulation could result in better correspondence to real world operation with updated gear shift model in an improved version of the LVD.

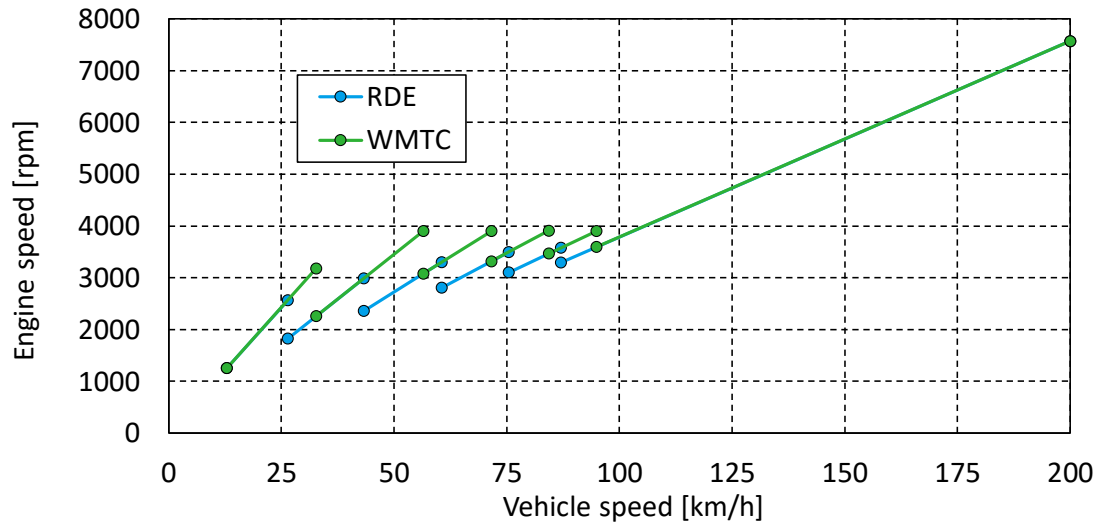


Figure 102: Comparison of upshifting scheme for type approval test WMTC and for on-road route “Arzberg” with the BMW F800GT test object.

Figure 102 and Figure 103 illustrate a comparison of gear shifting paradigm for type approval test WMTC and on-road driving pattern for the “Arzberg” route. Measurements were made by the same driver and one test was made for each test cycle/route. The shifting points are average points calculated from all occurring shifts per test cycle/route. One can see that upshifting is executed earlier than in type approval tests. Also, the downshifting paradigm of on-road driving clearly differs from the type approval test. Especially for low gears the downshifting happens at higher velocities and results in higher engine speeds.

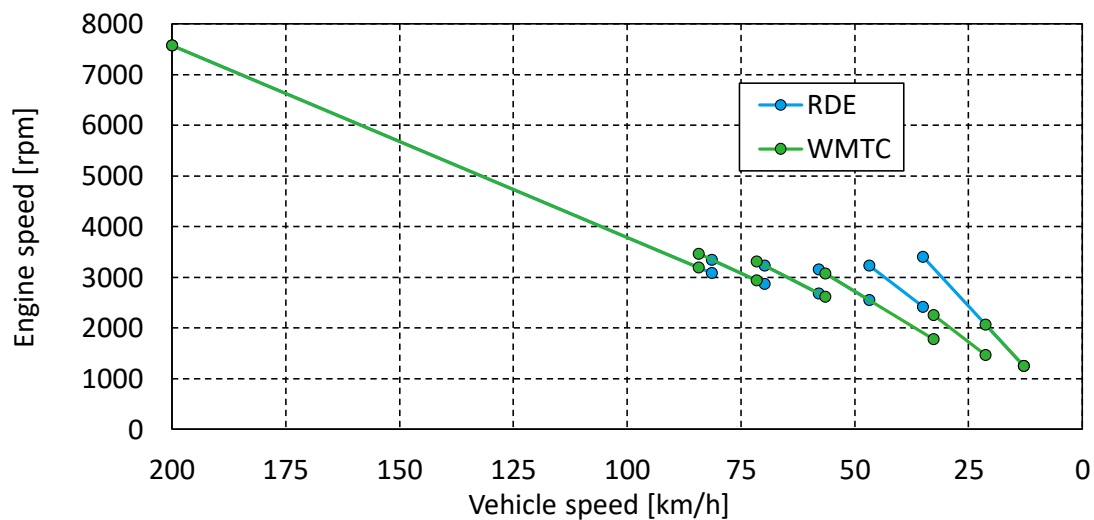


Figure 103: Comparison of downshifting scheme for type approval test WMTC and for on-road route “Arzberg” with the BMW F800GT test object.

4.1.4.1 Vehicle adaption test cases

The following section introduces three different vehicle adaption test cases, which were carried out for the simulated motorcycle. Namely, two engine adaptations were investigated in terms of their estimated effects on emissions and fuel consumption for the RDE test route “Arzberg”.

Furthermore, a third investigation is presented where the influence on emissions and fuel consumption of an additional mass of 70 [kg] is estimated for type approval tests and the RDE test route “Arzberg” as well. Cold start was not considered for all of these analysis.

At first, the relative change in overall RDE level was estimated for start-stop operation. Therefore, the simulation was carried out with neglected cooling of the catalyst during engine stop whilst the catalyst was assumed to have operation temperature. Additional start emissions and further phenomena like engine start followed by a stop were also neglected because no data was available at that time. The conditions for a motor stop in the LVD were chosen by a velocity smaller than 2 [km/h] and an engaged clutch or the engine in idling speed operation. As a second investigation, a stoichiometric engine setting was examined with ANNs trained with filtered data, notwithstanding the losses in engine performance. Figure 104 sums up the results of both investigations as deviation relative to normal operation for a simulated RDE test cycle. An improvement in total emission level can be seen for all investigated components and fuel consumption is also reduced for start-stop operation. The stoichiometric engine setting shows relative improving for fuel consumption and CO emissions but deterioration for NO_x and HC emissions. This result might correspond to reality as the engine of the investigated test object runs on stoichiometric operation anyways, except for acceleration enrichment and operation above 90 [%] throttle angle position. Therefore CO emissions could be lower as a result and NO_x emissions might increase. Nevertheless, with no more rich operation points HC emissions should also drop if one thinks of its usual relation over stoichiometric ratio for gasoline engines. So, the shown values must be considered with respect to the above shown training data variability (see Figure 86) and should serve as an estimation of possible trends in emissions caused by the engine operation adaption test cases. Therefore the illustrated values can be neglected and should just serve as an indicator of possible quantitative effects.

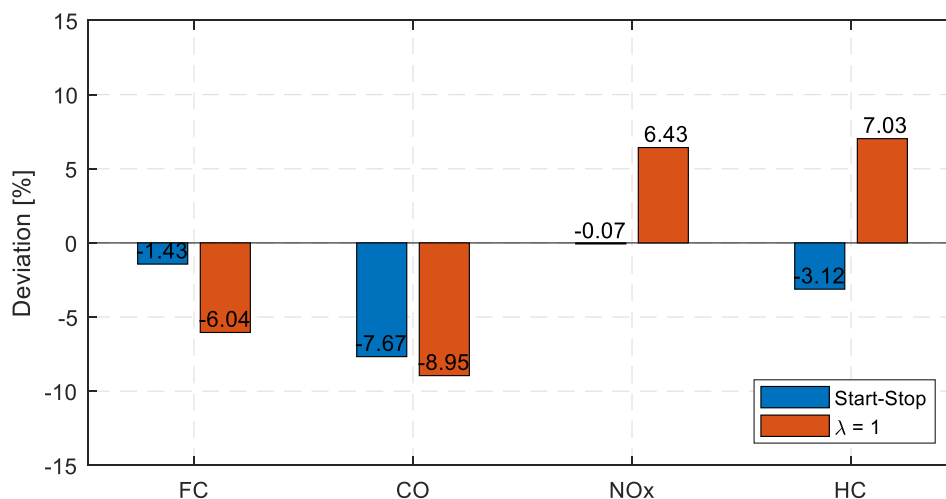


Figure 104: Estimated relative change in overall RDE level [g/km] for automatic start-stop system implementation and stoichiometric engine operation as relative deviation [%] to normal operation on RDE route “Arzberg”.

Moreover, the influence of an additional load on the motorcycle of 70 [kg] was investigated for type approval tests (WMTC stage 2) and RDE tests. This simulation was carried out with no changes in the ANNs but with adjusted test object weight in the LVD. The additional weight reflects the PEMS which was used for real world tests; therefore, the measurement result for RDE with tare weight plus drivers’ weight is missing. Figure 105 and Figure 106 sum up the evaluations for CO and NO_x emissions. The diagrams are cut at the given value for a more

detailed view of the deviations.

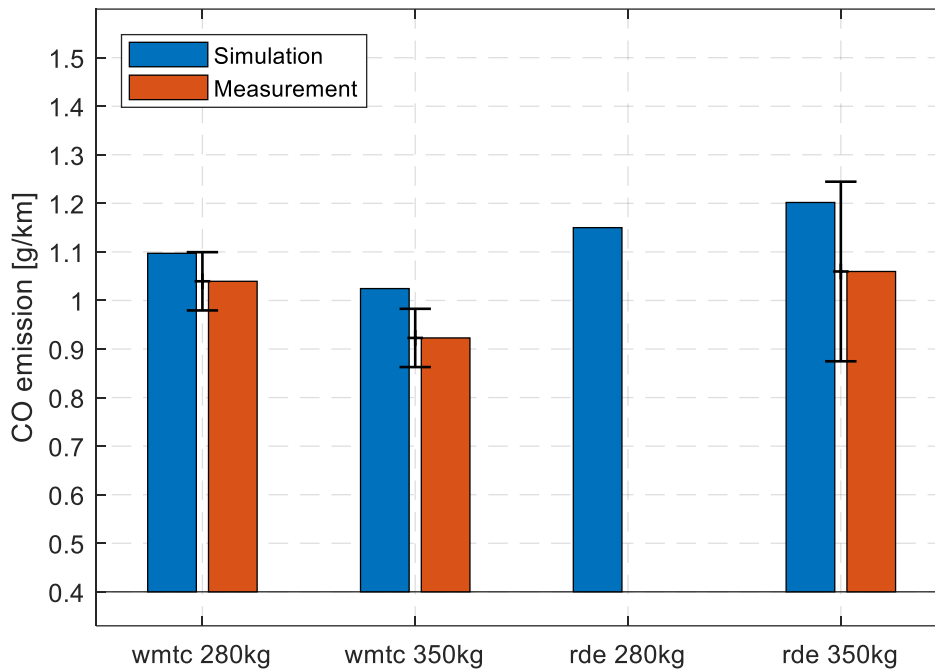


Figure 105: Comparison of CO emissions of WMTC and RDE simulation and measurement results for different additional load on a motorcycle; illustrated standard deviation based on multiple measurement results per WMTC and RDE in each case and plotted for the mean values of the measurement results; diagram is cut at 0.4 [g/km] for better illustration.

The reduction in CO emissions from the type approval test with 280 [kg] reference mass to 350 [kg] reference mass can be ascribed to the shift in engine operation towards better efficiency, which was proved by engine map evaluation. The simulation follows this trend and also the subsequent application to RDE test cycles for both investigated cases shows a realistic trend. Also, NO_x emissions out of emission simulation show the corresponding trend to reference measurement and the results lie in-between standard deviation of investigated measurement results.

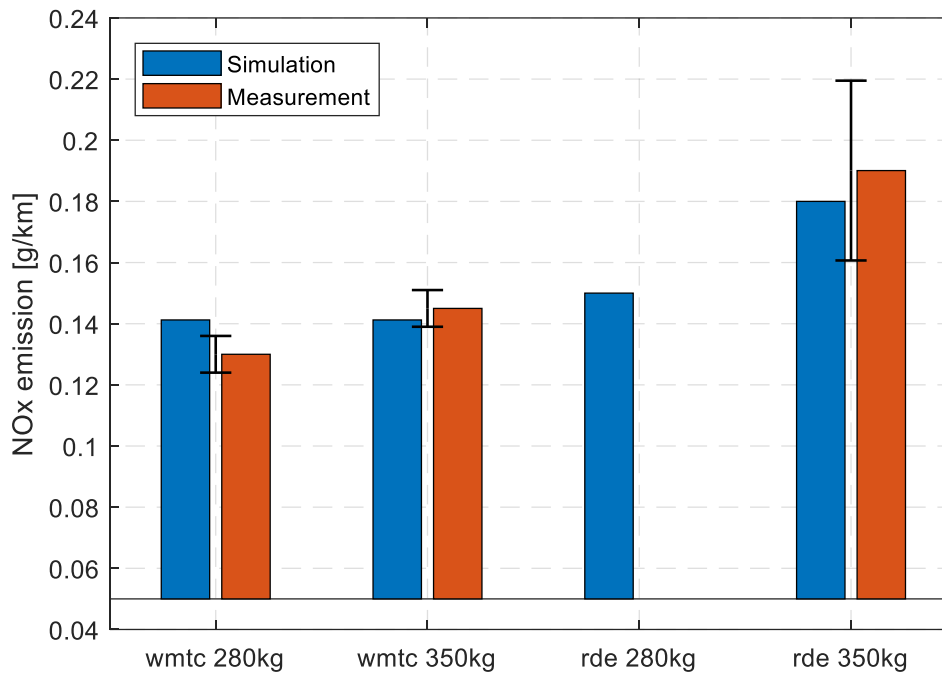


Figure 106: Comparison of NO_x emissions of WMTC and RDE simulation and measurement results for different additional load on a motorcycle; illustrated standard deviation based on multiple measurement results per WMTC and RDE in each case and plotted for the mean values of the measurement results; diagram is cut at 0.05 [g/km] for better illustration.

These exemplary test cases substantiate the applicability of the presented emission simulation model for the investigated motorcycle. As said above, improvements in the overall longitudinal vehicle dynamic can lead to even better accordance to reality and therefore to predicting results more accurately.

4.1.5 Model adaption to other motorcycles

It was stated that the introduced simulation methodology is adaptive to modifications and also to other motorcycles. This can be done very easily by the manipulation of training data as shown for the test cases in the previous section. The adaption to other motorcycles has to be done by the processing of new measurement data as learning input. According to the emission behavior of the test object, further adaptations of the network parameters, used input parameters and learning paradigm might be necessary (see also Table 18 for some of those values). In fact, any emission performance can be simulated with ANNs in a very simple way. The extrapolation of the model, as shown for RDE with test rig inputs only, is the uncertain part which must be considered very carefully. Herein shown models were optimized toward RDE prediction for the BMW F800GT Euro 3 motorcycle only. Subsequently, some very rough simulations were made for the BMW F800R and BMW G1200GS Euro 4 motorcycles too, but only to give some predictions for overall emissions and fuel consumption for the whole simulated test cycle. Nevertheless, it could be shown that this hasty simulations lead to satisfying results for overall emission level prediction. The summarizing diagrams for these simulations are presented in the last chapter 0 as base for a final discussion of a comprehensive RDE measurement and simulation methodology.

5 Conclusive discussion

Finally, the following figures Figure 107 to Figure 109 illustrate a conclusive comparison of type approval WMTC test results, real drive cycle RDC test results, real drive emission RDE results and RDE simulation results for the BMW F800GT Euro 3, BMW F800R Euro 4 and BMW G1200GS Euro 4. These diagrams have been discussed in section 3.4, except for the simulation results.

At a first glance, the simulation results seem to be reflecting operation scenarios between real drive cycles and on-road tests quite well. As these results are based on chassis dynamometer measurements only and on a quite small database, this is really satisfying. Nevertheless, on a closer look difficulties arise because the simulation model for the Euro 4 motorcycles is built on a very rough base and has to be optimized for each emission component and motorcycle for further analysis of emission relevant driving pattern as discussed in section 4.1.4.1 and section 4.1.5. Moreover, for the presented results for the Euro 3 motorcycle, the discussion about difficulties in simulating modal results for detailed analysis must be recalled at this point (see section 4.1.4).

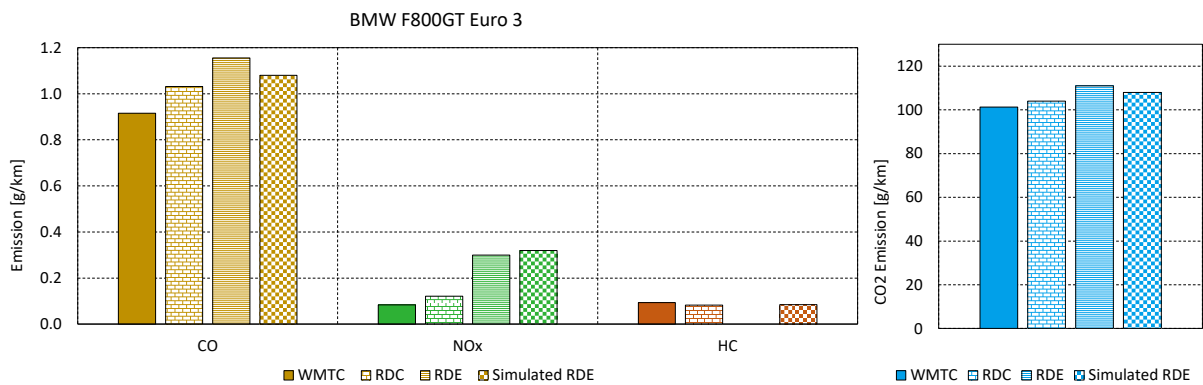


Figure 107: Comparison of WMTC, RDC, RDE measurement results and RDE simulation results for the BMW F800GT Euro 3 motorcycle.

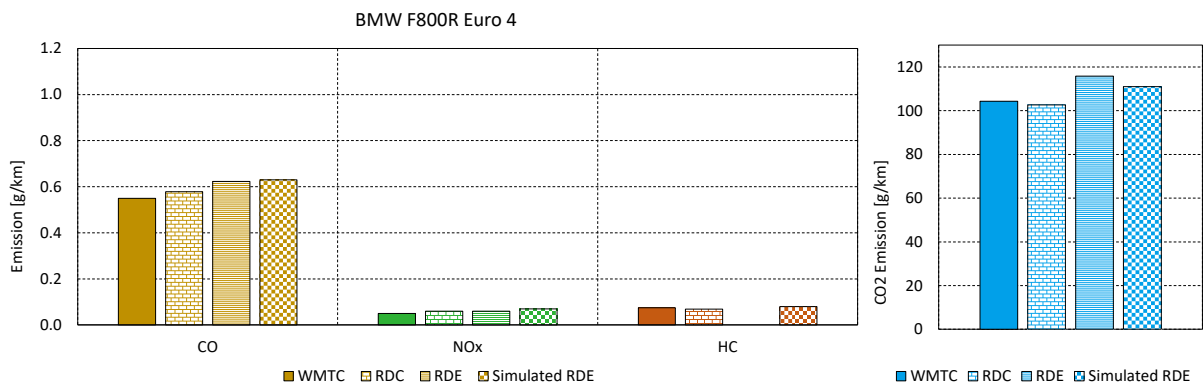


Figure 108: Comparison of WMTC, RDC, RDE measurement results and RDE simulation results for the BMW F800R Euro 4 motorcycle.

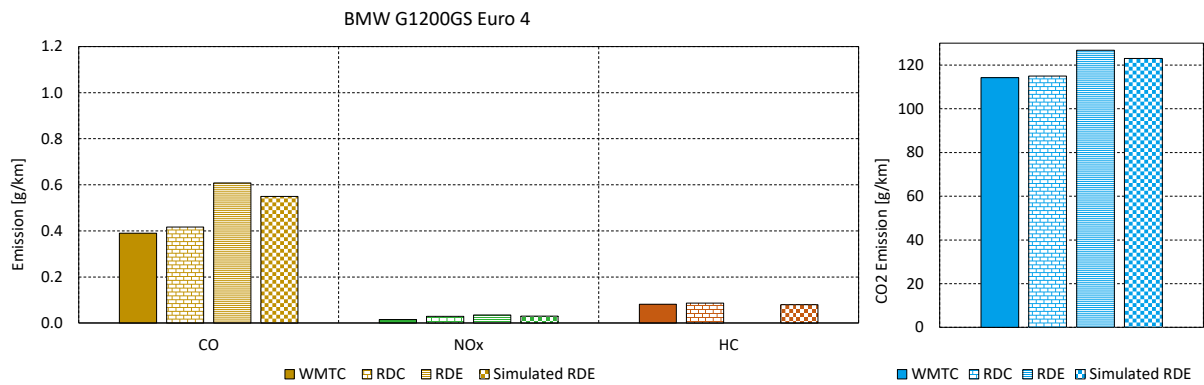


Figure 109: Comparison of WMTC, RDC, RDE measurement results and RDE simulation results for the BMW G1200GS Euro 4 motorcycle.

Hence, these results lead to the remaining need for on-road emission tests to adequately and reliably assess real drive emissions RDE for motorcycles as the presented simulation model serves as a tool for useful further emission estimations but not as substitution for any RDE measurement. Moreover, the presented real drive cycles RDC can serve as estimations too but will not substitute any real-world measurement with its vast variability of driving scenarios, route options, road parameters and driving pattern possibilities. In this context, possible cycle cheating must be reminded.

The following sections conclusively sum up some thoughts about the introduced research of this thesis. Firstly, a comprehensive RDE measurement methodology for motorcycles is shortly discussed based on the measurement investigations and emission results. Secondly, the presented RDE simulation methodology is summarized and some concluding thoughts are stated. Finally, further use of the introduced findings of this research project in general and the two main areas, measurement and simulation, are presented specifically at the end of each section.

5.1 RDE measurement methodology for motorcycles

Multiple emission and fuel consumption measurements with different motorcycles were conducted to broadly investigate and determine the effects of real world driving on powered two-wheelers. Therefore, on-road measurements with a state of the art PEMS and additional tests on chassis dynamometer were performed. In this context, the driving dynamic of motorcycles was investigated to determine relevant evaluation criteria for on-road measurements. Moreover, several real drive cycles were compiled to examine their purpose for RDE measurement. Furthermore, a variety of emission measurements were made with additional special gauges to confirm the accuracy of used PEMS and to display any occurring cross-influences. The results of emission and fuel consumption measurement underline the relevance of on-road measurements for adequate collection of representative emission data for motorcycles with various engine capacities and concepts. The gathered data also benefit in terms of better understanding of emission relevant real-world driving scenarios and, therefore, in terms of engine calibration for more stringent upcoming emission legislation.

Even with state of the art PEMS the measurement of real drive emissions is possible, although there are some restrictions concerning the size and weight. The actual measurement equipment cannot be applied on every motorcycle (compare with section 2.2.1) but a specifically developed equipment for motorcycles could be derived by adaptations of the state of the art

gauges. Nevertheless, RDE measurements can be performed without restrictions for motorcycles in the same category as the presented main test object BMW F800GT. Even bigger motorcycles show no more influence of the measurement equipment at all. Exemplarily, the BMW G1200GS is a motorcycle which is not influenced by a full PEMS equipment similar to the presented one. In fact, the driver is not feeling the equipment at all during on-road test cycles. Figure 110 depicts the full PEMS equipment (without EFM; compare to section 2.4.1.3) mounted on the BMW G1200GS motorcycle.

In fact, a more critical issue is the installation of and the measurement with and EFM. As discussed in section 2.4.1.2, the mounting of additional pipes and the EFM is disturbing exhaust gas flow behavior. Furthermore, some silencers even have to be modified to mount this equipment (see Figure 110). Moreover, the measurement principle itself has its a priori issues because of transient gas transport behavior like pulsations and backflow. Possible workarounds for the EFM, like using OBD signals, have been discussed in section 2.4.1.3.



Figure 110: Full PEMS equipment mounted on a BMW G1200GS motorcycle.

Conclusively, there can be said, that RDE measurements for motorcycles are possible and PEMS technology as well as measurement methodology can be adapted to motorcycles of the category L3e. Additionally, real drive test cycles, like the presented RDCs, can be used for fast forward estimation of effects on emissions and fuel consumption of on-road driving dynamic of motorcycles. Currently, the introduced real-world cycles are already applied in some projects for stocktaking of Euro 4 motorcycle emissions alongside their type approval tests. A lot of different models are investigated with these RDC tests and also with the introduced cold start test cycles, including mopeds with their real drive moped cycle (see section 2.6). The results from these investigations are currently not used for legislative purpose but for subsequent use of fleet emission calculations.

5.2 RDE simulation methodology

In the thesis, the applicability of ANNs to simulate regulated emissions and fuel consumption for real world driving scenarios for motorcycles RDE has been introduced. Chassis dynamometer measurement of a type approval WMTC test and a real drive cycle RDC test were used as training input for the emission model. An appropriate set of training data is a key to get good simulation results. Moreover, selection and adjustment of the best ANNs for the given fitting problem is crucial. Hence, the herein used neural network structures were described followed by the discussion of the optimization of network parameters for the given problem. Challenges of the presented solutions raised for training data selection and the mode of use of the longitudinal vehicle dynamic simulation itself:

- Correct temporal assignment of emission trajectories to engine specific operation trajectories is a key for subsequent exact emission simulation and usability of the model for further investigations. Therefore, constant and variable time delay of the sensor signals and correction of these effects was discussed.
- Moreover, the selection of the probe position for gas analysis and the choice of measurement principle were debated. This is an important issue to take the diminishing effects into account which lead to incorrect reproduction of transient effects in the simulation results.
- Furthermore, a big challenge is the implementation of real-world driving dynamic into the longitudinal vehicle dynamic simulation that serves as a base for the integrated emission model. Gear shifting paradigm, throttle angle gradient, the drivers' aggressiveness in vehicle operation respectively and the resulting change in engine operation are parameters that must be respected to fully display real world driving.

Hence, next steps for improvement of the simulation model can be as follows: as the used longitudinal vehicle dynamic and its emission model are extended more accurate to on-road requirements by above mentioned amendments, the emission simulation is likely to result in even better predictability of real-world operation. An additional cause for thought is the use of a single integrated ANN for all emission components which might implicate the advantage of combining the cross-sensitivity of gaseous emissions and thus resulting in better accordance to reality. As such, the optimization of the network parameters, training algorithms and the selection of the network type itself must be focused even more.

Three different examples were presented which demonstrate the applicability of the emission model. Summing up, it can be said that the presented approach for emission simulation is simple and fast forward in its applicability and eventuates in precious results for the presented vehicle adaption cases. Possibilities for application have been discussed.

Further use of the simulation model can be the analysis of engine adaptations or the determination of critical real-world operation scenarios in terms of emission formation.

6 Literaturverzeichnis

- [1] P. Mock, J. German, A. Bandivadekar and I. Riemersma, "Discrepancies between type-approval and "real-world" fuel-consumption and CO2 values," The International Council on Clean Transportation, 2012.
- [2] E. Burtynsky, Oil, Toronto: Steidl, 2009.
- [3] P. Nejat, F. Jomehzadeh, M. Mahdi Taheri, M. Gohari and M. Zaimi Abd. Majid, "A global review of energy consumption, CO2 emissions and policy in the residential sector (with an overview of the top ten CO2 emitting countries)," Elsevier Ltd., 2015.
- [4] H.-W. Schiffer, T. Kober and E. Panos, "World Energy Council's Global Energy Scenarios to 2060," Springer Fachmedien Wiesbaden GmbH, 2018.
- [5] I. W. E. B. 2018, "IEA International Energy Agency," 25 September 2018. [Online]. Available: <https://www.iea.org/>. [Accessed 25 September 2018].
- [6] BP, "BP Energy Outlook 2018," BP energy economics, 2018.
- [7] "Global Motorcycle Industry's Current Situation and Future Prospects," FOURIN Special Research, 2016.
- [8] S. Petit, "WARDS INTELLIGENCE: World Vehicle Population Rose 4.6% in 2016," 17 October 2017. [Online]. Available: <http://subscribers.wardsintelligence.com/analysis/world-vehicle-population-rose-46-2016>. [Accessed 25 September 2018].
- [9] J. M. Herrera, "Solid Growth in Global Auto Sales but US Protectionism May Shall Further Gains," Scotiabank, 2018.
- [10] OICA, "International Organization of Motor Vehicle Manufacturers," 2015. [Online]. Available: <http://www.oica.net/>. [Accessed 25 September 2018].
- [11] C. Gangloff, "InvestorIdeas.com: Global Demand for Motorcycles to Exceed 132 Million Units," 15 January 2015. [Online]. Available: <https://www.investorideas.com/news/2015/auto/01151.asp>. [Accessed 25 September 2018].
- [12] U. Bundesamt, "Umwelt Bundesamt: Europaweite Richtlinien regeln die Schadstoffemissionen von motorisierten Zweirädern," 2 November 2015. [Online]. Available: <https://www.umweltbundesamt.de/>. [Accessed 25 September 2018].
- [13] E. Commission, "COMMISSION REGULATION (EU) 2016/427 of March 2016 amending Regulation (EC) No 692/2008 as regards emissions from light passenger and commercial vehicles (Euro 6)," Official Journal of the European Union, Brussels, 2016.
- [14] E. Commission, "COMMISSION REGULATION (EU) 2016/646 of 20 April 2016 amending Regulation (EC) No 692/2008 as regards emissions from light passenger and commercial vehicles (Euro 6)," Official Journal of the European Union, Brussels, 2016.
- [15] E. Commission, "Regulation (EU) No 168/2013 of the European Parliament and of the Council of 15 January 2013 on the approval and market surveillance of two- or three-wheel vehicles and quadricycles," Official Journal of the European Union, Brussels, 2013.
- [16] P. Mock, "European Vehicle Market Statistics," International Council on Clean Transportation Europe, Berlin, 2016.

- [17] J. Hiesmayr, S. Schmidt, C. Zinner, P. Filips and S. Hausberger, "Current findings in measurement technology and measurement methodology for RDE and fuel consumption for two-wheeler-applications," SAE, 2017.
- [18] J. Hiesmayr, S. Schmidt, S. Hausberger, R. Kirchberger, C. Zinner, P. Filips, R. Wanker and H. Friedl, "Results, assessment and legislative relevance of RDE and fuel consumption measurements of two-wheeler-application.," SAE International, 2017.
- [19] J. Hiesmayr, S. Schmidt, R. Kirchberger and S. Hausberger, "Artificial neural network based predictive real drive emission and fuel economy simulation of motorcycles," SEC, Düsseldorf, 2018.
- [20] S. Schmidt, C. Zinner, J. Hiesmayr, R. Kirchberger and H. Eichseder, "Evaluation of measurement technologies for RDE and fuel consumption for two-wheeler-applications," AVL Propulsion Diagnostic Symposium, Baden Baden, 2018.
- [21] M. Kousoulidou, G. Fontaras, L. Ntziachristos, P. Bonnel, Z. Samaras and P. Dilara, "Use of portable emission measurement system (PEMS) for the development and validation of passenger car emission factors," Elsevier, 2013.
- [22] L. Ntziachristos, S. Geivanidis, Z. Samaras and e. Al., "Study on possible new measures concerning motorcycle emissions.," Report for EC, 2008.
- [23] A. T. Nguyen, "Asian Development Blog - Boosting fuel efficiency to cut motorcycle pollution in Viet Nam," 3 October 2016. [Online]. Available: <https://blogs.adb.org/blog/boosting-fuel-efficiency-cut-motorcycle-pollution-viet-nam>. [Accessed 29 March 2017].
- [24] J.-H. Tsai, H.-L. Chiang, Q.-C. Hsu, B.-J. Peng and R.-F. Hung, "Development of a local real world driving cycle for motorcycles for emission factor measurements," Elsevier, 2005.
- [25] S. Kasih, "Asian Human Network Databank," July 2011. [Online]. Available: http://www.asianhumannet.org/db/datas/9_transport/transport_jakarta_en.pdf. [Accessed 29 March 2017].
- [26] China Statistics Press, "China Statistical Yearbook 2017," China Statistics Press, 2017.
- [27] M. o. R. T. & H. Government of India, "Road Transport Year Book (2025-16)," Government of India, New Delhi, 2016.
- [28] I. Japan Automobile Manufacturers Association, "Motor Vehicle Statistics of Japan," Tokio, 2016.
- [29] E. A. M. A. ACEA, "ACEA," 2017. [Online]. Available: <https://www.acea.be/statistics/>. [Accessed 27 September 2018].
- [30] T. Schiller and K. Pillay, "Navigating the African Automotive Sector: Ethiopia, Kenya and Nigeria," Deloitte Africa, Johannesburg, 2016.
- [31] OICA, "International Organization of Motor Vehicle Manufacturers," 2017. [Online]. Available: <http://www.oica.net/category/sales-statistics/>. [Accessed 27 September 2018].
- [32] P. a. G. A. Office of Highway Policy Information, "Federal Highway Administration," 2016. [Online]. Available: <https://www.fhwa.dot.gov/>. [Accessed 27 September 2018].
- [33] F. Posada and C. Facaha, "Brazil Passenger Vehicle Market Statistics," International Council on Clean Transportation, Washington, 2015.

- [34] D. Savvidis, "Future of heavy duty vehicles CO₂ emissions legislation and fuel consumption in Europe," GreenDrive Project Conference "Tomorrow's vehicles: Challenges for industry and university", Antwerp, Belgium, 2016.
- [35] K. Chen, W. Wang, H. Chen, C. Lin, H. Hsu, J. Kao and M. Hu, "Motorcycle emissions and fuel consumption in urban and rural driving conditions," Elsevier, 2003.
- [36] W. Saleh, R. Kumar, H. Kirby and P. Kumar, "Real world driving cycle for motorcycles in Edinburgh," Elsevier, 2009.
- [37] H. Schmidt and J. Badur, "From laboratory to road - Real Driving Emissions," Springer Fachmedien Wiesbaden, Stuttgart, 2016.
- [38] B. Giechaskiel, T. Vlachos, F. Riccobono, F. Forni, R. Colombo, F. Montigny, P. Le-Lijour, M. Carriero, P. Bonnel and M. Weiss, "Implementation of Portable Emission Measurement Systems (PEMS) for the Real-driving Emissions (RDE) Regulation in Europe," Journal of Visualized Experiments, 2016.
- [39] K. Buchholz, "SAE International - New compact PEMS aims to plug the emission-compliance gap," 25 November 2015. [Online]. Available: <http://articles.sae.org/14429/>. [Accessed 11 April 2017].
- [40] S. Geivanidis and Z. Samaras, "Development of a dynamic model for the reconstruction of tailpipe emissions from measurements on a constant volume sampling dilution system.," Measurement Science and Technology, 2008.
- [41] B. Motorrad, "BMW Motorrad Österreich," 23 August 2016. [Online]. Available: http://www.bmw-motorrad.at/at/de/index.html?content=http://www.bmw-motorrad.at/at/de/bike/tour/2012/f800gt/f800gt_overview.html¬rack=1.
- [42] R. Moos, "Recent Developments in Automotive Exhaust Gas Sensing," AMA Conferences, 2009.
- [43] G. Hagen, A. Harsch and R. Moos, "A pathway to eliminate the gas flow dependency of a hydrocarbon sensor for automotive exhaust applications," Journal of Sensors and Sensor Systems, Bayreuth, 2018.
- [44] D. Y. Wang, S. Yao, M. Shost, J.-H. Yoo, D. Cabush, D. Racine, R. Cloudt and F. Willems, "Ammonia Sensor for Closed-Loop SCR Control," SAE International, 2009.
- [45] M. S. Zallinger, "Mikroskopische Simulation der Emissionen von Personenkraftfahrzeugen," Graz, 2012.
- [46] S. R. Gagandeep, S. Anil, C. Sasun and T. Rajasekaran, "Development of Real World Driving Cycle for Vehicle Durability Evaluation," SAE International, 2012.
- [47] B. A. Holmen and D. A. Niemeier, "Characterizing the effects of driver variability on real-world vehicle emissions," Elsevier, 1997.
- [48] S. Lipp and S. Hausberger, "CLEAR User Guide for Version 2.0," Forschungsgesellschaft für Verbrennungskraftmaschinen und Thermodynamik mbH, Graz, 2017.
- [49] C. Louis, Y. Liu, P. Tassel, P. Perret, A. Chaumond and M. André, "PAH, BTEX, caronyl compound, black-carbon, NO₂ and ultrafine particle dynamometer bench emissions for Euro 4 and Euro 5 diesel and gasoline passenger cars," Elsevier, Angers, 2016.
- [50] N. Heeb, A.-M. Forss, C. Saxer and P. Wilhelm, "Methane, benzene and alkyl benzene cold start emission data of gasoline-driven passenger cars representing the vehicle technology of the last two decades.," Elsevier, Dübendorf, 2003.

- [51] M. Weilenmann, P. Soltic, C. Saxer, A.-M. Forss and N. Heeb, "Regulated and nonregulated diesel and gasoline cold start emissions at different temperatures.," Elsevier, Dübendorf, 2004.
- [52] P. Rieger, J. Girstmair, S. Schmidt and R. Almbauer, "Development of a Thermal Model within a Complete Vehicle Simulation for Motorcycles and Powersport Applications," SAE International, Taipei, 2013.
- [53] N. Foxhall, S. Leiber and R. Rokita, "EC 2020 Emission Regulations - A Challenging Technology Roadmap for Powersport Vehicles," 13. Tagung: Der Arbeitsprozess des Verbrennungsmotors, Graz, 2011.
- [54] S. Qiang, D. Guangyu, O. Massimo, W. Zhijun and L. Liguang, "Design and Simulation of Serial Hybrid Electric Moped Powertrain," SAE International, Milwaukee, 2008.
- [55] C. Harrington, J. Allen, B. Smither and G. Farmer, "Low Cost Hybrid Optimisation Model," SAE International, Linz, 2010.
- [56] C. Dutzler, G. Heizinger and A. Mair, "Holistic Model Based Development Process," SAE International, Linz, 2010.
- [57] A. Fröberg and L. Nielsen, "Dynamic Vehicle Simulation - Forward, Inverse and New Mixed Possibilities for Optimized Design and Control," SAE International, Graz, 2004.
- [58] P. Hofmann, *Hybridfahrzeuge*, Heidelberg: Springer, 2010.
- [59] P. Rieger, C. Zinner, S. Stephan and S. Hausberger, "Analysis of Conventional Motorcycles with the Focus on Hybridisation," SAE International, Charleston, 2016.
- [60] MathWorks, "Matlab Documentation," The MathWorks, Inc., Natick, Massachusetts, 2018.
- [61] G. Vandi, D. Moro, F. Ponti, R. Parenti and G. Einaudi, "Vehicle Dynamics Modeling for Real-Time Simulation," SAE International, Teipei, 2013.
- [62] M. Puri, A. Solaki, T. Padawer, S. Tipparaju, W. Moreno and Y. Pathak, "Introduction to Artificial Neural Network (ANN) as a Predictive Tool for Drug Design, Discovery, Delivery, and Disposition: Basic Concepts and Modeling," in *Academic Press*, 2016.
- [63] M. Hagan, H. Demuth, M. Beale and O. De Jesús, "Neural Network Design," 2014.
- [64] M. Khare and S. M. S. Nagendra, *Artificial Neural Networks in Vehicular Pollution Modelling, Studies in computational intelligence*, 2007.
- [65] C. Sayin, M. Ertunc, M. Hosoz, I. Kilicaslan and M. Canakci, "Performance and exhaust emission of a gasoline engine using artificial neural network," 2007.
- [66] Z. Asher, A. Galang, W. Briggs, B. Johnston, T. Bradley and J. Shantanu, "Economic and Efficient Hybrid Vehicle Fuel Economy and Emissions Modeling Using an Artificial Neural Network," SAE International, 2018.
- [67] W. K. Yap, *Emissions Predictive Modelling and Simulation for a Plug-in Hybrid Electric Scooter*, Tasmania: University of Tasmania, 2005.
- [68] J. Layne, K. Passino and S. Yorkovich, "Fuzzy Learning Control for Antiskid Braking Systems," *IEEE Transactions on Control Systems Technology*, 1993.
- [69] O. Nelles, "Intelligent Tip: A Learning Driving Strategy for Automated Transmissions," SAE International, 2003.

- [70] J. Mohammadhassani, A. Dadvand, S. Khalilarya and M. Solimanpur, "Prediction and reduction of diesel engine emissions using a combined ANN-ACO method," in *Applied Soft computing*, 2015.
- [71] L. Pelkmans, P. Debal, T. Hood, G. Hauser and M.-R. Delgado, "Development of a Simulation Tool to Calculate Fuel Consumption and Emissions of Vehicles Operating in Dynamic Conditions," SAE International, 2004.
- [72] Z. Gao, J. C. Conklin, C. S. Daw and V. K. Chakravarthy, "A proposed methodology for estimating transient engine-out temperature and emissions from steady-state maps," 2010.
- [73] E. G. Giakoumis and A. I. Alafouzou, "Study of diesel engine performance and emissions during a Transient Cycle applying an engine mapping-based methodology," Elsevier, 2010.
- [74] N. Mizushima, K. Yamaguchi, D. Kawano, H. Suzuki and H. Ishii, "A study on High-Accuracy test Method for Fuel Consumption of Heavy-Duty Diesel Vehicles considering the Transient Characteristics of Engines," SAE International, 2016.
- [75] H. Li, K. Vutts, K. Zaseck, D. Liao-McPherson and I. Kolmanovsky, "Emissions Modeling of a Light-Duty Diesel Engine for Model-Based Control Design Using Mult-Layer Perceptron Neural Networks," SAE International, 2017.
- [76] C. J. Brace, M. Daecon, N. D. Vaughan, S. J. Charlton and C. R. Burrows, "Prediction of emissions from a turbocharged passenger car Diesel engine using a neural network," USA.
- [77] S. Javed, Y. V. V. Satyanarayana Murthy, R. Ulla Baig and D. Prasada Rao, "Development of ANN model for prediction of performance and emission characteristics of hydrogen dual fueled diesel engine with Jatropa Methyl Ester biodiesel blends.," Elsevier, 2015.
- [78] T. Ho, V. Karri, D. Lim and D. Barret, "An investigation of engine performance parameters and artificial intelligent emission prediction of hydrogen powered car.," Elsevier, 2008.
- [79] N. Sharma, K. Chaudhry and C. Rao, "Vehicular pollution modeling using artificial neural network technique: A review," *Journal of Scientific & Industrial Research*, 2005.
- [80] M. Deb, P. Majumder, A. Majumder, S. Roy and R. Banerjee, "Application of artificial intelligence (AI) in characterization of the performance-emission profile of a single cylinder CI engine operating with hydrogen in dual fuel mode: An ANN approach with fuzzy-logic based topology optimization.," Elsevier, India, 2016.
- [81] C. Zhang, O. Vinyals, R. Munos and S. Bengio, "A Study on Overfitting in Deep Reinforcement Learning," 2018.
- [82] E. Littmann and H. Ritter, "Cascade Network Architectures," *Proc. Intern. Joint Conference On Neural Networks*, Baltimore, 1992.
- [83] K. Weller, M. Rexeis, S. Hausberger and B. Zach, "A comprehensive evaluation method for instantaneous emission measurements".
- [84] M. Weilenmann, P. Soltic and D. Ajtay, "Describing and compensating gas transport dynamics for accurate instantaneous emission measurement," in *Athmosperic Environment*, 2003.